Electronic Theses and Dissertations

Theses, Dissertations, and Major Papers

1-1-2004

Active suspension simulation through software interfacing.

Joseph Maiorana
University of Windsor

Recommended Citation

ACTIVE SUSPENSION SIMULATION
THROUGH SOFTWARE INTERFACING

BY
JOSEPH MAIORANA

A THESIS
SUBMITTED TO THE FACULTY OF GRADUATE STUDIES AND RESEARCH THROUGH THE
DEPARTMENT OF MECHANICAL, AUTOMOTIVE, AND MATERIALS ENGINEERING IN
PARTIAL FULFILMENT OF THE REQUIREMENTS FOR THE DEGREE OF MASTER OF APPLIED
SCIENCE AT THE UNIVERSITY OF WINDSOR

WINDSOR, ONTARIO, CANADA

2004

© 2004, Joseph Maiorana

NOTICE:
The author has granted a non-exclusive license allowing Library and Archives Canada to reproduce, publish, archive, preserve, conserve, communicate to the public by telecommunication or on the Internet, loan, distribute and sell theses worldwide, for commercial or non-commercial purposes, in microform, paper, electronic and/or any other formats.

AVIS:
L'auteur a accordé une licence non exclusive permettant à la Bibliothèque et Archives Canada de reproduire, publier, archiver, sauvegarder, conserver, transmettre au public par télécommunication ou par l'Internet, prêter, distribuer et vendre des thèses partout dans le monde, à des fins commerciales ou autres, sur support microforme, papier, électronique et/ou autres formats.

The author retains copyright ownership and moral rights in this thesis. Neither the thesis nor substantial extracts from it may be printed or otherwise reproduced without the author's permission.

L'auteur conserve la propriété du droit d'auteur et des droits moraux qui protège cette thèse. Ni la thèse ni des extraits substantiels de celle-ci ne doivent être imprimés ou autrement reproduits sans son autorisation.

In compliance with the Canadian Privacy Act some supporting forms may have been removed from this thesis.

Conformément à la loi canadienne sur la protection de la vie privée, quelques formulaires secondaires ont été enlevés de cette thèse.

While these forms may be included in the document page count, their removal does not represent any loss of content from the thesis.

Bien que ces formulaires aient inclus dans la pagination, il n'y aura aucun contenu manquant.

Canada

ABSTRACT

Active suspensions provide favourable characteristics over traditional passive vehicle suspensions since they are able to find a better compromise between ride and handling, a conflict that plagues all conventional suspensions. However, active suspension has yet to break into production vehicles because of the technical issues that remain to be resolved to improve its implementation.

Effective virtual simulation of such a system requires a method of properly modeling a multi-domain system. Software interfacing is a method that may be used to solve such problems. It allows each sub-system to be modeled in its natural domain software and then links the sub-systems together, allowing the input and output values for each program to be exchanged with the rest of the model. With this technique, modelling simplifications of each domain is avoided by allowing a complete and accurate picture of the system to surface before prototyping begins.

This research focuses on simulating active suspension by combining the multibody dynamic software program of ADAMS (Automatic Dynamic Analysis of Mechanical Systems) with Matlab/Simulink. The purpose is to capture the dynamics of the system which would allow the user to tune and optimize the suspension before prototyping. Since it is geared towards passenger vehicles, this study focuses on the ride behaviour of the vehicle rather than its handling abilities.

A quarter car and full car model are implemented for both the traditional lumped mass model and the Bombardier Iltis utility truck. When interfacing with the Simulink controller, nonlinear and linear versions of the ADAMS vehicle model were used; also a fully-active and semi-active suspension was evaluated for comparison with the passive suspension. In addition, a Kalman filter for state estimation was used with the fully-active controller, while bushings are added to the full car Iltis vehicle.

The nonlinear ADAMS vehicle was able to successfully communicate with Simulink to simulate the above systems. Results also indicate that the linear vehicle models are reasonable in their performance and so are useful for quick preliminary studies. Additionally, the simple lumped mass vehicle demonstrated similar response patterns and features as the more complicated Iltis models, further proving the worth of these models.

Results demonstrate that a fully-active suspension is able to significantly increase ride performance over a passive suspension but at the cost of the suspension displacement. As expected the semi-active suspension performance was intermediate to that of the passive and fully-active system but with the advantage of only dissipating energy and not consuming it. Both semi-active and fully-active controllers performed reasonably well for this investigation, however, shortcomings in each were noticed. The Kalman filter was generally able to estimate the system states which make the fully-active controller use all the more viable for real world application.

DEDICATION

"The only true wisdom is in knowing you know nothing."
-*Socrates*

"Real knowledge is to know the extent of one's ignorance."
-*Confucius*

...and so this work is dedicated to those who know nothing, keep up the good work.

ACKNOWLEDGEMENTS

First I would like to thank Dr. Bruce Minaker who started it all by graciously agreeing to become my principal advisor. His encouraging guidance combined with his contagious enthusiasm for engineering made him a delight to work with.

My deepest appreciation goes out to my industrial advisor Dr. Dajun Zhang of DaimlerChrysler, whose support, humility and technical expertise is inspirational. He patiently sat through long discussions with me on the project while answering my questions carefully and thoughtfully.

In addition I would like to thank my co-advisor Dr. Peter Frise who supported this project and endorses others like it to the highest level.

Many thanks to Mr. Mohammed Malik of DaimlerChrysler who helped make it possible to conduct this research at the University of Windsor DaimlerChrysler Automotive Research and Development Centre (ARDC).

Furthermore I would like to acknowledge those at ARDC whose support of this project and others like it, expose students to cutting edge research that bridges the gap between academia and industry. I would also like to thank my co-workers at ARDC whose support was instrumental to the completion of this project.

Last but not least I would like to thank my parents Lina and Matthew and my sister Claudia without whom I would never have succeeded this far.

CONTENTS

3 THEORETICAL PRINCIPLES

TABLES

FIGURES

xiv

ADAMS – Automatic Dynamic Analysis of Mechanical System
ARDC – University of Windsor DaimlerChrysler Automotive Research and Development Centre
ARC – Active Roll Control
CM – Sprung mass
DAE – Differential algebraic equations
DET – The determinant of a matrix.
DIAG – Diagonal square matrix, its non-zero numerical values are listed in order of appearance

$$\text{i.e.} \begin{bmatrix} 1 & 0 & 0 \\ 0 & 2 & 0 \\ 0 & 0 & 3 \end{bmatrix} \text{ expressed as diag[1 2 3]}$$

DRES – Defence Research Establishment Suffield
E.C.U. – Electronic control unit
EOM – Equations of motion
GSTIFF – Gear Stiff integrator
LCA – Lower control arm
LQG – Linear quadratic guassian controller, the combination of using LQR for the controller with the Kalman filter to estimate the states
LQR – Linear quadratic regulator algorithm
L.V.D.T. – Linear voltage displacement transducer
nb – Number of bodies
m – Sum of the joint constraint equations
ODE – Nonlinear ordinary differential equations
RR – Ride rate
SP – Spindle
S & G Damping – Skyhook and ground-hook damping
UCA – Upper control arm

SYMBOLS

a – Vehicle lateral dimension.

$A^{\wp}$ – Closed loop system matrix, it includes the plant and controller.

A – Plant matrix (n x n).

$\hat{A}$ – System matrix where states are the desired states of the user.

A_{est} – System matrix (n x n).

A_1 – Ill conditioned plant matrix.

A_2 – Plant matrix in partitioned form.

b – Vehicle lateral dimension.

B – Plant input matrix (n x $(r_{1+}\, r_2)$).

B_1 – Control force input matrix (n x r_1).

B_2 – Road displacement input matrix (n x r_2).

$\hat{B}$ – Input matrix where states are the desired states of the user.

B_{est} – Input matrix of control input force and sensor output measurements (n x (r_1+m)).

B_1 – Ill conditioned plant input matrix.

B_2 – Plant input matrix in partitioned form.

c – Vehicle longitudinal dimension.

c_{gh} – Ground-hook damper coefficient.

c_{sky} – Skyhook damper coefficient.

c_s – Semi-active damping rate.

c_{st} – Strut damper coefficient.

C – Output matrix ((n+m) x n).
    i) if full state feedback desired- an (n x n) identity matrix.
    ii) for measured outputs- an (m x n) matrix.

$\hat{C}$ – Output matrix where states are the desired states of the user.

C_1 – Output matrix where output is desired states.

C_{est} – Output matrix of sensor output measurements and state estimates ((m+n) x n).

C_s – Measured sensor outputs.

d – Vehicle longitudinal dimension.

D – Output matrix ((n+m) x (r_1+r_2)).

$\hat{D}$ – Output matrix where states are the desired states of the user.

D_1 – Output matrix where output is desired states.

D_{est} – Matrix of size ((m+n) x (r_1+m)).

D_s – Measured sensor outputs.

E – Expected value.

f – Vector of applied forces.

F_{sky} – Force generated from skyhook damper.

$F_{desired}$ – Desired force for the semi-active damper.

F_{gh} – Force generated from ground-hook damper.

F_{max} – Maximum force from semi-active damper.

F_{min} – Minimum force from semi-active damper.

F_s – Spring strut force.

F_D – Damper strut force.

F_t – Tire force.

$F_s(x_0)$ – Spring preload for the linear spring.

F_{lnr} – Linear spring force.

F_{sc} – Suspension force.

F_u – Active force.

$F(q,\dot{q},t)=\begin{bmatrix} f \\ \bar{n} \end{bmatrix} \in \mathbf{R}^6$ – Vector of applied forces.

g – Acceleration of gravity, 9.81m/s^2.

g – Set of DAE describing a general multibody system.

G – State matrix corresponding to process noise.

h – Height of road profile.

h – Integration step size.

H – Output matrix corresponding to process noise.

I – Identity matrix.

I_y – Inertia about y-axis.

I_x – Inertia about x-axis.

I_z – Inertia about z-axis.

J – Quadratic cost function.

J – Jacobian matrix of **g**.

$\bar{J}$ – Generalized inertia matrix, expressed in the local body reference frame reference frame.

k – Step size/sample rate.

k_{tire} – Radial spring rate stiffness of tire.

k_{spsn} – Suspension spring stiffness.

k_{lqr} – The optimal gain matrix from LQR solution, $(r_1 \times n)$.

k_s – Strut spring stiffness.

k_t – Tire radial stiffness.

K – Full state feedback gain.

K_{est} – Matlab object consisting of state-space matrices that describe the Kalman filter.

K – Kinetic energy, $K = \dfrac{1}{2}\mathbf{u}^T\mathbf{Mu} + \dfrac{1}{2}\bar{\omega}^T\bar{J}\bar{\omega}$.

l_f – The horizontal distance between the front axle and the center of gravity.

l_r – The horizontal distance between the front axle and the center of gravity.

L – Proportional error feedback gain for state estimator.

m_{sprng} – Sprung mass.

m_{usprng} – Unsprung mass.

m_s – Sprung mass.

m_u – Unsprung mass.

m_t – Total mass of the vehicle body (excludes the mass of the unsprung mass).

m – Sum of the joint and motion constraint equations, equals the number of Lagrange multipliers.

M – Generalized mass matrix.

$\bar{n}$ – Vector of applied torques.

nb – Number of bodies in the system.

nj – Number of joints in the system.

p – Matrix of the body position of a rigid body.

P – Generalized momentum.

P – Riccati equation solution matrix.

P_e – Riccati matrix for Kalman filter.

q – Matrix of the generalized coordinates of a rigid body.

Q – Weight matrix, is a positive definite or semi-definite matrix $(n \times n)$.

Q_n – Covariance of process noise.

$Q(q,\dot{q},t) \in \mathbf{R}^6$ – Generageneralized coordinates, $Q = \left[(\Pi^r)^T f \quad (\Pi^R)^T\bar{n} \right]^T$ .cting the applied force **F** on the generalized coordinates, $Q = \left[(\Pi^r)^T f \quad (\Pi^R)^T\bar{n} \right]^T$.

R – Weight matrix, is a positive definite or real symmetric matrix $(r_1 \times r_1)$.

R_n – Covariance of measurement noise.

ss – Initial tire deflection.

t – Time.

TL – Tire lift off tracking function measure.

$\mathbf{T}$ – Transformation matrix relating body angular velocity in the local coordinate system with that defined. in the generalized coordinate system.

$\mathbf{u}$ – Unconstrained control force input (r_1 vector).

$\mathbf{u}^*$ – Input, from both control and road.

$\delta\mathbf{u}$ – Dependant variables.

$\mathbf{u}$ – Vector of the body translational velocity.

U_k – Inputs to plant model in discrete solver model.

v – Damper velocity.

υ – Measurement noise.

$\mathbf{v}^p$ – Velocity of point of application P of the external force $\mathbf{F}$.

$\delta\mathbf{v}$ – Independent variables.

w – Road displacement input (r_2 vector).

w_{sprng} – Undamped sprung mass natural frequency.

$w_{unsprng}$ – Undamped unsprung mass natural frequency.

w – Process noise.

$\bar{\omega}$ – Vector of the body angular velocity, expressed in the local body reference frame.

W – Road input frequency.

x – State vector, the minimum set of independent variables that fully describe the system (n vector).

x_0 – Set point/operating point.

x_{actual} – Actual/current value of the states.

$x_{desired}$ – Desired value of the states.

$\tilde{x}$ – State error, difference between actual and estimated state.

$\hat{x}$ – Estimated state.

x_1 – Set of independent variables.

x_2 – Set of dependent variables.

x_A – Set of independent states in the ADAMS model.

x_D – Damper displacement.

x_{actual} – Actual state-space variable value.

$x_{desired}$ – Desired state-space variable, for this study this value is zero.

$\hat{x}$ – States desired by user.

x_u – Undesired state space matrix.

Δx – Spring deflection.

x – Distance between the strut mounting points.

X – Displacement in the x direction.

y – User defined output ((n+m) vector).

$\hat{y}$ – Estimated output.

Y – Displacement in the y direction.

$\mathbf{Y}$ – Solution vector, $\mathbf{Y}=[q,\dot{q},\lambda]^T$.

$\Delta\mathbf{Y}$ – Correction of $\mathbf{Y}$.

$\mathbf{Y}^*$ – User specified set-point.

z – State variables of controller in cosimulation mode.

z_u – Unsprung mass absolute vertical displacement.

z_s – Sprung mass absolute vertical displacement.

z11 – Vertical displacement of corner 11.

z12 – Vertical displacement of corner 12.

z21 – Vertical displacement of corner 21.

z22 – Vertical displacement of corner 22.

z_{road} – Road vertical profile.

z_t – Tire vertical movement.

$\mathbf{z}$ – Complex constant vector.

z_{cm} – Displacement of sprung mass in z direction.

Z – Displacement in the z direction.

x,y,z – Coordinate position of a rigid body.

ε – Array of the body orientation of rigid body.

β – Rotation about the z-axis.

ζ – Time derivative of ε.

$\lambda \in \mathbf{R}^m$ – Lagrange multiplier array. The number of multipliers is equal to the number of joint constraint equations (m).

Γ – Angular momenta.

$\mathbf{P}^P$ – Projection operator.

$\mathbf{P}^R$ – Projection operator.

ψ, θ, ϕ – Third, first and third Euler angle sequence of rotation.

α, β_0, β_j – Gear integration constants.

σ – Complex constant vector.

Φ – Algebraic constraint equation.

Φ_u – Constraint equation as a function of dependent variables.

Φ_v – Constraint equation as a function of independent variables.

θ – Angle.

φ – Rotation about the x-axis.

θ – Rotation about the y-axis.

1 INTRODUCTION

1.0 Problem Synthesis

A passenger automobile suspension is a compromise between ride and handling and as such it is the aim of the vehicle dynamicist to find settings that give the best of both worlds. Since passive suspension has existed throughout the age of the automobile, much is known of the system and engineers today are very good at extracting the most performance from it. In fact it is commonly thought that the performance of today's passive suspension has little more improvement left in it. This, combined with a highly competitive automotive market, with hard to please consumers, has sent companies searching for alternative solutions to the conventional system.

As defined by Wong {23} ride is concerned with the sensation or feel of the passenger in the environment of a moving vehicle. Problems arise mainly from vibrations of the vehicle body, induced by sources such as aerodynamic forces and vibrations from the powertrain, drivetrain and road. As stated by Hrovat {31}, vertical ground input disturbances caused by road roughness are the most relevant for ride studies. Handling, on the other hand, deals with the vehicle's response to steering, braking and environmental inputs. In part handling is a measure of the ability to manoeuvre turns since this deals mostly with the vehicle's response to inertial body input forces. The main criteria for optimizing the dynamics of a vehicle are:

- Body motion caused from road surface irregularities.
- Body motion caused from road inputs, aerodynamic loading and inertial forces.
- Road holding related to the contact force between the tire and road surface (through controlling wheel motion).
- Suspension travel, which is limited by the packaging restrictions of the vehicle.
- Maintain directional stability during manoeuvres.

An active suspension is better able to find a compromise between these conflicting requirements and as such can offer greater performance than a passive suspension. However, even with the most sophisticated system, no suspension can simultaneously optimize each of the above criteria since they are all coupled. Although the concept of active suspension has existed since the 1950's when companies like

- 1 -

Citroen and Westinghouse experimented with prototypes, the technology has yet to fully break into production for different reasons.

This research simulates active suspension vehicles using various methods; it carves out a process for developing vehicle models in which the characteristics of such a system can be evaluated and optimized. From such an analysis, problems in the initial design phase can be identified before prototyping and so money and time can be saved in development, helping to further usher this technology into the automotive market.

1.1 Ride versus Handling

1.1.1 Model Description

A vehicle is a complex multi-degree of freedom system that requires sophisticated multibody dynamic algorithms to describe its behaviour. However, to reveal its fundamental response and limitations, a simple lumped mass model of a quarter of the vehicle may be considered; in this way the following discussion will be simpler to outline.
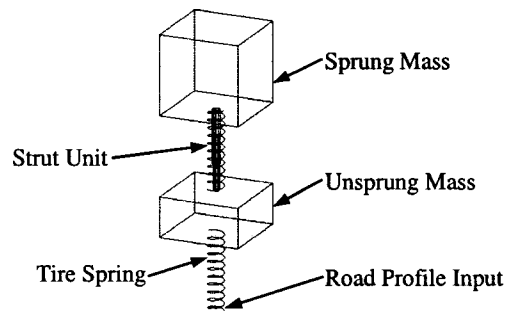
Figure 1.0: Quarter car model

From Figure 1.0, the sprung mass represents the vehicle body; in this model it is roughly one quarter the weight of the entire body, while the unsprung mass represents the mass of one wheel unit. Here the strut unit contains both the suspension spring and damper; it provides the link between the two masses. At the same time the tire spring represents the radial stiffness of the tire with negligible damping (as assumed by most ride studies). The road input is specified at the end of the tire spring in the form of a vertical displacement and since both masses are constrained to only move vertically, the system has two degrees of freedom system.

During operation, it is the suspension spring that absorbs most of the disturbance movement, while the damper dissipates this energy input from the road. Of the variables that affect the vehicle response, the damper and spring rate of the strut unit are two that the dynamicist has direct control over; their chosen parameters contribute to the conflict between ride and handling.

1.1.2 Spring Conflict

When solving the equations of motion for the quarter car model, since damping is typically small, the damped natural frequencies may be approximated by the undamped natural frequencies of:

$$w_{spng} = \left(\frac{RR}{m_{spng}} \right)^{\frac{1}{2}} \tag{1.0}$$

$$w_{unspng} = \left(\frac{k_{spsn} + k_{tire}}{m_{unspng}} \right)^{\frac{1}{2}} \tag{1.1}$$

$$RR = \left(\frac{k_{spsn} \cdot k_{tire}}{k_{spsn} + k_{tire}} \right) \tag{1.2}$$

From these equations, the suspension spring rate is related to both natural frequencies and is the only value in the equations that the dynamicist has control over. Due to the difference in mass, the natural frequency of the unsprung mass is an order higher than the sprung mass (around 10Hz and 1Hz respectively). When the unsprung mass becomes excited by the road the sprung mass becomes excited by the unsprung mass. As a result, for high frequency inputs when the unsprung mass is vibrating near its natural frequency, the sprung mass is mostly unaffected, since its resonant frequency is much lower. However for low frequency inputs, disturbances are passed by the wheel to the body, even amplified at times.

In examining the characteristics of a typical random road profile the vertical acceleration intensity increases with road frequency. As a result, minimizing the natural frequency of the sprung mass decreases the intensity of its response when excited and results in a better ride. This implies that the strut spring should be as soft as possible.

Another way to see the effects of the suspension spring rate on the sprung mass is by considering the frequency response plot[†] of the sprung mass acceleration of Figure 1.1. Frequency plots generate the sinusoidal response amplitude to a vertical sine wave road profile of varying frequency. As shown, the softer the suspension the lower the acceleration levels of the sprung mass, especially in the area of its natural frequency. However the softness of the strut spring is limited by the amount of space in which the suspension can move within - both while the car statically sits and when it encounters road disturbances.

[†]*Notice: All graphs in this study are 'normalized' by dividing the y-axis values by the maximum value attained.*
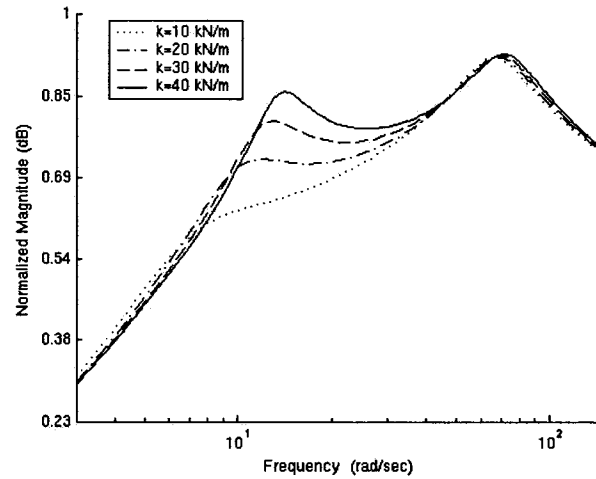
*Figure 1.1: Sprung mass acceleration response versus road input
frequency for various strut spring rates*

Although a softer suspension produces less sprung mass motion, it also leads to deterioration in handling due to a loss of tire grip. When the vehicle performs a cornering manoeuvre the sprung mass shifts to the outside tires increasing the normal tire loading on the outside tires and decreasing it on the inside. The generated lateral tire force is related to the normal tire load, yet at a decreasing rate as illustrated in Figure 1.2. As such, the more the vehicle rolls the less lateral tire grip is produced from the combined outside and inside lateral tire force. Hence for handling purposes stiff springs should be used.
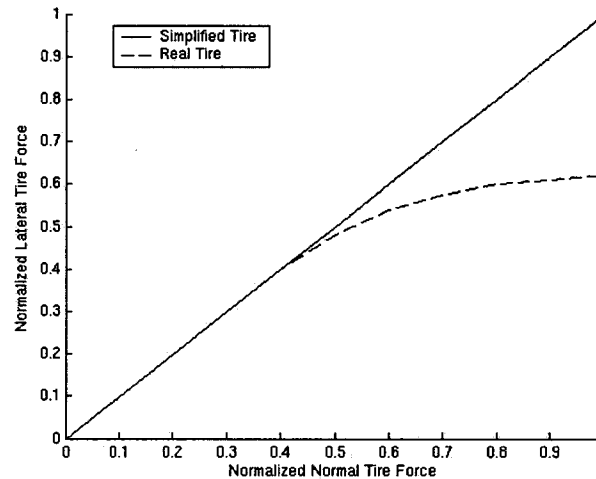
*Figure 1.2: A typical relationship between the
tire lateral force and vertical force*

For ride manoeuvres, softer springs lead to greater wheel movement which will increase the fluctuation in tire force. This is confirmed in Figure 1.3, which shows the frequency response of the tire force. For road input frequencies near the unsprung mass resonant frequency, a softer suspension leads to greater tire force fluctuation, which decreases the longitudinal grip of the vehicle.

- 4 -
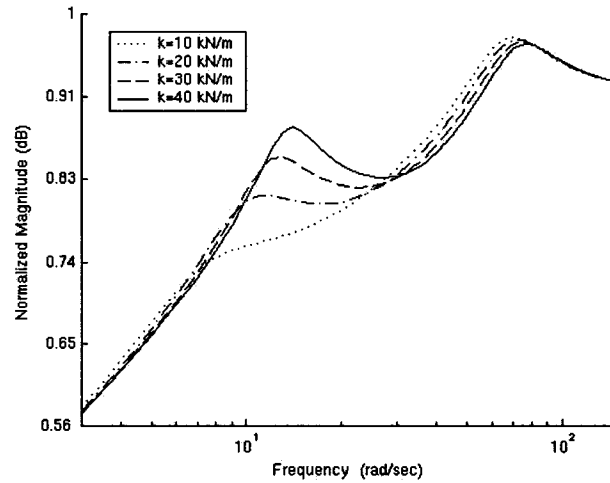
*Figure 1.3: Tire force response versus road input frequency
for various strut spring rates*

1.1.3 Damper Conflict

The ideal damping coefficient depends on the natural frequencies of the system and the road input frequency and so it continuously changes as the vehicle operates. In looking at the frequency response of the body acceleration in Figure 1.4 for different damping rates, for input frequencies around the natural frequencies high damping is best, yet at all other frequencies low damping is preferred. A similar pattern emerges for the tire force frequency response in Figure 1.5, high damping is ideal near the body and wheel natural frequencies with low damping ideal everywhere else in minimizing tire deflection.
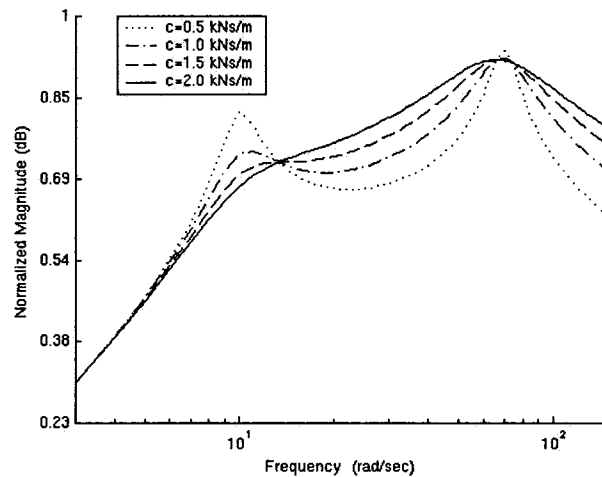
*Figure 1.4: Sprung mass acceleration response versus
road input frequency for various damping rates*

- 5 -
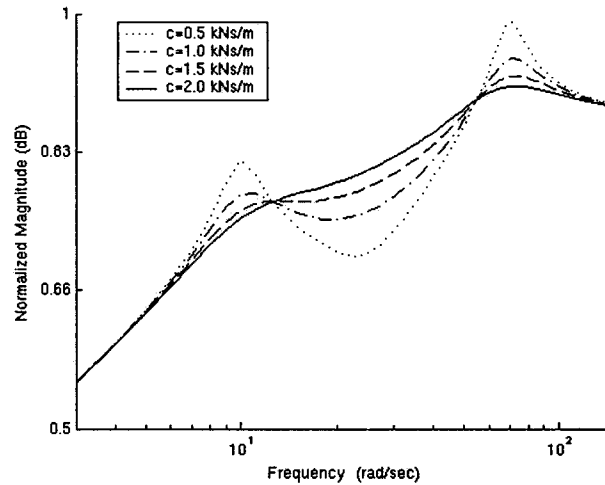
*Figure 1.5: Tire force response versus
road input frequency for various damping rates*

1.2 The Active Solution

A way of addressing the above conflicts is a suspension with a variable stiffness that changes according to measured parameters such as body movement, spring displacement, steering angle, etc. Using feedback from sensors, an electronic control unit (E.C.U.) finds the optimal action that produces the best combination of ride and handling. An active element within the suspension then generates the action that the E.C.U. deems optimal.

1.2.1 Fully-Active Suspension

A fully-active system typically makes use of hydraulic power. A pump, driven by a belt from the engine supplies a source of oil. As the vehicle operates, sensors throughout the vehicle send data to the E.C.U., which determines the optimal suspension force. The controller then sends a current/voltage to the power valve which regulates the flow rate of oil to enter/exit the actuators. In the final phase, the double acting piston actuators convert the pressure difference between their upper and lower chambers into a net force on the suspension. Other elements are required such as accumulators, relief valves, throttle valves, etc.

Fully-active suspension differs from passive and semi-active suspension in its ability to inject energy into the vehicle. Only a high-bandwidth active system will be considered for this project; it is defined by having the capability of controlling road frequency inputs as high as 25Hz. This system typically uses a spring to carry the static weight of the vehicle along with a double acting hydraulic actuator placed parallel to it. Since it controls both sprung and unsprung mass resonance motion, the requirements and demands of the system components are relatively high. Peak power requirements in the range of 4 to 10kW have been quoted in the past, corresponding to an increase of 10-20% in fuel consumption, with the system hardware adding anywhere from 49 to 136kg.

1.2.2 Semi-Active Suspension

A semi-active suspension varies the rate of energy dissipation based on a closed loop feedback of sensor data. This is accomplished through an active damper that varies the damping coefficient and is used

- 6 -

in parallel with a conventional spring. The system is relatively simple, affordable, and quick (response times of 30 to 150ms) with the promise of increased ride performance. As a result, it is seeing an increased presence in production cars.

Three commonly used methods to alter the damping coefficient are: on-off, continuously variable and rheological fluid damping. The first method switches between discrete states of damping resistance through the use of motor/solenoid driven internal valves that switch between different orifice areas. Continuous damping is similar to the first method except that it now has the ability to continuously vary the orifice area between a maximum and minimum value. In the last method no moving parts are used to vary the damping coefficient, instead the viscosity of the damper fluid is altered in response to the intensity of an applied energy field.

1.2.3 System Problems

To this day few fully-active suspension vehicles have made it to production. The main reasons include, but are not limited to, the increased power consumption and response time of the suspension, the reliability and serviceability of the hydraulic system, increased cost, added weight and achieving system robustness.

Also, over the years designers have become very good at dealing with the ride/handling trade-off and extracting performance from the passive suspension. Designs used to increase passive performance include:

- nonlinear spring, damper and bushing stiffness
- stiffer body structures to maintain a more accurate suspension geometry
- low profile tires with high lateral stiffness
- anti-roll bars and anti-dive suspension geometry to resist roll and pitch
- lighter unsprung components
- more complicated suspension geometry

As a result consumer demand for a better suspension has to this day not been strong, contributing to the reluctance of implementing active systems.

1.3 Software Interfacing

Most engineering systems are multi-domain, where the distinct sub-systems are difficult to simulate in a single software program, requiring many simplifications and inaccuracies. In a fully-active suspension three distinct domains exist: the vehicle, the E.C.U. and the hydraulic system. To properly model all three domains and capture how they interact with the rest of the system, software interfacing techniques are suggested.

In short, different software programs are connected to one another to solve different aspects of the same problem. This interfacing allows each sub-system to be modeled in its natural software domain which more accurately captures the dynamics of the sub-systems. With the tools used in this study, the user has the option of either having the solver of each software integrate its own model (known as discrete

mode/cosimulation) or letting the integrator from the control software solve the entire system (known as continuous mode).

Although the above methods solve nonlinear multibody systems, a linearized version may be exported to the controller software. Linear models, although not as accurate, gives the user access to tools such as frequency response plots and allow eigen analysis to be performed. These linearized versions are also sometimes necessary for designing controllers.

Software interfacing is relatively new and unused for active suspension simulation (at least in academia) but should gain in popularity as software developers refine the interfacing capabilities of their products.

1.4 Objectives

The objective of this research is to determine the feasibility of synthesizing procedures to simulate active suspensions by interfacing different software programs. Attention is focused on the ride response of the vehicle and so this research does not evaluate the handling behaviour of active suspension. It should also be emphasized that focus is not on trying to design a road-worthy control algorithm with an ultra detailed vehicle model, but rather on performing a preliminary evaluation on the usefulness of the simulation techniques developed.

More specifically to:
- Implement a quarter and a full car model of a generic lumped mass passenger vehicle and of the Bombardier Iltis utility truck.
- Model the vehicle in ADAMS, the E.C.U. in Matlab/Simulink.
- Use algorithms related to skyhook damping for the semi-active suspension.
- Use linear optimal control techniques (LQR controller) to design the fully-active controller.
- Implement a Kalman filter to estimate the system states for the LQR.
- Add suspension bushings to the full vehicle Iltis model for increased realism.

And to compare:
- The differences of the various procedures developed and the available solver modes.
- Explore the differences of using linear and nonlinear models of the vehicle.
- The different vehicle models.
- Compare passive, semi-active and fully-active suspension.

All research is conducted at the DaimlerChrysler Automotive Research and Development Centre in Windsor, Ontario.

2 LITERATURE REVIEW

2.0 Active Suspension Application

2.0.1 Active Anti-Roll Bar

Anti-roll bars are laterally placed tubes that link the left and right suspension together through drop links to the suspension control arms (Figure 2.0). When both wheels move up the same amount, the roll bar rotates about its lateral axis and exerts negligible force on the wheels. However when the vehicle rolls, the left and right control arms rotate relative to one another and as a result the roll bar twists and exerts an opposing force to reduce body roll.
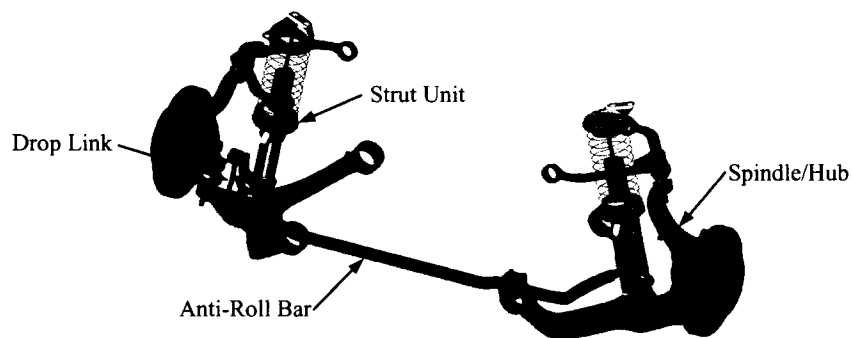
Figure 2.0: Configuration of a typical front suspension

Active anti-roll bars have entered production vehicles with the ability to vary its torsional stiffness. In BMW's Dynamic Drive system, the active anti-roll bar consists of two halves that are connected through a hydraulically operated swivel motor. The motor, through transforming hydraulic pressure into a stabilizing counter-torque resistance, varies the stiffness of the roll bar according to the lateral acceleration of the vehicle. When the acceleration is negligible, the system depressurizes so as to not influence the roll dynamics. In this way the understeer and oversteer characteristics of the vehicle can be modified in response to the lateral acceleration of the body by varying the front and rear roll resistance. BMW claims that for lateral accelerations from up to 0.3g, no roll occurs and for an acceleration of 0.6g an 80% reduction is achieved.

TRW's system named Active Roll Control (ARC) varies the stiffness of the roll bar by replacing one anti-roll bar drop link with a computer controlled linear actuator that uses hydraulic pressure to apply a

resisting force. The actuator is driven by the power steering pump and is controlled by a servo-valve in response to sensor outputs. Lateral accelerometers, a steering angle sensor and other sensors determine the roll force and directs a control valve to apply a counterbalancing force to the sway bar. TRW claims that the system eliminates body lean up to 0.4g of lateral acceleration, which translates into moderately hard cornering. Above this level the system allows some body roll to warn the driver of an impending loss of tire traction.

2.0.2 Variable Geometry Suspension

With this system the geometry of the suspension is altered to vary the suspension stiffness in response to vehicle motion. Past research is sparse compared to active suspension systems and the concept is relatively new. The 1965 Velocette Thruxton motorcycle is one of the earliest production examples; it allows the driver to manually adjust the top mount location of the spring. Experimental cars that automatically vary the strut or leaf spring mount locations have also been built with success. A main focus in their design is having the actuator apply forces perpendicular to the main suspension forces, minimizing the energy needed to change the mount position.

In another design, Minaker {15} moved the body attachment points of the lower control arms through hydraulic or electric actuators. In this manner the location of the vehicle roll center relative to the vehicle center of gravity is controlled and changes the handling characteristics of the vehicle. Under closed loop control the system consumed a peak power consumption of under 100W with a reduction in roll and heave during cornering manoeuvres. Overall the concept showed potential for future application.

2.0.3 Rheological Semi-Active Damper

A rheological fluid exhibits a change in flow when an energy field is applied to it since the particles, that are randomly dispersed, group together to follow the path of the applied field. As the fluid flows the particle bonds are broken only to be reformed to follow this energy field while absorbing energy in the process. Since the tendency to bond varies with the strength of the field, the level of energy dissipation is controllable. These fluids are used within dampers to continuously vary their viscosity according to a control input signal that in certain designs change according to the road input frequency. Additional information on this topic may be found in {37}.

2.0.4 Active Body Control

Currently used in Mercedes road cars, the Active Body Control (ABC) system is a fully-active hydraulic suspension system that relies on thirteen vehicle sensors. As Merker et al. {34} explains, at each corner of the vehicle a hydraulic actuator is connected in series with the top of the strut spring. By extending/retracting the cylinder the spring preload changes and varies the suspension stiffness. Since the system is low-bandwidth, meaning it's only effective for frequencies just greater than the sprung mass vibration mode, it requires little energy compared to a high-bandwidth system. ABC uses a system pressure of 20MPa and weighs an additional 42kg.

2.0.5 Lotus Active Suspension

In 1980 a joint venture formed between Cranfield Institute of Technology and Lotus Engineering to develop high-bandwidth hydraulic active suspensions for the Lotus Esprit and the Lotus Formula One race cars. The purpose was to address the high aerodynamic loading on ground effect racing cars (up to 3 times its static weight) by minimizing the weight transfer on the tires. The system was first fitted to the Esprit with the E.C.U. aimed at controlling the hydraulic pressure and the car attitude with the capability of altering the damping, the body attitude and its rate of change. Additionally, the roll stiffness distribution was adjustable and the modes of vibration could be separated/decoupled.

Road induced dynamic loads transmitted through the tires were around half those of a passive system and an improvement in handling in the order of 10-20% was claimed. The road version of the system was driver controllable, allowing the passengers to completely eliminate body motion during bumps and transient manoeuvres. The system pressure was in the neighbourhood of 17.2MPa with a response time of approximately 3ms at a cost of 4-7kW and 20-45kg in mass. In spite of the increased weight the F1 car was noticeably quicker than its passive version since cornering speeds increased by 10%. More information on the program is available from {45}, {49} and {50}.

2.0.6 Citroen Hydraulic Suspension

A pioneer in active suspension, Citroen has a long history of offering hydraulic suspension. As summarized by Merker et al. {34} its current 'hydractive' system uses six accumulators: one at each corner, one between the front wheels and one between the rear wheels. Conventional springs and dampers are therefore not needed as their function is replaced by the accumulators. Suspension stiffness is varied by switching the central accumulators in and out of the hydraulic circuit which changes the total volume of fluid and gas in the system (less gas-more stiff). In addition all four suspensions are interconnected by the high pressure fluid that further smoothes the ride. Another important characteristic of the system is that the hydraulics has a variable effect - it becomes harder as the loads are increased.

2.0.7 Iltis Active Suspension

Commissioned by the Defence Research Establishment Suffield (DRES) in the late eighties, a fully-active hydraulic suspension system was fitted to the Bombardier Iltis utility jeep by researchers from Queen's University. The system used hydraulic servo-actuators with a hydraulic system pressure of 20.6MPa and an 80386DX-20MHz IBM-PC compatible microcomputer for the E.C.U. Tests indicated that simultaneous improvements in ride and handling were achieved.

Another feature of the truck was its preview system. Using electronic ultrasonic sensors, the road profile at the front bumper was measured and the information sent to the main controller. The strategy was to have the active system anticipate and act *as* the vehicle encountered road irregularities, rather than having the suspension react after the disturbances occurred. It has the added advantage of reducing the overall energy consumption. For more information refer to {33} and {44}.

2.1 Virtual Active Research

Unless stated, the following studies ignore the dynamics of the hydraulics, assuming that the desired force calculated from the controller is the force applied to the suspension with no time delay.

2.1.1 Linear Quadratic Regulator (LQR)

Thompson {43} generated a two degree of freedom lumped mass quarter car model. The LQR weighting function consisted of the mass velocities and the tire and suspension dynamic deflections. Results to a unit step input indicated a reduction in body overshoot at the cost of the unsprung mass motion. In comparing the eigenvalues, the LQR system increased the sprung mass damping and decreased the unsprung mass damping, this explained why the body settled more quickly. The author concluded that the active suspension was better in practically all respects predicting that further refinement of the controller weighting matrices and the addition of dynamic vibration absorbers would improve the unsprung mass oscillations.

As a bridge between chassis models that can perform nonlinear handling manoeuvres and control design studies, Haycock {30} looked at a two degree of freedom quarter car model which incorporated the geometry of a short long arm suspension. The author conducted a ride study with a ramp road input by implementing a full state feedback LQR controller and compared it to a passive suspension. Although encouraged by the ride response, it was noticed that depending on the weights used, the solution still contained an inherent compromise of vehicle response. This led the author to suggest a frequency dependent compensation controller be used since the required response depends on the changing conditions and road disturbances.

Aimed at analyzing the effects of changing suspension parameters, road disturbance and seat position, an eight degree of freedom lumped mass full car ride model was created by Bouazara et al. {25}. A fully-active system was implemented using the LQR algorithm and compared with a semi-active and passive suspension. Here the weight function included the body accelerations, the suspension deflection and wheel velocity and was weighted most heavily towards the suspension displacement. The wheel and sprung mass velocities were hardly weighted. As the authors state, the final weighting values were chosen for a good trade-off between comfort and road holding capability. The fully-active suspension was able to most of the time give a slightly superior response in both sprung and unsprung mass motion for a double bump road input (note: the LQR gain used was not aggressive). In addition the semi-active vehicle response rivalled that of the fully-active system giving a slightly worse performance.

Hrovat {31} reviewed the application of LQR applied to various vehicle models. It is claimed that for this controller, either ride or handling can be improved by choosing the weighting matrices accordingly. He states that the full advantage of active suspensions stems from adaptive tuning/gain scheduling of the controller parameters depending on the driving conditions. A situation is suggested where if the steering and wheel position and lateral acceleration sensors indicate straight line operation of the vehicle, then the wheel motion weighting can be relaxed.

As for nonlinear control, Hrovat {31} stated that for many operations a linear control system is appropriate as suggested by past empirical validations. The shortcomings of such a controller are seen during situations which amplify discrete disturbances such as when the suspension bottoms out due to potholes or speed bumps. He supports an algorithm in which a linear controller is used for normal operation and switches to a nonlinear scheme for discrete event disturbances.

2.1.2 Linear Quadratic Gaussian Regulator (LQG)

Sharma et al. {39} addressed the requirements of full-state feedback for using an LQR algorithm with a quarter car model. They suggested incorporating a Kalman filter to estimate the immeasurable states and compared the model to one without the filter. Available measurements were assumed to consist of suspension deflection and body acceleration which were used as inputs to the Kalman filter. Although a slight degradation was noted with the Kalman filter, the authors were pleased with the results. Also encouraging was when the vehicle traversed a road of different roughness and speed than the one used to tune the controller. Performance was virtually maintained, leading the authors to state that there was no need to implement an adaptive time varying estimator.

Taghirad et al. {42} taking passenger acceleration as an indication of ride comfort used a half-car model that incorporated the seat dynamics with an LQG algorithm. Despite a random road profile, the state estimates followed the true states quite closely, while assuming a typical sensor arrangement that measured suspension travel and passenger bounce. In addition the authors found that their model decreased body acceleration while producing tire forces on par with the passive system.

2.1.3 Semi-Active Control

In the now classic paper {26} by Karnopp et al., skyhook and semi-active damping was proposed to increase the ride of a vehicle suspension. The ideal skyhook damper scheme was synthesized for a one degree of freedom model by connecting a damper from the mass to an inertial reference so that the damping was proportional to the mass absolute velocity. While the conventional damper reduces the relative velocity between the sprung and unsprung mass, effectively stiffening the suspension when a soft suspension is desired, the skyhook damper reduces the absolute body motion.

Karnopp et al. {26} theorized that a practical active system that approximated the unrealistic skyhook damper configuration would perform better than a passive suspension. They went on to devise such a system that switched between high and zero damping force for an active strut element whose power was restricted to being dissipative. Through simulation it was shown that this semi-active system had a performance intermediate to the passive and ideal skyhook damper, yet required less power and complexity than a fully-active system.

A shortcoming of the work by the previous study was that with a skyhook damper, the unsprung mass was not damped, leading to a degradation of tire forces. Valasek et al. {46} addressed this issue with a quarter car model by adding a damper that connected the unsprung mass with the ground, known as a ground-hook damper. Although conceived to minimize road damage from trucks, the authors concluded

that the extended system decreased the tire-road dynamic loading and increased body comfort throughout the entire range of exciting frequencies.

Oueslati et al. {35} compared different semi-active control systems with passive and fully-active systems for a four degree of freedom half car model. Among the controllers implemented were the fully-active LQR controller and the switch algorithm created by Karnopp et al. {26}. Relative to the passive system, the LQR system increased ride and the tire dynamic force and suspension displacement for high input frequencies. The semi-active system was not as effective as the fully-active algorithm in reducing body acceleration while increasing suspension displacement and tire force relative to the passive suspension. Of the semi-active control algorithms considered, that devised in {26} demonstrated the best performance.

2.1.4 Software Interfacing

Villec {47} investigated the merits of using cosimulation to explore how control systems affected vehicle behaviour during handling manoeuvres. ADAMS/Car modeled the vehicle and Xmath the E.C.U. and hydraulic system; they were linked in an attempt to simulate an attitude control system. ADAMS used inputs of steering wheel and vehicle speed from real track data. After responding to the inputs, the vehicle lateral acceleration and actuator velocity from ADAMS were passed to Xmath as input to the control algorithm. The controller then determined actuator forces which were returned to ADAMS.

To better evaluate the performance of cosimulation an additional ADAMS model was constructed that included the vehicle, the E.C.U. and the hydraulics. At the same time, data collected from track testing was compared with these virtual models. All three results showed reasonable correlation with the cosimulation solver times within the range of the 'ADAMS only' solve times. The results led the author to conclude that cosimulation provides an effective method of analyzing control systems integrated within vehicle systems.

To analyze the movements of a boom lift of an aerial work platform Jansson et al. {32} used a multi-domain approach of combining ADAMS/View with AMESim. Three models were constructed: i) a multibody ADAMS model with no hydraulics, ii) an AMESim hydraulics model with a simplified boom lift model, iii) a detailed ADAMS model of the boom with a detailed hydraulics model in AMESim. The latter model was formed by linking AMESim with ADAMS and using the ADAMS solver to perform the numerical integration. The results from this last model were significantly different from the first two models, most notably the forces involved with the boom were quite dissimilar and the system was initially badly tuned. It was concluded that interfacing software packages will become necessary in future efforts to simulate multi-domain systems.

ADAMS/Car was linked with Simulink in developing a simulation of a suspension system using semi-active dampers in an Alfa Romeo car. Danesin et al. {27} used nonlinear controls to perform a cosimulation of handling manoeuvres such as lane changes. The vehicle was modeled in ADAMS/Car and the controller in Simulink. The nonlinear controller was designed to optimize the vehicle dynamics subject to a predefined set of manoeuvres such as standard lane changes. The authors found this tool useful in

- 14 -

integrating different chassis control systems while predicting interaction problems with the vehicle and the controller.

Feng et al. {28} used cosimulation to model an off road vehicle with a hydro-pneumatic suspension with the aim to minimize the sprung mass vertical and pitch acceleration. The vehicle was modeled in ADAMS/View as a twelve degree of freedom full car and the suspension and controller were created in Simulink. Since the hydro-pneumatic suspension was difficult to model, empirical models were implemented from previous experimental test data. The software interface exchanged the suspension vertical displacements, velocities and accelerations and the cabin pitch and vertical velocity from ADAMS to Simulink with the actuator forces passed the other way. Without having to simplify the vehicle, the authors obtained positive results showing an increase in ride quality versus the passive vehicle.

3 THEORETICAL PRINCIPLES

3.0 Global Coordinate System

For this study the axis system adopted is shown below. The forward longitudinal axis is along the x-axis, the vertical axis is along the z-axis and the lateral axis is along the y-axis. Roll rotation (φ) is the rotation of the vehicle about the x-axis; pitch rotation (θ) is about the y-axis and yaw rotation (β) about the z-axis.
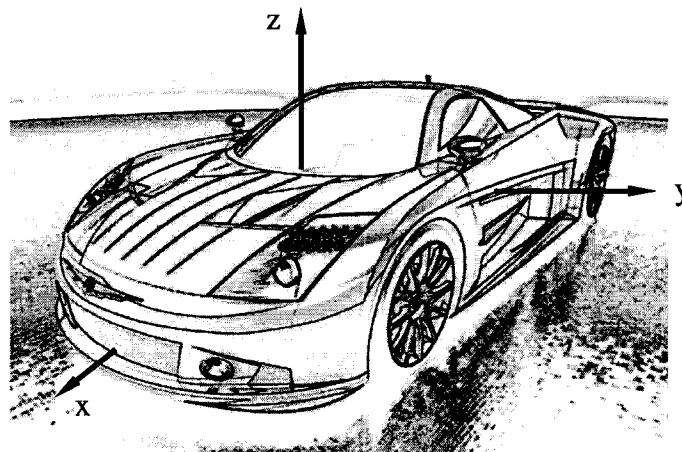
Figure 3.0: The global coordinate system adopted for all vehicle models

3.1 ADAMS

3.1.1 Multibody Dynamics

Multibody dynamics arise in everyday systems where multiple bodies are interconnected with one another through joints. These joints govern and constrain how the system behaves. As Sharp {40} mentions, multibody dynamic problems arise naturally in biomechanics, machine dynamics, robots, vehicles and spacecraft. He goes on to say that since the advent of computers and well developed numerical methods it is now possible to solve such computationally intensive problems.

An industry standard in solving general multibody systems, ADAMS solves the equations of motion through numerical integration. Integration takes the following form, replacing a first order time derivative with a linear combination of future and past values of the unknown solution vector.

$$\dot{Y}(t^i) \xrightarrow{\text{(integration)}} Y(t^i + \Delta t) \tag{3.0}$$

- 16 -

ADAMS adopts an approach which has been found to be the simplest way in generating the governing equations. It describes the motion of each body in a fixed Cartesian space, as if each body were isolated from the other bodies in the system, and separately considers the constraint equations. In this manner the equations of motion are in a standard and repetitive form. The dynamic equations of the bodies are a set of nonlinear ordinary differential equations (ODE) derived from the Newton-Euler equations and the constraint equations are algebraic equations. Combined together the system is described by a set of differential algebraic equations (DAE). The unknown variables consist of displacements, velocities, angular momenta of the bodies and constraint forces.

In ADAMS the DAE are solved by first reducing the second order dynamic equations to first order form, increasing the number of equations and forming a set that is said to be 'maximal', since its size is more than need be. These equations are now a set of nonlinear algebraic sparse equations that leads to considerable redundancy when solving. Although time is wasted in solving for variables of no interest to the analyst, the form of the equations are relatively simple to solve. As Nikravesh {17} mentions, ADAMS treats the algebraic constraint equations as a form of differential equations where the time derivative of the variables do not appear.

Solving these DAE causes the system to become 'stiff' (in which the corresponding linear system has eigenvalues of widely differing magnitudes) by introducing high frequency components. These artificially high frequency components result from numerical rather than physical sources, and so stiff integrator schemes must be used with relatively small time steps (because of the fast varying modes). However small time steps can cause solver instabilities as explained in section 3.1.2.1. Another reason why stiff integrators are used is because any nonlinear system has eigenvalues that vary unpredictably from step to step and so all nonlinear systems are in danger of being stiff.

The following sections summarize the structure of ADAMS as outlined by Harris et al. {29}.

3.1.1.1 Generalized Coordinates

The location of the center of each body is:

$$\mathbf{p}=[x \; y \; z]^{\mathrm{T}} \tag{3.1}$$

while the orientation of the rigid bodies is defined using Euler angles that correspond to the 3-1-3 rotational sequence with respect to the global reference frame. They are stored as an array in the following form:

$$\varepsilon=[\psi \; \theta \; \phi]^{\mathrm{T}} \tag{3.2}$$

These coordinates combine to form a set of generalized coordinates that uniquely define the position of the mechanical system:

$$\mathbf{q}_i=[\mathbf{p}_i \; \varepsilon_i]^{\mathrm{T}} \tag{3.3}$$

The body translational and angular velocity defined in the local coordinate system become:

$$\mathbf{u} = \dot{\mathbf{p}} \tag{3.4}$$

$$\bar{\omega}=\mathbf{T}\dot{\varepsilon}=\mathbf{T}\zeta \tag{3.5}$$

- 17 -

Where:

$$T=\begin{bmatrix} \sin\phi\sin\theta & 0 & \cos\phi \\ \cos\phi\sin\theta & 0 & -\sin\phi \\ \cos\theta & 1 & 0 \end{bmatrix}$$ (3.6)

Considering a system of nb bodies, there will be $6nb$ coordinates describing the position and orientation of each body. These coordinates populate the following array.

$$\mathbf{q}=\begin{bmatrix} \mathbf{q}_1^T & \mathbf{q}_2^T & \cdots & \mathbf{q}_{nb}^T \end{bmatrix}^T = \begin{bmatrix} q_1 & q_2 & \cdots & q_{nb} \end{bmatrix}^T$$ (3.7)

3.1.1.2 Joints

Depending on the topology of the system, joint constraint equations act upon certain coordinates; they take the mathematical form:

$$\Phi(\mathbf{q})=0$$ (3.8)

The exact relation depends strictly on the type of joint defined, with each degree of freedom removed represented by one equation. For example, a translational joint allows for one direction of translational movement between two bodies, removing five degrees of freedom. In this case the joint is described with five constraint equations. The joint collectively forms the following:

$$\Phi(\mathbf{q})=\begin{bmatrix} \Phi_1^T(\mathbf{q}) & \Phi_2^T(\mathbf{q}) & \cdots & \Phi_{nj}^T(\mathbf{q}) \end{bmatrix}^T = \begin{bmatrix} \Phi_1(\mathbf{q}) & \Phi_2(\mathbf{q}) & \cdots & \Phi_m(\mathbf{q}) \end{bmatrix}^T$$ (3.9)

Here nj is the number of joints in the system and m is the sum of the joint constraint equations. Usually the number of generalized coordinates is larger than the number of constraints they satisfy. For the system to correctly move, the generalized coordinates of the system must satisfy the constraint equations along with its velocity and acceleration relations.

3.1.1.3 Motion

Represented as a time dependant constraint equation, the motion of the generalized coordinate becomes a function of time and adopts the form:

$$\Phi(\mathbf{q}, t)=0$$ (3.10)

The generalized coordinates must also satisfy the first and second time derivative of this equation to ensure that the intended motion is produced.

3.1.1.4 Dynamic Equations of Motion

Assume the equations of motion are presented in Lagrangian form:

$$\frac{d}{dt}\left[\left(\frac{\partial K}{\partial \dot{\mathbf{q}}}\right)^T\right] - \left(\frac{\partial K}{\partial \mathbf{q}}\right)^T - \mathbf{Q}=0$$ (3.11)

This can be reformulated with the introduction of Lagrange multipliers as:

$$\frac{d}{dt}\left[\left(\frac{\partial K}{\partial \dot{\mathbf{q}}}\right)^T\right] - \left(\frac{\partial K}{\partial \mathbf{q}}\right)^T + \left(\frac{\partial \Phi}{\partial \mathbf{q}}\right)^T \lambda - \mathbf{Q}=0$$ (3.12)

- 18 -

Where generalized momentum is defined as $\mathbf{P} = \dfrac{\partial K}{\partial \dot{\mathbf{q}}}$ (3.13)

In considering the prior definition of $\mathbf{q}$, the above equation is rewritten for a rigid body as:

$$\frac{d}{dt}\begin{bmatrix} \left(\frac{\partial K}{\partial \mathbf{u}}\right)^{\mathrm{T}} \\ \left(\frac{\partial K}{\partial \zeta}\right)^{\mathrm{T}} \end{bmatrix} - \begin{bmatrix} \left(\frac{\partial K}{\partial \mathbf{p}}\right)^{\mathrm{T}} \\ \left(\frac{\partial K}{\partial \varepsilon}\right)^{\mathrm{T}} \end{bmatrix} + \begin{bmatrix} \Phi_{\mathbf{p}}^{\mathrm{T}}\lambda \\ \Phi_{\varepsilon}^{\mathrm{T}}\lambda \end{bmatrix} - \begin{bmatrix} (\Pi^{r})^{\mathrm{T}}\mathbf{f} \\ (\Pi^{R})^{\mathrm{T}}\bar{\mathbf{n}} \end{bmatrix} = \mathbf{0}$$ (3.14)

Where:

$$\Pi^{P} = \frac{\partial \mathbf{v}^{P}}{\partial \mathbf{u}}$$ (3.15)

$$\Pi^{R} = \frac{\partial \bar{\omega}}{\partial \zeta}$$ (3.16)

These equations of motion (EOM) may be obtained by stacking together the EOM for the bodies in the multibody system. Notice that:

$$\frac{d}{dt}\left(\frac{\partial K}{\partial \mathbf{u}}\right)^{\mathrm{T}} = \mathbf{M}\dot{\mathbf{u}}$$ (3.17)

$$\left(\frac{\partial K}{\partial \mathbf{p}}\right)^{\mathrm{T}} = \mathbf{0}$$ (3.18)

With Γ defined as angular momenta $\Gamma \equiv \dfrac{\partial K}{\partial \zeta} = \mathbf{T}^{\mathrm{T}}\bar{\mathbf{J}}\mathbf{T}\zeta$

The equations of motion may now be rewritten as:

$$\mathbf{M}\dot{\mathbf{u}} + \Phi_{\mathbf{p}}^{\mathrm{T}}\lambda = (\Pi^{r})^{\mathrm{T}}\mathbf{f}$$ (3.19)

$$\dot{\Gamma} - \frac{\partial K}{\partial \varepsilon} + \Phi_{\varepsilon}^{\mathrm{T}}\lambda = \left(\Pi^{R}\right)^{\mathrm{T}}\bar{\mathbf{n}}$$ (3.20)

As Harris et al. {29} notes, these first order differential equations relate how external forces influence the time variation of the translational and angular momenta. In combining the kinetic and kinematic differential equations a set of 15 partial differential equations form to describe each body. The set is comprised of: six 1st order motion equations, six 1st order equations that define the velocity states and three 1st order angular momenta equations. The combined system takes the form:

$$\mathbf{M}\dot{\mathbf{u}} + \Phi_{\mathbf{p}}^{\mathrm{T}}\lambda - (\Pi^{r})^{\mathrm{T}}\mathbf{f} = \mathbf{0}$$

$$\Gamma - \mathbf{T}^{\mathrm{T}}\bar{\mathbf{J}}\mathbf{T}\zeta = \mathbf{0}$$

$$\dot{\Gamma} - \frac{\partial K}{\partial \varepsilon} + \Phi_{\varepsilon}^{\mathrm{T}}\lambda - \left(\Pi^{R}\right)^{\mathrm{T}}\bar{\mathbf{n}} = \mathbf{0}$$ (3.21)

$$\dot{\mathbf{p}} - \mathbf{u} = \mathbf{0}$$

$$\dot{\varepsilon} - \zeta = \mathbf{0}$$

To solve the entire system requires solving a total $15nb + m$ DAE.

3.1.2 Solver Techniques

Let the above set of DAE be written as:

$$g(\ddot{q},\dot{q},q,\lambda,Q,t)=0 \qquad (3.22)$$

To use a standard numerical integration method the equations are converted to a set of 1st order equations by introducing velocity as a solution variable, this produces:

$$g(\dot{Y},Y,Q,t)=0 \qquad (3.23)$$

Where:

$$Y=[q,\dot{q},\lambda]^{T} \qquad (3.24)$$

Notice: Numerical integration of equation 3.23 yields the solution vector Y.

3.1.2.1 ADAMS Solver

ADAMS offers a multitude of solvers, each having particular advantages. For this project the default 'stiff' solver Gear Stiff (GSTIFF) is employed for its relative robustness. GSTIFF finds the system states by approximating the solution with polynomials. These functions pass through the previous solution values to satisfy the equations of motion at every time step. Since the velocity and acceleration kinematic constraint equations are only periodically enforced they may have errors associated with them. All stiff integrators used are based on the Backward-Difference Formula and occur in two phases: a prediction and a correction phase.

Prediction Phase

The prediction of Y^{n+1} is based on the previous values of Y and its derivatives; it fits a polynomial through past values and then extrapolates to the current time. The form taken is:

$$Y^{n+1}=-h\beta_{0}\left(\frac{dY}{dt}\right)^{n+1}+\sum_{j=1}^{k}\left(\alpha_{j}Y^{n-j+1}+h\beta_{j}\left(\frac{dY}{dt}\right)^{n-j+1}\right) \qquad (3.25)$$

This step assumes that past values are sufficient indicators of the current values, however these predicted values do not necessarily satisfy the equations of motion and so a corrector algorithm is used.

Correction Phase

In the next step the residual of the governing equations from using the predicted values is reduced by repeated use of the corrector formulation until a convergence criterion is met. The integrator estimates the solution error and compares it against a specified level at which point the integrator either rejects the solution and takes a smaller time step or moves to the next time step. This process continues until the end solution time is reached. The corrector formula is:

$$\left\{\frac{\partial g}{\partial Y}-\left(\frac{1}{h\beta_{o}}\right)\frac{\partial g}{\partial \dot{Y}}\right\}\Delta Y=-g=0 \qquad (3.26)$$

and may be rewritten as:

$$J\Delta Y=-g \qquad (3.27)$$

This equation relates the derivative of the states with the states themselves and transforms the nonlinear differential equations of the system to nonlinear algebraic difference equations. The equation is solved with a modified Newton-Raphson algorithm to obtain the state variables; it has the disadvantage of diverging from the solution if the initial guess is poor.

The Jacobian matrix (J) represents the partial differentials of each equation of motion with respect to each state variable in the system. ADAMS needs to invert this matrix, using indirect methods, to find the state corrector. To make these indirect methods more efficient, the rows and columns of the Jacobian are constantly rearranged during the simulation. This process can cause instability since terms consisting of the inverse of the step size exist within the matrix. Hence the Jacobian becomes ill conditioned and singular as the step size approaches zero.

3.1.2.2 Alternative Strategy

An alternative to solving this mixed set of DAE is to convert it to a set of ODE and solve it using relatively simple non-stiff Runge-Kutta integrators[†]. A process called coordinate partitioning is used, it involves using the constraint equations to express coordinates considered as dependent on the remainder considered as independent. Due to equation complexity this is performed at every time step and involves intensive matrix inverting. One may rewrite the equations of motion and the constraint equations as:

$$M(q)\ddot{q} + \Phi_q^T \lambda = Q(q,\dot{q}) \tag{3.28}$$

$$\Phi(q) = 0 \tag{3.29}$$

by differentiating the constraint equation twice, the acceleration constraint equation is:

$$\ddot{\Phi}(q) = \Phi_q \ddot{q} + \dot{\Phi}_q \dot{q} + \dot{\Phi}_t = 0 \tag{3.30}$$

This is appended to the dynamic equation of motion and so the equations to solve become:

$$\begin{bmatrix} M(q) & \Phi_q^T \\ \Phi_q & 0 \end{bmatrix} \begin{Bmatrix} \ddot{q} \\ \lambda \end{Bmatrix} = \begin{Bmatrix} Q(q,\dot{q}) \\ -\dot{\Phi}_q \dot{q} - \dot{\Phi}_t \end{Bmatrix} \tag{3.31}$$

Since only acceleration constraints are considered, the body displacement and velocity may accumulate error causing drift; as a result penalty stabilizing algorithms are needed. However, unlike the ADAMS solver, when unable to solve this method will not diverge; instead, it will produce results that are unrealistic.

For stiff integrators, the integration step is limited by the inverse of the highest *active* frequency and for non-stiff integrators the step is limited by the inverse of the highest frequency (active or not). An example of an inactive frequency is one that has an associated overdamped eigenvalue and so although capable of oscillating at high frequency it usually does not due to its high damping. As a result non-stiff integrators are inefficient in dealing with stiff problems while stiff integrators generally sacrifice speed for robustness and efficiency.

[†]*Notice: This is the approach taken by the popular DADS multibody dynamic software program.*

3.1.2.3 Linearization Algorithm

The process used in ADAMS in linearizing the equations of motion is explained by Sohoni et al. {41} and yields a complete set of eigenvalues and eigenvectors. Once rewritten as first-order equations, the system is linearized about a user specified operating point of $Y^* = (Y_o, \dot{Y}_o, Q_o, t_o)$ as:

$$\delta g = A_1 \big|_Y \cdot \delta Y - B_1 \big|_Y \cdot \delta \dot{Y} + \frac{\partial g}{\partial Q} \bigg|_Y \cdot \delta Q + \frac{\partial g}{\partial t} \bigg|_Y \cdot \delta t = 0 \qquad (3.32)$$

Where:

$$A_1 = \frac{\partial g}{\partial Y} \bigg|_{Y^*} \qquad (3.33)$$

$$B_1 = -\frac{\partial g}{\partial \dot{Y}} \bigg|_{Y^*} \qquad (3.34)$$

and $\delta Y, \delta \dot{Y}, \delta Q, \delta t$ are variations about $Y_o, \dot{Y}_o, Q_o, t_o$

It is assumed that g is in a state of equilibrium such that A_1 and B_1 are time invariant and so $\partial g / \partial t = 0$. Furthermore if the linearized equation 3.32 is homogeneous by letting $\delta Q = 0$ then:

$$\delta Y = e^{\sigma t} z$$

and...

$$\delta \dot{Y} = \sigma e^{\sigma t} z$$

Substituting these two equations into 3.32 leads to the generalized eigenvalue problem of:

$$A_1 z = \sigma B_1 z \qquad (3.35)$$

To solve this problem the A_1 and B_1 matrices are first needed. Sohoni et al. {41} notices that the Jacobian matrix, defined in equation 3.27 calculates these matrices for the corrector formula during the numerical integration procedure. He goes on to state that the problem is not well posed since the B_1 matrix is singular and claims the source of the problem is from the fact that no Lagrange multiplier terms appear in g, more specifically some of the eigenvalues are undefined due to the presence of the constraint equations. Sohoni et al. {41} also states that the presence of the algebraic equations creates infinite eigenvalues; these equations may be viewed as elements of infinite stiffness leading to eigenvalues of infinite magnitude.

Element Condensation

To cope with this problem, Sohoni et al. {41} condenses out the elements that result from the algebraic constraint equations. To begin, the constraint equations are rewritten as linear algebraic equations:

$$\delta \Phi = \frac{\partial \Phi}{\partial q} \bigg|_{Y^*} \delta q = 0 \qquad (3.36)$$

From this it is possible to express the dependant components of δq in terms of the remaining independent coordinates. From coordinate partitioning equation 3.36 can be written as:

$$[\Phi_u \quad \Phi_v] \cdot \begin{bmatrix} \delta u \\ \delta v \end{bmatrix} = 0 \qquad (3.37)$$

Now the above equation can be used to write the dependent variables in terms of the independent coordinates as:

$$\delta\mathbf{u} = \left(-\frac{\Phi_v}{\Phi_u}\right)\delta\mathbf{v} \tag{3.38}$$

In partitioned form the original eigenvalue problem is rewritten as:

$$\mathbf{A}_2 \begin{bmatrix} \delta\mathbf{u} \\ \delta\mathbf{v} \\ \delta\dot{\mathbf{u}} \\ \delta\dot{\mathbf{v}} \\ \delta\lambda \end{bmatrix} = \sigma\mathbf{B}_2 \begin{bmatrix} \delta\mathbf{u} \\ \delta\mathbf{v} \\ \delta\dot{\mathbf{u}} \\ \delta\dot{\mathbf{v}} \\ \delta\lambda \end{bmatrix} \tag{3.39}$$

Substituting equations 3.38 into 3.39 yields:

$$\mathbf{A} \begin{bmatrix} \delta\mathbf{v} \\ \delta\dot{\mathbf{v}} \\ \delta\lambda \end{bmatrix} = \sigma\mathbf{B} \begin{bmatrix} \delta\mathbf{v} \\ \delta\dot{\mathbf{v}} \\ \delta\lambda \end{bmatrix} \tag{3.40}$$

Upon further manipulation $\delta\lambda$ can be algebraically eliminated to give a condensed form which cannot be reduced any further. In this form the system matrices are well suited for eigen analysis.

3.2 Control Algorithm

3.2.1 Linear Quadratic Regulator

Optimal control involves finding the best control within the confines of satisfying conflicting requirements. An example is the linear time invariant quadratic regulator; it is derived from a linear plant in the standard state space form:

$$\dot{x}(t) = Ax(t) + B_1 u(t) + B_2 w(t) \tag{3.41}$$

$$y(t) = Cx(t) + Du^*(t) \tag{3.42}$$

$$B = \begin{bmatrix} B_1 & B_2 \end{bmatrix} \tag{3.43}$$

$$u^* = \begin{bmatrix} u & w \end{bmatrix} \tag{3.44}$$

The full state feedback control is:

$$u = -k_{lqr}x \tag{3.45}$$

where k_{lqr} is the optimal LQR gain. The best possible gain is one that minimizes the quadratic cost function comprised of weighting matrices Q and R:

$$J = \int_0^\infty (x^T Qx + u^T Ru)dt \tag{3.46}$$

The gain that satisfies this requirement is:

$$k_{lqr} = R^{-1}B_1^T P \tag{3.47}$$

where the P matrix is unique and found by solving the algebraic matrix Riccati equation:

$$A^T P + PA - PB_1 R^{-1}B_1^T P + Q = 0 \tag{3.48}$$

- 23 -

By substituting equation 3.45 into equation 3.41 one obtains:

$$\dot{x}=Ax-B_1k_{lqr}x+B_2w=(A-B_1k_{lqr})x+B_2w \tag{3.49}$$

$$\text{let } A^{\wp}=A-B_1k_{lqr} \tag{3.50}$$

$A^{\wp}$ is the closed loop system matrix that includes the plant and the controller. Its properties describe the behaviour of the controlled system.

3.2.1.1 Cost Function

The penalty function can be interpreted as follows.

$$\int_0^\infty (u^TRu)dt \tag{3.51}$$

This term is a measure of the amount of control effort and in many cases can be interpreted as the control energy. The function is a least effort measure that minimizes the expended energy; the term u^TRu is always positive because of the definition of R.

$$\int_0^\infty (x^TQx)dt \tag{3.52}$$

This is the integral of the error squared of a tracking system where $x=x_{actual}-x_{desired}$. For this application $x_{desired}$ is zero. Hence the controller tracks a desired state value of zero; this type of controller is called a regulator. From the definition of Q, x^TQx is always positive or zero.

Notice that while the integral in equation 3.46 spans infinity, J is a finite number. This implies that since it is an integral consisting of the states, the state error goes to zero as time goes to infinity, which guarantees the closed loop stability of the system.

The Q and R matrices are numerically defined by the user and determine the relative importance of the input energy and state response. They are weighting matrices which control the system response. For example, selecting a numerically large Q matrix implies that to keep J small the state response must be small. This results in closed loop poles that are further left in the s-plane. Also a numerically large R matrix means that less control effort will be used, this implies that the poles are generally slower and result in a larger state response value.

The weightings can also differ between the control input and the states. For example, by changing the relative numerical values within the Q matrix, certain states are weighted more than others such that the system response can be controlled as desired. For this research the Q and R matrix are chosen as diagonal matrices where each value corresponds to a certain state and control input.

Example.

$$\text{let } Q = \begin{bmatrix} 10 & 0 & 0 \\ 0 & 1 & 0 \\ 0 & 0 & 3 \end{bmatrix} \text{ and } x = \begin{pmatrix} x_1 \\ x_2 \\ x_3 \end{pmatrix}$$

Here 10 corresponds to x_1, 1 to x_2 and 3 to x_3. As a result x_1 is weighted the most and will have the smallest response, followed by x_3 and then x_2. The state variables used for all the models are listed in Appendix A and B.

3.2.1.2 Solution Condition

The requirements for an LQR solution are:

i) (A,B) is stabilizable.

<u>Definition.</u>

If a system is stable or controllable then it is stabilizable.

Hence the system is stabilizable if its uncontrollable states/modes are stable, while its controllable states/modes may be unstable. Thus the pair (A,B) is stabilizable if A^p can be made asymptotically stable (negative real eigenvalues), else J will be infinite.

If controllable, there exists a control that will transfer any initial state to any desired state, allowing any set of eigenvalues to be assigned. This property guarantees that the optimal cost is finite and so can replace the weaker condition of stabilizability.

ii) (A,C) is at least detectable or observable.

This condition ensures the uniqueness of the positive semi-definite solution to the Riccati equation and the stability of the closed loop system. If detectable any unstable modes are observable and its unobservable modes, if any, are stable.

iii) R>0, a positive definite or real symmetric matrix

Q≥0, a positive definite or semi-definite matrix

Note that no constraint is placed on the stability of the original plant; this is because stability is guaranteed regardless of whether the original system is stable when using LQR.

3.2.2 State Observer

If not all state variables are available for measurement by sensors, they may be estimated. First let:

$$\underset{\text{error}}{\tilde{x}} = \underset{\text{actual}}{x} - \underset{\text{estimate}}{\hat{x}} \tag{3.53}$$

and assume the following state estimator form:

$$\dot{\hat{x}} = A\hat{x} + Bu^* + L(y - \hat{y}) \tag{3.54}$$

The last term is a correcting term that reacts to the output error of the state estimator; it takes the form of proportional error feedback. Now differentiate equation 3.53 and substitute accordingly (D matrix is zero):

$$\dot{\tilde{x}} = \dot{x} - \dot{\hat{x}} \tag{3.55}$$

$$\dot{\tilde{x}} = (Ax + Bu^*) - (A\hat{x} + Bu^* + LC(x - \hat{x})) \tag{3.56}$$

$$\dot{\tilde{x}} = (A - LC)\tilde{x} \tag{3.57}$$

- 25 -

Thus the response of the estimation error is determined by the eigenvalues of (A-LC). If (A,C) is stable, the error will converge to zero regardless of the initial values used. It is possible to choose L to attain any desired error dynamics as long as (A,C) is observable.

3.2.2.1 Kalman-Bucy Filter

This filter has been applied to inertial navigation, sensor calibration, radar tracking, manufacturing, economics, signal processing and freeway traffic modeling. It was also implemented in the trajectory estimation and control problem for the Apollo project. Grewal et al. {4} claim that it is one of the greater discoveries in the history of statistical estimation theory and possibly the greatest discovery in the twentieth century.

As an optimal estimator it provides the best estimate of the states for a system perturbed by random noise. Like LQR it is optimal with respect to a quadratic cost function, taking a quantitative consideration of the noise and finding the best estimate despite its presence. In addition the filter provides a compromise between the speed of state reconstruction and its level of vulnerability to noise. This balance is determined by the magnitudes of the noise intensities.

The Kalman filter meets two criteria:

1. The expected value of the estimate equals the expected value of the state. Hence "on average" the estimate of the state will equal the true state.
2. Of all possible estimation algorithms, the Kalman filter minimizes the expected value of the square of the estimation error. Hence "on average" the algorithm gives the smallest possible estimation error.

Now let the plant be described as:

$$\begin{aligned} \dot{x} &= Ax + B_1 u + B_2 w + Gw \\ y &= Cx + Du^* + Hw + v \end{aligned} \tag{3.58}$$

Here the process and measurement noise (w and v respectively) are assumed to be uncorrelated, zero mean, stationary white noise. Probabilistic information about noise is summarized by its covariance and usually attained from test data, its form is as follows.

$E(w) = E(v) = 0$

$E(ww^T) = Q_n$

$E(vv^T) = R_n$

The filter takes the form of equation 3.54 with output:

$$\begin{bmatrix} \hat{y} \\ \hat{x} \end{bmatrix} = \begin{bmatrix} C \\ I \end{bmatrix} \hat{x} + \begin{bmatrix} 0 \\ 0 \end{bmatrix} u \tag{3.59}$$

And the optimal estimator gain is mathematically derived to equal:

$$L = P_e C^T R_n^{-1} \tag{3.60}$$

where P_e is determined from solving the matrix Riccati differential equation:

$$AP_e + P_e A^T - P_e C^T R_n^{-1} CP_e + GQ_n G^T = 0 \tag{3.61}$$

In this way the following quadratic error function is minimized.

$$\lim_{t \to \alpha} E((x-\hat{x})(x-\hat{x})^T)$$

(3.62)

The requirements for the Kalman creation are:

i. (A,G) is stabilizable

ii. (A,C) is detectable

3.2.3 State Estimate Feedback Control

To combine the ideal plant, the full state feedback controller and the state estimator, the full state feedback control input force becomes a function of the estimated states:

$$u = -K\hat{x} = -K(x-\tilde{x})$$

(3.63)

Using this equation with the plant (equation 3.41) and estimator (equation 3.54) but ignoring the road input disturbance yields the combined system, (D is a zero matrix):

$$\begin{pmatrix} \dot{x} \\ \dot{\tilde{x}} \end{pmatrix} = \begin{bmatrix} A\text{-}BK & BK \\ 0 & A\text{-}LC \end{bmatrix} \begin{pmatrix} x \\ \tilde{x} \end{pmatrix}$$

(3.64)

Since the combined system has a characteristic equation of det[A-BK-sI]*det[A-LC-sI]=0 the dynamics of the observer and controller (their eigenvalues) are independent of one another. Thus their design can be done separately. However, the real components of the eigenvalues of the estimator should be much further left in the s-plane than the eigenvalues of the LQR. This will ensure that the estimated error will die quickly compared to the dynamics of the controlled system.

3.2.4 Skyhook and Ground-Hook Damper

In this idealized system, the vehicle model is configured as shown in Figure 3.1. Here the skyhook damper generates the force:

$$F_{sky} = c_{sky} \dot{z}_s$$

(3.65)

and the modified ground-hook damper generates the force:

$$F_{gh} = c_{gh} \dot{z}_u$$

(3.66)
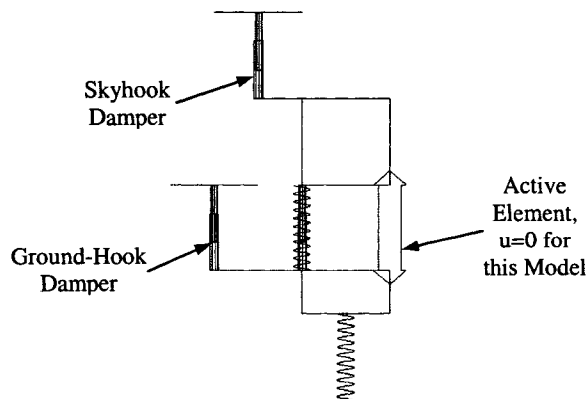
Figure 3.1: Implementation of S & G damping
within ADAMS for the quarter car model

3.2.5 Semi-Active Control

The following switching law is taken from that first derived by Karnopp et al. {26}.

In deriving switching laws for a semi-active damper, one must ensure that the active element does not inject energy into the system; rather the element should only dissipate energy (i.e. the system loses energy). As a result the element is restricted to generating forces whose associated power is dissipative. For the damper, work is the transferred energy to the system and power is the rate at which work is done. The following equations and sign conventions are adopted by Karnopp et al. {26} as:

$$Work = F_D x_D \tag{3.67}$$

$$Power = F_D \dot{x}_D \tag{3.68}$$

where:

$F_D > 0$ indicates a tensile force

$F_D < 0$ is a compressive force

x_D is the relative displacement of the damper and

if $x_D > 0$ then the element is extended

if $x_D < 0$ then the element is compressed

In using the above definitions, dissipative work and power occur when:

$$F_D x_D > 0 \tag{3.69}$$

$$F_D \dot{x}_D > 0 \tag{3.70}$$

This implies that if the relative displacement is increasing, F_D is tensile and if decreasing F_D is compressive. With the above restrictions one may derive switching control laws that ensure the element behaves as a damper. The damper is instructed to switch to low/off damping during situations where energy is required to be injected into the system, one possible scheme is:

$$F_{max} \quad if \quad F_D \dot{x}_D > 0 \tag{3.71}$$

$$F_{min} \quad if \quad F_D \dot{x}_D \leq 0 \tag{3.72}$$

To create this changing desired force in a real damper the damping coefficient is altered according to the following.

$$F_D = F_{desired} \tag{3.73}$$

$$c_s \dot{x}_D = F_{desired} \tag{3.74}$$

$$c_s = \frac{F_{desired}}{\dot{x}_D} \tag{3.75}$$

3.3 Software Interface

When interfacing ADAMS with Simulink, ADAMS/Control gives the user two distinct options in solving the system. These two methods are significantly different and are outlined below. With both solve methods, the user can choose any of the available Matlab integrators.

- 28 -

3.3.1 Function Evaluation Method/Continuous Mode

In this mode, numerical integration of both the ADAMS and Simulink models are done by Matlab, ADAMS is nothing more than a function evaluator. The ADAMS plant model is represented by the equations:

$$\dot{x}=f(x,u,t) \tag{3.76}$$

$$y=f(x,u,t) \tag{3.77}$$

As mentioned previously the ADAMS plant is a set of DAE that consists of the dynamic equations of motion and the constraint equations. The output function (y) on the other hand is a set of complex nonlinear equations. The Simulink model is of the form:

$$\dot{z}=f(z,y,t) \tag{3.78}$$

$$u=f(z,y,t) \tag{3.79}$$

As before the state equation is a set of DAE while the output is a set of complex nonlinear equations.

Since the ADAMS equations are written in a non-minimal form they are reduced to minimize the number of states that Simulink must integrate. ADAMS achieves this by using coordinate partitioning via the Adams Bashforth-Adams Moulton integrator formula. The reduced form distinguishes between the independent and dependent variables (x_1 and x_2 respectively):

$$\dot{x}_1=f_1(x_1,x_2,u,t) \tag{3.80}$$

$$0=f_2(x_1,x_2,t) \tag{3.81}$$

ADAMS isolates the dependent variables by solving the implicit algebraic equation f_2; here the dependant variables are expressed as algebraic functions of the independent variables. These dependent variables are then substituted into f_1 resulting in a compact set of ODE based on a minimum set of independent states. The resulting ODE takes the form:

$$\dot{x}_A=f(x_A,t) \tag{3.82}$$

During a simulation ADAMS receives x_A and u from Simulink. It then calculates the dependant variables (by evaluating f_2), the Lagrange multipliers (constraint forces) along with $\dot{x}_A$ (based on equation 3.82) which it sends to Simulink. From this, Matlab forms a set of ODE that describes the entire system; using these equations it integrates for x_A and the process advances to the next time step.

3.3.2 Cosimulation Method/Discrete Mode

With cosimulation, integration of the ADAMS and Simulink model is performed by their respective solver. At every time interval Matlab and ADAMS stops and updates one another with new state values. The ADAMS plant is now represented as:

$$\dot{x}=f(x,U_k,t) \tag{3.83}$$

$$y=f(x,U_k,t) \tag{3.84}$$

ADAMS considers the input U_k constant in the interval [kt,(k+1)t] while it performs the integration. It sends its output to Matlab at the end of each interval while receiving U_{k+1} from Matlab for the

- 29 -

next interval. Where in the previous method the plant and controller were treated as one continuous system, here the two are discretized with sampling rates. The output step size (sampling rate) is the interval at which information is exchanged between Simulink and ADAMS.

To effectively capture the response of the system, the developers of ADAMS suggest sampling the mechanical system at more than twice the highest frequency of interest in on the mechanical side. Below this value, false frequencies may develop or high frequency noise might be converted into a lower frequency (these events are known as aliasing).

As such, the highest frequency of interest for the vehicle is chosen to be 20Hz, which is well above the sprung mass natural frequency (in the range of 10-14Hz). Hence, a sample frequency at 40Hz would be adequate. However, to achieve a smooth response a sample frequency of 1kHz was used instead; at this rate the solving times were still reasonable.

3.3.3 Interface Notes

Function Evaluation Method/Continuous Mode

• Typically this method is numerically more difficult to solve.

• Within Matlab one large system of equations are formed that represent both the control and mechanical scheme. When integrating these equations the integrator 'sees' a continuous system, ensuring that the system dynamics are captured and so a very accurate result is achieved. Hence it should be used when the two domains are highly coupled.

• Has a tendency to fail when the ADAMS model is stiff.

Cosimulation Method/Discrete Mode

• Most useful when the ADAMS model is numerically stiff since the Matlab integrators can't handle it as well.

• For most problems cosimulation is the more efficient method. It is faster and handles complex systems better.

• Since cosimulation discretizes the system, it is more suitable to solving discontinuous system, for example controllers that are digital.

• Even when properly sampled, this method may at times not capture all the dynamics because of the software decoupling. However, for this study, no differences were noticed compared to the function evaluation method results.

4 VIRTUAL MODEL

4.0 Vehicle

Since the vehicle is traveling straight for all simulations, the lateral forces produced by the tires are typically small, and therefore not considered. Thus, the tires are modeled as vertical springs representing the radial stiffness, and only vertical disturbances are considered. Also, in all vehicles the tire damping is neglected since its effect is also small, an assumption used in most ride studies.

In connecting the tire spring to the unsprung mass, a 'dummy' massless body is first created. It is constrained to the unsprung mass using a translational joint, according to Figure 4.0b. With the other end of the body constrained by the road motion, the body is fully constrained and has no effect on the dynamics of the model. The spring is then created and connected to the spindle and to the opposite end of the dummy body. The dummy body is needed because in ADAMS, the ends of a spring must be defined by two separate parts and motion is not considered a part.

All vehicle models developed have two types of inputs, the road disturbance and the force from the active element. The road input is modeled as a vertical displacement in the form of step functions, sine waves, etc. It is imposed on the end of the dummy body that coincides with the end of the tire spring at the ground. Hence, at the ground the model is only constrained vertically. The active force element (whether for a semi-active or fully-active system) is placed in the same location as the passive strut unit and is modeled as an equal and opposite force element in ADAMS.

In modeling the fully-active suspension, the same conventional struts used in the passive vehicles are retained. As a result, differences between passive and active systems can only be attributed to the addition of the active element.

- 31 -

(a)   *(b)*
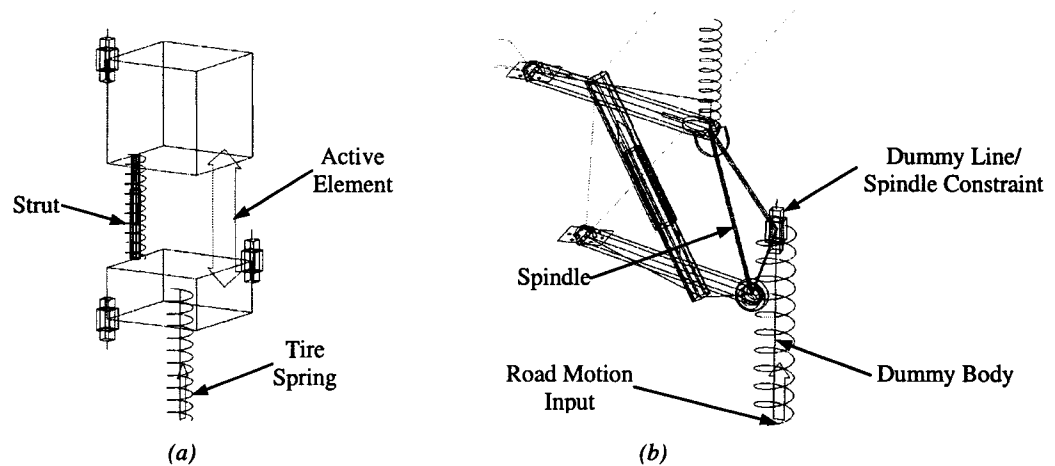
Figure 4.0: The quarter car lumped mass model (a) and the Iltis model (b)

4.0.1 Lumped Mass Vehicle

For these preliminary models, the suspension is not modeled since the control arms are ignored. Instead the body and wheel assembly are represented as separate lumped masses with a strut unit/force element linking them (Figure 4.0a). In these models the unsprung mass is constrained to move vertically using translational joints within ADAMS. Furthermore, only linear spring and damper rates are employed by using the ADAMS spring/damper element. These springs have no preload and gravity is turned off, which means that the initial vehicle configuration is in static equilibrium. Although not representative of reality, the settings simplify these models so that modeling procedures could be more quickly and easily developed.

Due to the simplicity of these models they need only be described by linear ordinary differential equations and do not require the use of algebraic constraint equations. As a result their symbolic equations are derived and cast into state-space form with relative ease. The matrices are then solved in Simulink and compared with the other modeling methods for validation.

The parameters used for the lumped mass models are taken from Bouazara et al. {25}; they are values that correspond to a typical passenger car. The values quoted are for a seven degree of freedom full vehicle model and are adjusted accordingly for the quarter and half car models.

4.0.1.1 Quarter Car Model

As discussed in the introduction, one quarter of the vehicle is modeled with two masses that are constrained to move vertically using the ADAMS translational joint. The values used represent the front corner of the full vehicle model from Bouazara et al. {25}.

4.0.1.2 Half Car Model

To capture the pitching characteristics of a vehicle, a half car model is constructed according to Figure 4.1. The body now represents half the weight of the vehicle while both the front and rear unsprung masses are included. Here the body is allowed to translate vertically and rotate about the lateral axis and as a result this model has four degrees of freedom. To restrict the body motion in ADAMS the sprung mass is

- 32 -

constrained using the parallel and in-line axis primitive joints. In the interest of space the results from this model are not discussed. The response of this model is consistent with both the quarter and full car models and so presents no new insight into these systems.
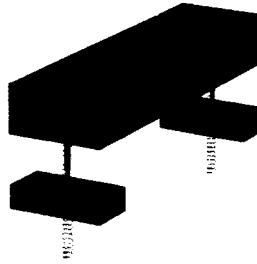
Figure 4.1: ADAMS half car model

In this model and others that follow, linearization is required to put the model in state-space form. This need arises in part from the nonlinear sine and cosine terms that describe the rotational motion. These terms are simplified by assuming only small rotations exist, it is assumed that:

$$\sin\theta = \theta \qquad (4.0)$$

$$\cos\theta = 1 \qquad (4.1)$$

This is a reasonable assumption since the associated error is relatively small for typical rotations experienced by the vehicle (generally <10° for body pitch and roll).

4.0.1.3 Full Car Model

The models above are extended to a full car in which all four wheels are included and the entire vehicle body mass used. The body has three degrees of freedom: vertical translation, pitch and roll. This coincides with the model developed by Bouazara et al. {25} where body yaw is ignored due to previous studies that indicate that its effects on comfort and road holding is negligible. In removing the undesired motions from the sprung mass, inline and perpendicular primitive joints in ADAMS are applied.
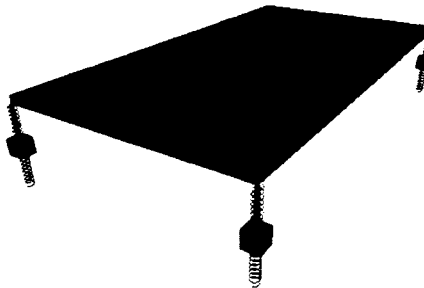
Figure 4.2: ADAMS full car model

4.0.1.4 S and G Model

Known as S & G damping, this model replaces the strut damper with a skyhook and a ground-hook damper. For this idealized ADAMS model, the skyhook damper is installed between the sprung mass and absolute ground, while the ground-hook damper is connected from the unsprung mass to absolute ground. The configuration can be seen for a quarter car model in Figure 3.1 and is implemented to compare with the semi-active controller. Since this configuration is thought to be the best case scenario for semi-active

control, it is ideal to evaluate the performance of the semi-active switch controller. Results for only the quarter car model are shown in this study.

4.0.2 Bombardier Iltis Utility Truck

The Bombardier Iltis utility truck is currently used by the Canadian military. It employs independent suspension consisting of a lower control arm with one common leaf spring serving as the upper control arm for both left and right suspension units. Bump stops are placed on the body to limit the movement of the wheel in bounce. For ease of design and manufacture, the front and rear suspension units are the mirror image of one another.

In a 1990 workshop hosted by the International Association of Vehicle System Dynamics called 'Multibody Systems Analysis Methods and Computer Codes', problems were selected to compare the results from using different multibody dynamic software packages. The Iltis was among the systems chosen and was modeled by researchers at Queen's University. Measurements were taken from the vehicle and published in {7} to encourage duplication. The intent of this virtual model was to leave nothing to the interpretation of the user when creating it.
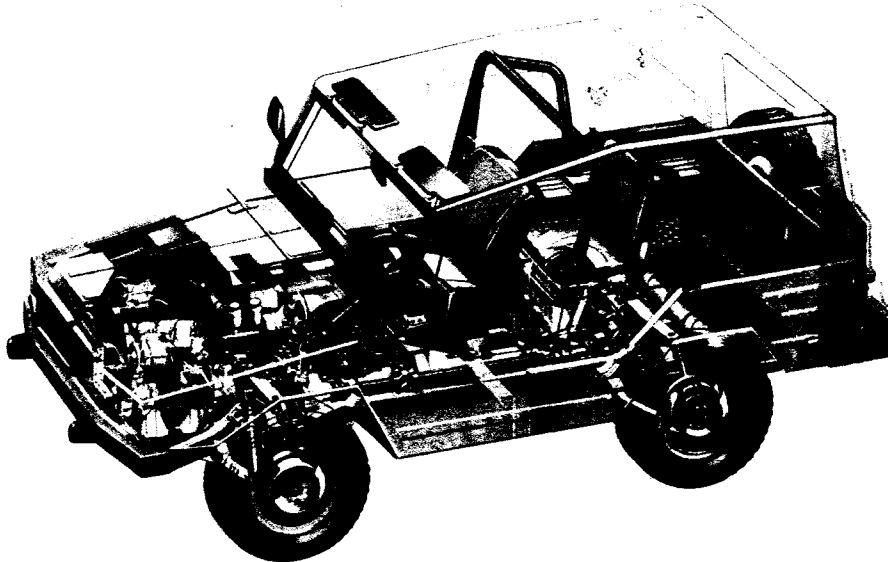
Figure 4.3: Iltis utility truck

In this benchmarking model all bodies are considered rigid and the data is given for the vehicle nominal position, i.e. the position of the vehicle just as it is about to sit on the ground. This is not the static equilibrium position, but rather the designed position of the suspension before equilibrium. The leaf springs are modeled as in Figure 4.6 and consist of a rigid massless upper control arm with a vertical spring connected between the cabin body and the top of the spindle. Incorporated into the stiffness of this vertical spring is the bump stop stiffness.

- 34 -
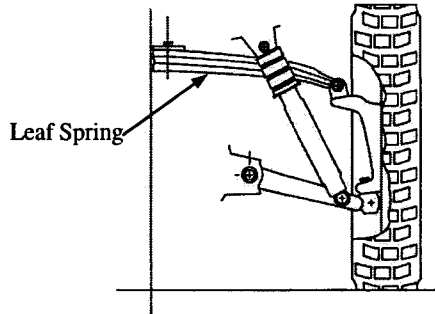
Figure 4.4: Iltis utility truck suspension unit

4.0.2.1 Force Elements

The strut spring for the benchmarking vehicle is described as:

$$F_s = -4.0092 \times 10^6 + (2.8397 \times 10^7)x - (6.7061 \times 10^7)x^2 + (5.2796 \times 10^7)x^3 \qquad \text{for } x \text{ in [m]} \qquad (4.2)$$

In this form, a positive position of x corresponds to a tensile force. Meanwhile the strut damper force is a combination of three equations:

$$F_D = 9945.627v + 33955.72v^2 - 59832.25v^3 - 395651.0v^4 \qquad \text{for } -0.2 < v < 0.21\text{m/s} \qquad (4.3)$$

$$F_D = -416.42 + 1844.3v \qquad \text{for } v < -0.2\text{m/s} \qquad (4.4)$$

$$F_D = 1919.1638 + 1634.727v \qquad \text{for } v > 0.21\text{m/s} \qquad (4.5)$$

Where v is in [m/s] and like before, a positive direction of velocity corresponds to a force in tension.

To model the effects of the bump stop the vertical spring has two distinct stiffness values. When the bump stop is not engaged the vertical spring stiffness is 35906N/m and jumps to 10^7N/m when contact occurs. Engagement occurs for a vertical wheel displacement of 70mm from the nominal position; through simulation it is found that this corresponds to when the vertical spring displacement is 63.85mm in the front and 63.40mm in the rear (relative to the spring length in the nominal position).

4.0.2.2 Virtual Model

Both a quarter and full vehicle model of the Iltis are built in ADAMS. Since handling manoeuvres are not considered, steering effects are not important and so the wheels are constrained to not steer and the tie rods are not included. Here gravity and spring preloads are used, unlike the lumped mass models.

Revolute joints are used to connect the control arms with the cabin, the top connection of the control arm and the spindle uses a hooke joint and the lower connection employs a spherical joint. This combination of joints is chosen since it does not produce any redundant constraint equations. It should be noted that when redundant equations existed, ADAMS either could not find static equilibrium (and thus could not linearize the vehicle) or if linearized, the resulting modal analysis gave inconsistent solutions.

The strut spring is modeled in ADAMS by defining a general force element between the sprung and unsprung mass; it uses equation 4.2 as its definition. This equation references markers within the model to determine the length of the spring; in this way the resulting force is generated.

On the other hand both the vertical spring and strut damper are modeled with the spring/damper element. Their nonlinear rates are defined by inputting force versus spring displacement/damper velocity

- 35 -

numerical values that satisfy the above equations. This data is then used to construct a best fit polynomial spline that ADAMS uses to calculate and generate the associated force based on the current spring displacement/damper velocity. This feature is used instead of the generalized force element since the definitions of these elements are discontinuous and so cannot be modeled with a single equation like the nonlinear strut spring.

	X	Y
1	-100.0	-1.8484642E+05
2	-50.0	-9.263142E+04
3	-15.0	-2.808092E+04
4	-9.0	-1.701512E+04
5	-7.0	-1.332652E+04
6	-3.0	-5949.32
7	-0.7	-1707.43
8	-0.6	-1523.0
9	-0.5	-1338.57
10	-0.4	-1154.14
11	-0.3	-969.71
12	-0.25	-877.495
13	-0.21	-803.723
14	-0.205	-794.5015
15	-0.195	-776.6544
16	-0.19	-769.0946
17	-0.15	-726.2048
18	-0.1	-634.7384
19	-5.0E-02	-407.3858
20	0.0	0.0
21	5.0E-02	572.2188
22	0.1	1234.7226
23	0.15	1853.6156
24	0.18	2126.0979
25	0.209	2260.7137
26	0.2099	2262.2919
27	0.2105	2263.2466
28	0.211	2264.0912
29	0.25	2327.8456
30	0.3	2409.5619
31	0.4	2573.0546
32	0.5	2736.5273
33	0.6	2900.0
34	0.7	3063.4727
35	1.0	3553.8908
36	5.0	1.00927988E+04
37	9.0	1.66317068E+04
38	14.0	2.48053418E+04
39	50.0	8.36555138E+04

Name SPLINE_1

Type y=f(x) (2D)
View as Tabular Data
Units no_units
☑ Linear extrapolation

Append row to X and Y data
Prepend row to X and Y data

Insert Row After
Remove Row

OK   Apply   Cancel

Figure 4.5: ADAMS graphical user interface of the nonlinear damping element

4.0.2.3 Quarter Car Model

The quarter car model has two degrees of freedom, one from the suspension and the other from the vertical movement of the cabin. A translational joint is used to constrain the body, whose weight is roughly one quarter the weight of the vehicle body.

- 36 -
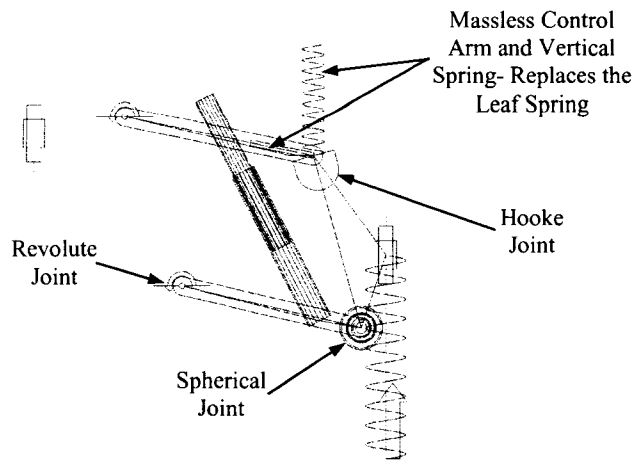
Figure 4.6: ADAMS quarter car model of Iltis

4.0.2.4 Full Car Model

With the full car model the sprung mass is a free body and so the model has a total of ten degrees of freedom. Although the ends of the tires are constrained to move vertically, there are no lateral or longitudinal constraints on the entire system. If a net force results in either of these directions the model could drift. To deal with this, bushings are attached to the ends of the tire with translational stiffness values of 10N/m in the global x, y and z directions. This insignificantly small stiffness is enough to keep the vehicle stable during a five second simulation. The quarter car version does not need these bushings since the translational joint on the car body supplies a lateral and longitudinal constraint while the road motion supplies a vertical one.
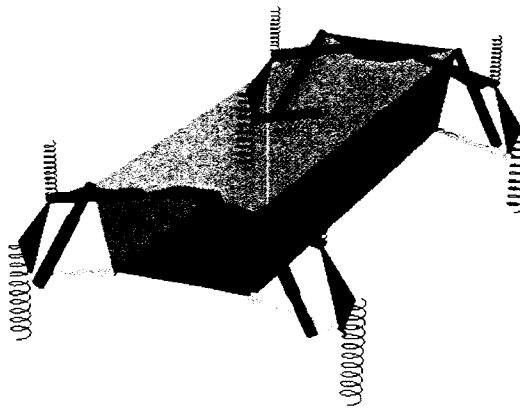
Figure 4.7: ADAMS full car model of Iltis

4.0.2.5 Full Car Model with Suspension Bushings

Suspension bushings are used at component interfaces (such as connecting the control arms to the body) to give compliance to the suspension, reduce static friction, reduce noise, minimize stress failures due to shock loading, etc. These components are normally made of rubber compounds or other elastomer materials. In adding bushings to the full car model, the number of degrees of freedom rises dramatically. This is because the two bodies that a bushing connects are not constrained to move in a defined way relative to one another. Instead a bushing produces an opposing force in response to the relative movement of the bodies it connects. As a result, the two bodies may move in any direction relative to each other.

- 37 -

To limit the number of degrees of freedom of the model, bushings are only placed between the mounting points of the control arms and the cabin body. When added, the degrees of freedom of the Iltis jump from ten to thirty-eight. Since bushings are not included in the original benchmarking Iltis model, values are estimated and are based on the work of Wood {24}. He gives the translational and rotational bushing stiffnesses used in a production sport utility vehicle. Since this vehicle is similar in size and layout to the Iltis, the values he quoted should be appropriate for use in the ADAMS model. However these values were modified when implemented in this model, but because the values used have the same order of magnitude as the original values they should still be reasonable.

Since the model only uses one link to represent each control arm and since the tie rods are not modeled, only the bushings prevent the suspension from yawing relative to the cabin. It is found through simulation that the rotational stiffness of the bushings about the vertical axis had to be significantly increased from the values quoted from Wood {24} to ensure the suspension did not yaw excessively with respect to the sprung mass. Although an unrealistic situation, the purpose of adding the bushings is to see if the LQR algorithm and the software interface can handle the increased model size and the increased data being passed back and forth.

4.1 Controller

4.1.1 Linear Quadratic Regulator

Calculation of the LQR gain is straightforward within Matlab. Knowing the state space matrices of the ADAMS model, and defining the weighting matrices correctly, the LQR gain matrix is found using the Matlab command:

$$k_{lqr}=lqr(A,B_1,Q,R)$$

For the function to solve, all four matrices that it refers to must be defined in the Matlab workspace and must comply with the restrictions outlined in Chapter Three. Within Simulink this gain is implemented using the gain block shown below.

Figure 4.8: Simulink block representation
of the LQR controller

4.1.2 Kalman-Bucy Filter

As with the LQR algorithm, the Kalman filter design within Matlab requires knowledge of the vehicle state space matrices along with the noise co-variance matrices. The state space matrices of the vehicle must be defined as a state space object using the command:

$$sys=ss(A,B,C_s,D_s)$$

The Kalman filter is then created using the function:

$$K_{est} = kalman(sys,Q_n,R_n)$$

K_{est} is an object containing state space matrices that describe the filter, these matrices are extracted with the command:

$$[A_{est}, B_{est}, C_{est}, D_{est}] = ssdata(K_{est})$$

Following this function the matrices are now in the Matlab workplace environment, and are referenced by Simulink using the state-space block shown below.
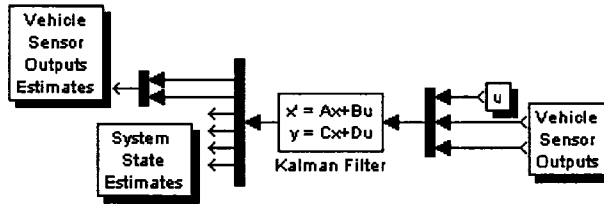
Figure 4.9: Simulink block representation of the Kalman filter

4.1.3 Semi-Active Control

In accordance with the equations developed in chapter three, for this project F_{min} is set to zero which is the most ideal situation and $F_{max} = c_{sky} \dot{z}_s$, hence the active damper simulates skyhook damping when damping is provided and so $F_D = c_{sky} \dot{z}_s$. Although unrealistic since a damper will always generate a force in response to motion, this algorithm provides a best case scenario.

The semi-active switching relations (equation 3.71 and 3.72) can be implemented in Simulink using various methods. The method applied involves the creation of a Matlab function that is saved as an Matlab m-file. It is then referred to by Simulink using the Simulink function block and the switching is performed according to the block input. The block arrangement is shown in Figure 4.10. In considering a quarter car model, the switching function of equations 3.71 and 3.72 are modified as follows. Since

$$F_{desired} = F_{sky} = c_{sky} \dot{z}_s \tag{4.6}$$

then

$$c_{sky} \dot{z}_s \quad \text{if} \quad (c_{sky} \dot{z}_s)(\dot{z}_s - \dot{z}_u) > 0 \tag{4.7}$$

$$0 \quad \text{if} \quad (c_{sky} \dot{z}_s)(\dot{z}_s - \dot{z}_u) \leq 0 \tag{4.8}$$

By ignoring the scalar c_{sky} in the switching criteria, the following is developed:

$$c_{sky} \dot{z}_s \quad \text{if} \quad \dot{z}_s (\dot{z}_s - \dot{z}_u) > 0 \tag{4.9}$$

$$0 \quad \text{if} \quad \dot{z}_s (\dot{z}_s - \dot{z}_u) \leq 0 \tag{4.10}$$

The Matlab function switches its output between c_{sky} and zero depending on the magnitude of its input $\dot{z}_s (\dot{z}_s - \dot{z}_u)$.
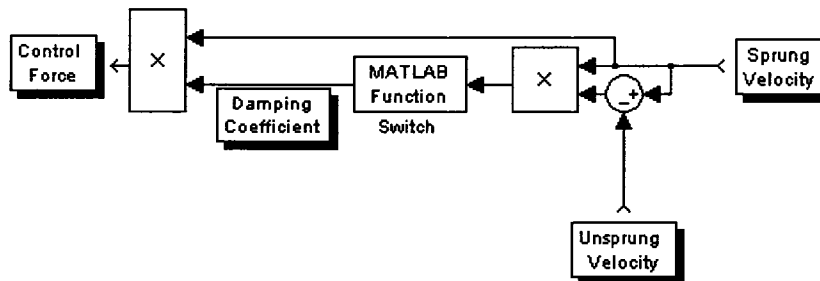
Figure 4.10: Semi- active, ideal skyhook damping switch block diagram

Although the controllers discussed are for implementation with the quarter car model, the principals are simply extended to the more complicated full car models. For these models, when damping is on, a dissipative damping force proportional to the absolute vertical velocity of the corner of the vehicle body is applied by the suspension strut. For the Iltis models, the switching functions use the same relations, except now the strut velocity equation is complicated because of the kinematic suspension. This is dealt with by outputting this measure from the ADAMS vehicle plant instead of deriving its analytical form.

5 INTERFACE PROCESS

Although a powerful tool, ADAMS/Controls is not flexible in that it does not offer many options, and certain shortcomings force the interface process to be adopted accordingly. Oddly enough, it is the requirement of linearizing the ADAMS model to solve the LQR algorithm and the Kalman filter that presents most of the challenges. The overall process for this linearization is likened to simplifying, within ADAMS, the model for proper exportation and then rebuilding it within Simulink.

5.0 ADAMS/Matlab Interface

A brief overview of the procedure for interfacing ADAMS with Matlab follows, for a detailed description refer to {11}.

After building the model in ADAMS, the input and output variables are defined by creating 'state variables'. These are the measures that the user wishes to use as inputs and outputs for the ADAMS block in Simulink. The ADAMS/Controls interface window is then opened, within which the plant inputs and outputs are specified by referring to these state variables.

An available option is whether to export a linear or nonlinear model into Simulink. The linear option exports the time invariant state-space matrices of the ADAMS model and all calculations are performed by Matlab with no communication between the two programs. Directly before exporting the linear ADAMS model, the program must solve for static equilibrium, without doing this the system *will not* linearize. The nonlinear option creates a direct-feedthrough interface to link the two software suites by creating a Simulink block of the ADAMS model. With this option the user does not have to perform a static analysis before exporting the block to Simulink.

After exporting the system, ADAMS is abandoned and Simulink is entered. Using designated Matlab commands, a block representation of the ADAMS model is created. At this point the user creates the Simulink system and connects it to the ADAMS block accordingly. Subsequent simulations are controlled within Simulink in terms of executing the run and specifying its duration. For nonlinear simulations the communication sample rate and simulation type (i.e. continuous versus discrete mode) are also specified within Simulink. Results are viewed within Simulink and for nonlinear simulations can also be exported into ADAMS for use with its post-processor.

- 41 -
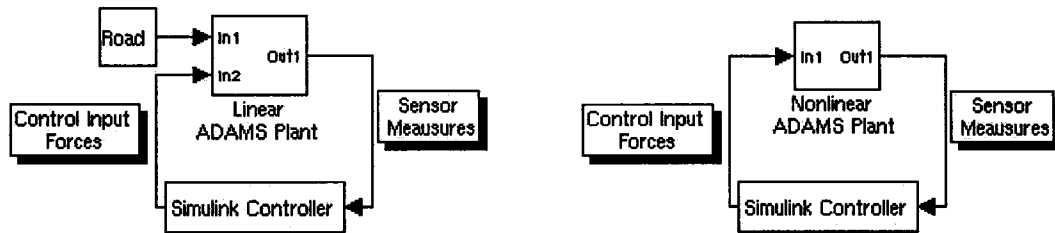
Figure 5.0: ADAMS Simulink interfacing configurations within Simulink

5.0.1 Linear Lumped Mass Model Extraction

A drawback of the LQR controller is that it's based on a linear version of the plant. A linear model may be viewed as a photograph; it captures a continuously changing system at an instant in time and so is limited in its description. Since the eigenvalues for nonlinear systems change with time, the LQR gain is only optimal for the nonlinear vehicle configuration that coincides with the linear model used to construct the gain. Hence it is important that the multibody system be linearized about a reasonable configuration; for vehicle models this is usually the static equilibrium position.

When attempting to obtain the linear system matrices of the vehicle, capturing the vertical displacement of the road input proves problematic. Since motion is a constraint that removes the degree of freedom in its direction, the vertical degree of freedom of the tire contact patch is eliminated. But when ADAMS constructs the B_2 matrix for the linear model, the input variables must have an associated degree of freedom. Also motion function expressions can only be functions of time but during linearization time is frozen. Because of these conflicts the resulting B_2 matrix generated by ADAMS is zero. In short, motions within ADAMS cannot be captured as inputs in the state-space matrices.

For simple models this is not serious as the B_2 matrix can be derived and constructed in Simulink. However for a complicated multibody system, having the user derive the nonlinear equations and then synthesize the corresponding linear equations is too complicated a task. Hence a procedure is needed to automatically extract the B_2 matrix from the virtual ADAMS model.
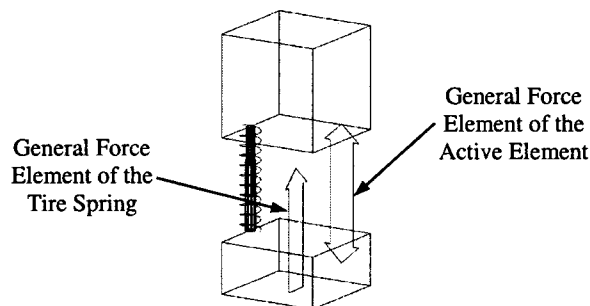
Figure 5.1: ADAMS quarter car model with the tire force input

Since force is not a constraint it can be captured as an input when linearizing a system. Using this property, the tire spring in ADAMS is eliminated and replaced by a generalized force element whose magnitude is defined as an input from Simulink. The tire force is now calculated within Simulink and fed into the plant as shown in Figure 5.1 and 5.2. For the lumped mass models, the reconstructed tire force in Simulink is:

- 42 -

$$F_t = -k_t(z_u - z_{road})$$ (5.0)
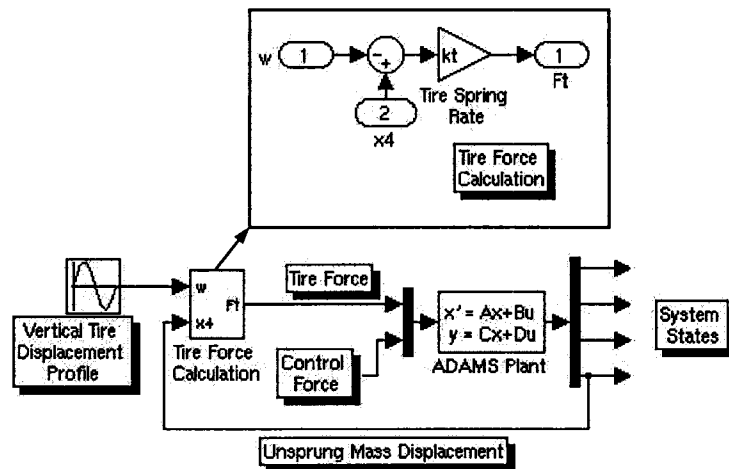
Figure 5.2: Simulink diagram of the tire force construction

The plant matrices now use tire force as its input, however to find the LQR gain system matrices with the road displacement as input is required. To change the input for the matrices a separate Simulink file is created as illustrated in Figure 5.3 for the quarter car model.
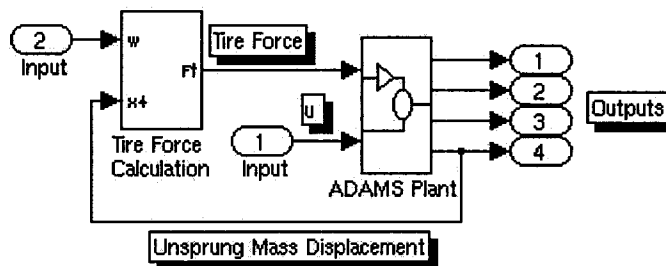
Figure 5.3: Block diagram for linmod function <filename>

The following command in Matlab, which refers to this Simulink file, extracts the desired matrices.

[A,B,C,D]=linmod('<filename>')

The linmod command linearizes and extracts the state-space model of the block diagram specified within the file <filename>. The new inputs and outputs are defined using the inport and outport blocks while the state space variables of the original ADAMS plant are preserved.

An alternative method to the above procedure exists. One may feed the road profile from Simulink directly into ADAMS and then calculate and apply the tire force within ADAMS. This method has the advantage of not having to perform the linmod command since the linearized ADAMS plant matrices would have the desired inputs for the creation of the LQR controller. Also this method linearizes the system once using one software whereas the previous method requires linearization by ADAMS and then by Matlab.

For this study the first method is implemented. Since the radial stiffness of the tire is linear the linmod calculation in Matlab is straightforward and so introduces negligible error. This was confirmed by numerous simulations on the matter.

- 43 -

5.0.2 Nonlinear Exchangeable Measures

In using the nonlinear interface, information is continuously passed back and forth between the two software suites. In this mode it is desired to define the vertical road profile within Simulink and feed it into ADAMS. In this way changing the road input can be done easily, quickly and conveniently without having to reopen and resave ADAMS to change the road profile. However exchanging motion between the two programs is not a straightforward matter since the solvers tend to find the scenario unacceptable. This inability to solve is due to how the information is used/applied in the receiving program and on the solver methods.

An imposing motion is defined as a driving motion (i.e. fixing a body to accelerate at a specific rate) that is treated as a constraint in ADAMS, whereas a measured motion is the resulting movement of the body measured by sensors; it is not a constraint. Motion can be transferred from Simulink to ADAMS if it is not used as an imposing motion in ADAMS, for example, if the motion input is used by ADAMS to calculate and apply a force on the system. It has also been found that passing measured motion from ADAMS to Matlab is acceptable.

Motion cannot be passed to ADAMS when in ADAMS it is defined and treated as an imposing motion. This restriction stems from the fact that the communication of the two programs occurs at a discrete sampled rate (in discrete mode). As a result motion is treated as discrete and a discrete step in motion gives an infinite acceleration. In addition, because of the internal formulation of ADAMS, an imposed motion is never allowed to depend on anything but time and must be continuous with continuous first and second time derivatives. The end result is that this scenario usually prevents the simulation from proceeding (regardless if using the discrete or continuous mode) depending on the solvers used.

In light of these findings the road profile, which is an imposing motion, is defined in ADAMS and only force values are passed from Simulink to ADAMS with measured motion passed from ADAMS to Simulink.

The lumped mass models are produced in three ways:
1. Linear vehicle derived from analytical equations and implemented in Simulink.
2. Linear vehicle modeled partially by ADAMS and exported to Simulink for completion.
3. Vehicle modeled in ADAMS and solved in its nonlinear form by software interfacing.

5.0.3 Linear Iltis Model Extraction

The previous problems encountered with the lumped mass models also apply to the implementation of the Iltis vehicle models with the addition of the following issues.

5.0.3.1 Solving Static Equilibrium

As mentioned for the lumped mass models, to obtain their state-space matrices from ADAMS the tire spring is replaced by a generalized force that is defined in Matlab (see Figure 5.1 and 5.2). The only way to solve static equilibrium for the lumped mass models is to remove all external forces that exist in the model. This is because in the current form the model is not constrained vertically, since only the vertical tire

- 44 -

force that is not a constraint is applied to the wheel hub. Hence with the presence of an external vertical force there is no static equilibrium solution and so linearization is not possible. So gravity and spring preload are turned off and the vehicle configuration is assumed to initially be in the static position, in this way linearization by ADAMS is possible.

The Iltis models present a much different scenario. As before the tire springs are replaced with their equivalent applied force, but now the known vehicle configuration is not the equilibrium position and both the vertical and strut spring have preload. As a result both gravity and spring preload have to be active to find the sitting position of the ADAMS model. But since the system is not globally constrained, a static equilibrium position does not exist and so the system cannot linearize. Because of these circumstances the procedure adopted for the lumped mass models cannot be applied to this vehicle and so two processes are developed to linearize the Iltis models.

5.0.3.2 Static Export Method

This procedure has the aim of changing the Iltis model so that its conditions before linearization are equivalent to the conditions when linearizing the lumped mass models. Hence the model is modified so that when finding the static position (before linearization occurs) there is neither spring preload nor gravity present. In this way the static equilibrium position of the vehicle can be determined with the tire force acting as an input.

Achieving this goal involves a multi-step procedure. First the motion driven tire spring is included in the ADAMS model. With both spring preload and gravity on, static equilibrium is found since the vehicle is vertically constrained by the road motion. The vehicle is now in the desired configuration with gravity balancing out the static force of the springs. Using a feature within ADAMS, this configuration is saved as a separate file using the following steps:

1. From the top menu press 'Simulate' then 'Interactive Controls'.

2. Press the icon on the bottom row of the new box, second from the left (has the tooltip:

   "Save the model, at a simulated position, into the database under a new name").

3. Name the new file and save.

This creates a second model in the view session that has the configuration found in the static run. Now using this new model, gravity is turned off and the definition of the springs is modified to remove preload. In addition the tire radial spring is replaced with the input tire force on the spindle.

Now the model is equivalent to the scenario found with the lumped mass vehicles and static equilibrium can be solved a second time to find and export the linear system. When static equilibrium is solved this time the system configuration does not change since neither gravity nor spring preloads nor any other external forces are present in the model.

Because the model lacks gravity and spring preload before the final linearization, its linear version should also exhibit these characteristics. For a vertically constrained spring this effect is minimal since the spring preload is completely cancelled by gravity when in equilibrium. However, complete cancellation does not occur for a tilted spring since the preload force can now be resolved into a vertical and horizontal

component. The vertical component is offset by gravity, but the horizontal component is not, instead it exerts a moment on the suspension. Hence by removing both preload and gravity the suspension effectively stiffens since the moment exerted by the spring preload is now absent. This feature should be observed in the resulting linear matrices.

General Force
Element of the
Tire Spring
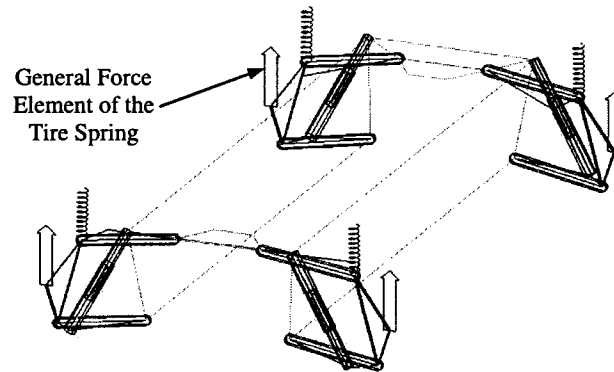
Figure 5.4: Iltis full model of the static export method

5.0.3.3 Gravity Export Method

In the second linearization procedure the effects of gravity and spring preload are included by using a dummy spring. In this process the tire spring is turned into a 'ghost' spring by decreasing its stiffness to a value of 2N/m while preserving its preload value. Since the ghost spring has such a small stiffness compared to the tire its presence is negligible.

The bottom end of the ghost spring is then constrained to move laterally and longitudinally but not vertically; this is accomplished by defining a zero vertical velocity on the end of the spring. At the same time the tire equivalent input force is applied to the spindle in the same manner as the static export method. The model is now constrained vertically with the ability of accepting the tire force from Simulink and is ready to be linearized. Static equilibrium is found once and the system linearized thereafter.

5.0.3.4 Tire Lateral Tracking

With a kinematic suspension there is a direct coupling between the vertical displacement input disturbance at the tire contact patch and a corresponding lateral reaction movement. In other words a vertical tire movement causes a lateral reaction movement which is dictated by the kinematic design of the suspension. If the model cannot produce this lateral movement then the suspension locks up. For the nonlinear interface model the relationship between these two motions is taken care of by ADAMS, all the user specifies is the vertical displacement profile.
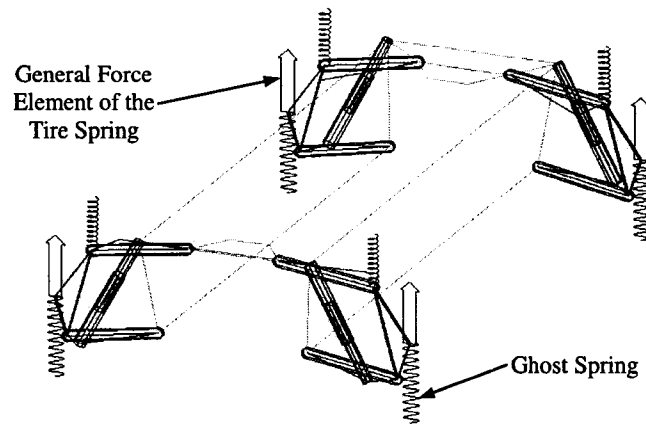
Figure 5.5: Iltis full model of the gravity export method

However in the linear model, where the road profile and tire force is constructed by the user, the lateral movement of the tire needs to be modeled in Simulink. This was thought important since the lateral tire movement affects the displacement of the tire spring and so directly influences the tire force applied to the upright. After extensive simulation it was concluded that the corresponding lateral movement of the tire, for the road profiles considered, was negligibly small. As a result the lateral motion can be ignored in Simulink without sacrificing model accuracy. In light of these findings, for the linear Iltis models the force equation for the tire is still represented by equation 5.0.

For the Iltis, three model versions are created:

1. Linear vehicle produced thru the static export method.

2. Linear vehicle produced thru the gravity export method.

3. Vehicle modeled in ADAMS and solved in its nonlinear form by software interfacing.

5.0.4 Linear Control of the ADAMS Model

The fully-active and semi-active controllers are used with both linear and nonlinear vehicle models. Most notably the constant LQR gain, which is created from a linear model, is used with linear and nonlinear vehicle models. The controller weights are tuned through trial and error until an acceptable response is achieved for the particular vehicle model and input being used. When combined with the nonlinear ADAMS model, the system is not ideal for two reasons:

1. The constant LQR gain is not optimal for the nonlinear model since the eigenvalues of the nonlinear model change with time, meaning that the optimal gain changes also.

2. Although the LQR algorithm guarantees stability with the linear vehicle model, it does not with the nonlinear version.

The first issue may not be serious if the vehicle configuration and behaviour does not change drastically during the disturbance. In this case the vehicle will have characteristics similar to its static equilibrium position and so LQR will be close to optimal.

- 47 -

5.0.5 Changing the System States

When ADAMS performs the linearization the user has no choice as to what states are used to describe the system. Rather ADAMS automatically chooses the states on the basis of which variables yield the best numerical conditioning of the state matrices. The following procedure outlines a method of changing the states, within Matlab, after ADAMS has formed the state-space matrices and before applying the linmod command for the LQR. Let the original system with the undesired states take the form:

$$\dot{x}_u = Ax_u + Bu^* \tag{5.1}$$

$$y = Cx_u + Du^* \tag{5.2}$$

The strategy is to have ADAMS/Controls output specific variables which generate matrices that can be used to later change the states. In ADAMS define two output sets:

$$y = \begin{vmatrix} y \\ \hat{x} \end{vmatrix} = \begin{vmatrix} C \\ C_1 \end{vmatrix} x_u + \begin{vmatrix} D \\ D_1 \end{vmatrix} u^* \tag{5.2}$$

Where $\hat{x}$ is the vector of states desired by the user and y is the output of the Simulink plant block. D_1 can be assumed zero since the old states can be mapped to the new states without external inputs. Now rearrange the second relationship of equation 5.3 to give:

$$x_u = C_1^{-1}\hat{x} \tag{5.3}$$

and substitute into equations 5.1:

$$\dot{\hat{x}} = C_1AC_1^{-1}\hat{x} + C_1Bu^* \tag{5.4}$$

$$y = CC_1^{-1}\hat{x} + Du^* \tag{5.5}$$

Hence the new system is defined as:

$$\dot{\hat{x}} = \hat{A}\hat{x} + \hat{B}u^* \tag{5.6}$$

$$y = \hat{C}\hat{x} + \hat{D}u^* \tag{5.7}$$

Where:

$$\hat{A} = C_1AC_1^{-1} \tag{5.8}$$

$$\hat{B} = C_1B \tag{5.9}$$

$$\hat{C} = CC_1^{-1} \tag{5.10}$$

$$\hat{D} = D \tag{5.11}$$

To attain the required matrices, first export from ADAMS the system with the y vector as output, this will yield the matrices A,B,C,D. Then select and export the desired set of state variables $\hat{x}$ as output that will generate C_1 and D_1. The new state space equations can then be calculated in Matlab by using the above relations.

5.1 Model Schematics

Shown below are Simulink block schematics of how the ADAMS plant and controller are linked for various arrangements.

5.1.1 Linear Quadratic Regulator
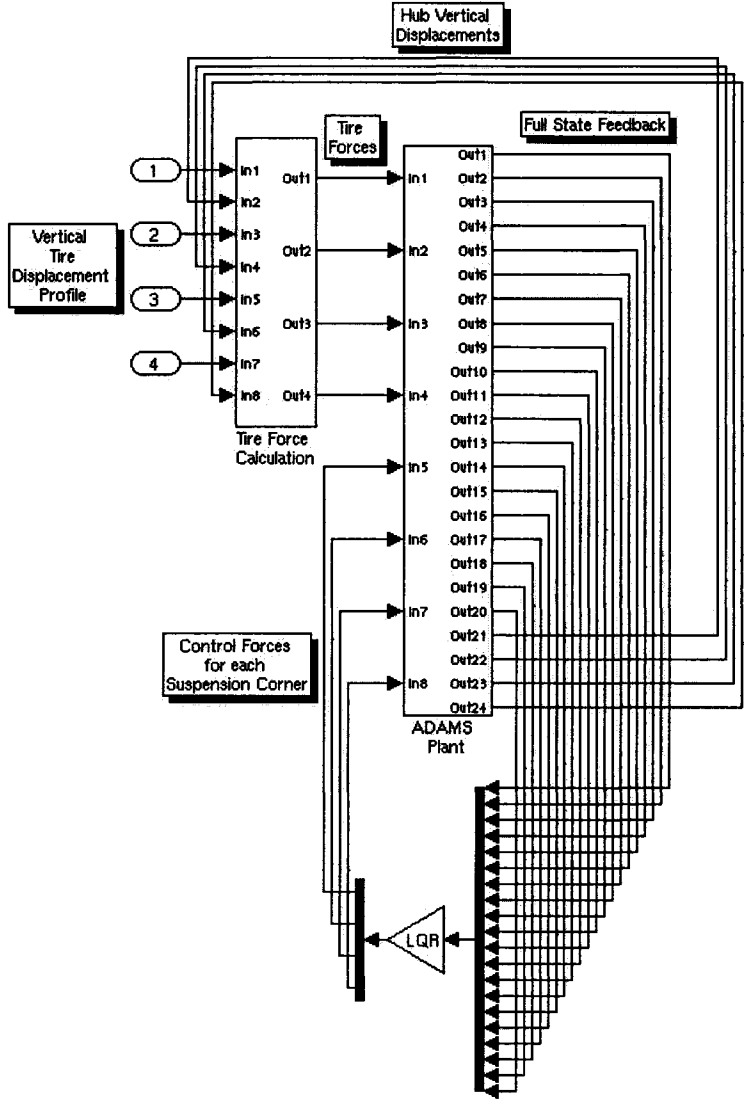
Figure 5.6: Linear Iltis full car model (no bushings)

- 49 -

5.1.2 Linear Quadratic Gaussian Regulator

This model combines the LQR controller with the Kalman filter.
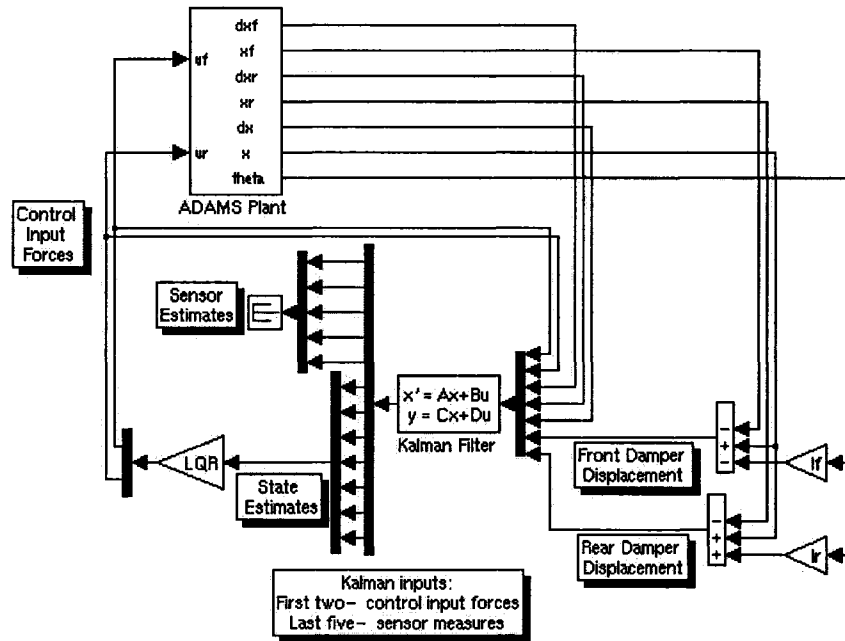
Figure 5.7: Nonlinear lumped mass half car model

5.1.3 Semi-Active Skyhook Switch
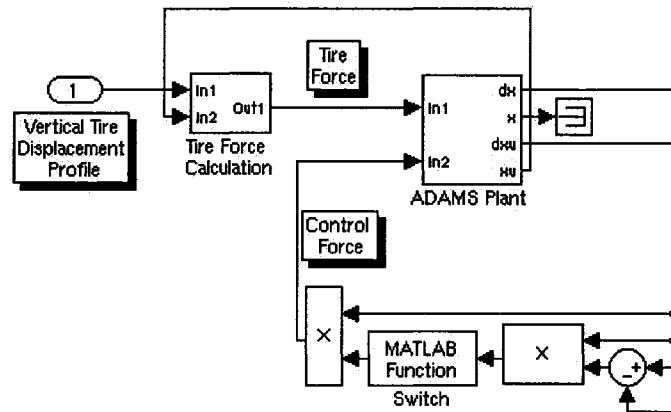
Figure 5.8: Linear lumped mass quarter car model

5.2 Algebraic Loop

For nonlinear simulations between Matlab and ADAMS, algebraic loops may develop that prevent the system from solving. In this case an algebraic loop is when the dynamics of the controller and plant are not present, i.e. when no differential variables are included in the model. The Simulink block representing the nonlinear ADAMS plant should be described by the differential equations:

$$\dot{x}=f(x,u,t) \tag{5.12}$$

$$y=f(x,u,t) \tag{5.13}$$

When using the cosimulation solve mode the integration of x occurs in ADAMS and so the ADAMS interface Simulink block behaves as an algebraic function with direct feed-through taking the form of:

$$y=y(u,t) \tag{5.14}$$

As a result this block contains no differential variables, and if the rest of the Simulink model has no differential variables, then an algebraic loop will exist. Since the LQR controller (without the Kalman filter) and the semi-active switch controller do not use any differential variables, algebraic loops form when solving in the cosimulation mode.

To break the loop, without disturbing the system response, different Simulink blocks may be added so that a differentiable element exists. Of the methods tested, using the memory block seems to provide the most robust solution. It applies a one integration step delay, meaning that its output is the previous input value. The result is that this block shifts its input forward by the communication interval used between Simulink and ADAMS (a negligible 1ms for most simulations). As shown in Figure 5.9, the block is inserted between the controller and the vehicle.
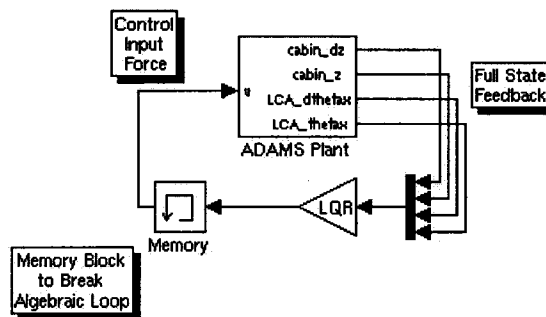
*Figure 5.9: Technique used to break algebraic loop
for the nonlinear Iltis quarter car model*

6 MODEL SETTINGS AND RESULTS

For this study the active suspension controllers are tuned toward delivering performance for a passenger road car rather than a race car. Hence the primary aim is to demonstrate active suspensions ability in increasing the ride quality of the vehicle during ride manoeuvres by decreasing the sprung mass acceleration. For the remainder of this study, simulations that link Adams with Simulink (either through the discrete or continuous calculation mode) are referred to as 'interfacing models'.

6.0 Preliminary Notes
6.0.1 Road Profile

For time domain simulations, the quarter car vehicle is disturbed as if traveling over a speed bump at 5km/h. Figure 6.0 shows the road profile used, the y-axis represents the vertical displacement and the x-axis is the forward distance traveled and its associated time. In ADAMS the profile is implemented using the step function command:

step(time, t_0, h_0, t_1, h_1)+step(time, t_2, h_2, t_3, -h_1)

step(time, 1, 0, 1.021, 5e-2) +step(time,1.0857, 0, 1.107, -5e-2)

This profile is also duplicated in Matlab by constructing its mathematical equation that is given in {12}. Each step function is described as:

$$a=h_1-h_0 \tag{6.0}$$

$$\Lambda=\frac{(t-t_0)}{(t_1-t_0)} \tag{6.1}$$

$$Step=\begin{cases} h_0 & :t \le t_0 \\ h_0+a\cdot\Lambda^2(3-2\Lambda) & :t_0 < t < t_1 \\ h_1 & :t \ge t_1 \end{cases} \tag{6.2}$$

The equation is implemented by creating a Matlab function describing this discontinuous relation; it is introduced into Simulink using the function block. For convenience, the speed bump is encountered after one second of simulation time.
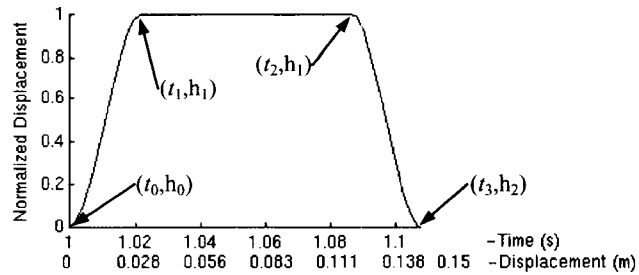
Figure 6.0: Vertical displacement profile of speed bump

For full car models, a road input is chosen to simultaneously excite the sprung mass bounce, pitch and roll modes. A plot of the road disturbance for each of the four corner wheels is illustrated in Figure 6.1. In this way a more complete picture of the system response is seen since the performance of the active system is evaluated when all rotational degrees of freedom of the sprung mass are excited.
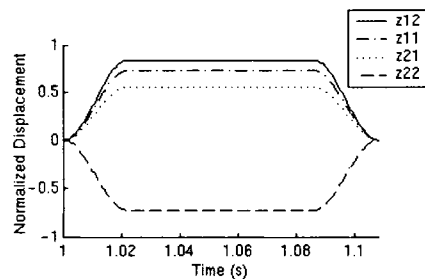
Figure 6.1: Speed bump profiles for each corner of the full car

6.0.2 Ride Assessment

Ride quality is associated with the level of vibration felt by the passenger. To date there is no one agreed upon standard to quantitatively describe ride comfort limits. This is attributed to the variations in individual sensitivity to vibration that makes it difficult to map out a ride comfort boundary and to a lack of agreement among researchers on common test methods.

Because of this, focus will be on the vibration isolation capabilities of the cabin body and not on assessing the acceleration experienced by the occupants. Generally, the movements of the sprung mass in vehicle models are regarded as indicators of the level of vibration felt by the passengers where the acceleration levels are inversely proportional to the ride quality of the vehicle. As such it is the aim of the suspension system to minimize the acceleration of the vehicle body by filtering out as much vibration as possible.
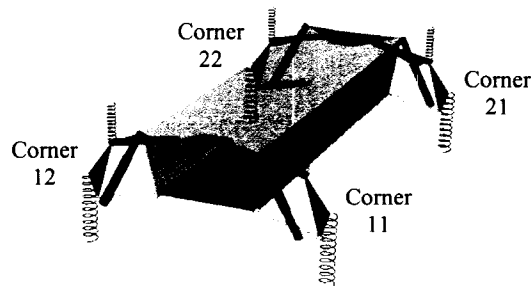
Figure 6.2: Suspension corner notation of full car model

- 53 -

6.1 Linear Lumped Mass Model Validation

To gain confidence in the software and process developed, two methods are used to extract the linear lumped mass vehicle models. The equations of motion are derived by hand, linearized and then cast into state-space form. The resulting matrices are defined in Matlab and implemented in Simulink with the E.C.U. In another process the models are partially built in ADAMS, then linearized and exported into Simulink where the tire input force and E.C.U. is constructed to complete the model.

These two methods of attaining the linear models yield equivalent state-space matrices except for some negligibly small non-zero numbers in the ADAMS matrices. These values are attributed to numerical errors within the ADAMS routine. Comparing the results of these two procedures helps confirm the validity of the linear vehicle models attained from ADAMS for both the quarter car and full car models.

6.2 Lumped Mass Quarter Car Model

6.2.1 Fully-Active Suspension

A drawback of the LQR algorithm is the requirement of optimizing the response by picking the Q and R weighting matrices by trial and error. As a result a better set of weighting matrices than those used for these results may exist. Nonetheless, the following still lends insight into the behaviour of fully-active suspension. Tuning the LQR controller involves finding the values of the weighting matrices by running simulations with different Q and R magnitudes until a reasonable ride response is achieved. For this model the numerical values of the diagonal Q and R weight matrices are:

Q=diag[1e8 100 100 1e8]

R=[1]

The Q matrix is equally weighted on the first and last state which is the sprung mass velocity and unsprung mass displacement respectively, thus the controller should decrease these state responses the most to give a better trade-off between ride and handling.

6.2.1.1 Time Domain Simulation

Figure 6.3 outlines the response of the sprung mass acceleration of the LQR system compared to the linear passive suspension. Graphed are two different model responses for the LQR controller, one by constructing and calculating the linear active suspension model entirely in Simulink ('LQR Simulink' series) and the other by linking the ADAMS model with the Simulink controller ('LQR Interface' series). As seen in the results, for this vehicle there are no noticeable differences between the two active models, confirming that these two modeling methods should give the same results for an inherently linear vehicle model.

- 54 -
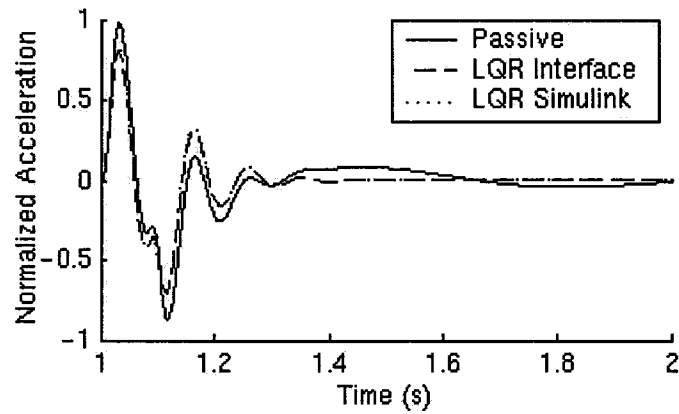
Figure 6.3: Sprung mass vertical acceleration[†]

In this response the fully-active system slightly reduces the acceleration peaks while allowing the body acceleration to settle more quickly compared to the passive system. However the increase in ride comfort from using fully-active suspension is not considerable and is due to the moderate settings of the weighting matrices. For the other vehicle models a more aggressive controller setting is used to achieve a greater improvement in ride.

Any suspension design must seek to minimize changes in tire force since these fluctuations may cause insufficient contact with the road causing the car to loose traction. Additionally the tire normal force is an important measure since it directly influences cornering force, tractive effort and braking performance of the tire. Ideally the tire normal force remains at its preload force throughout vehicle operation.

The forces produced by the radial tire spring, in Figure 6.4, indicate that for the weights chosen no significant change in the tire force takes place with the fully-active system. At some instances the tire force peaks are larger than the passive suspension and at other times they are smaller.
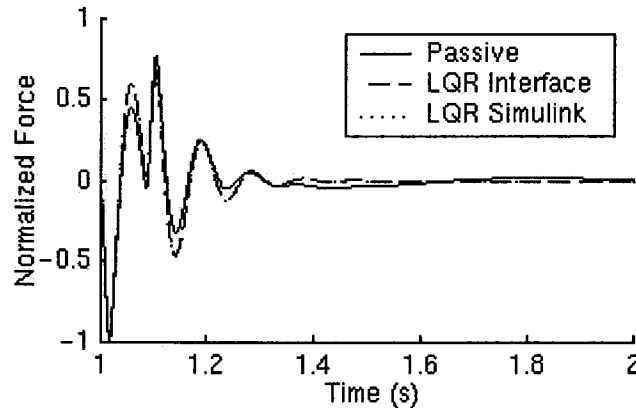
Figure 6.4: Tire dynamic force[†]

Although not a direct indicator of either ride or handling, suspension displacement does provide useful insight into the differences between passive and active suspension. This measure is one of practicality; with a reduced suspension working space more flexibility exists in the vehicle packaging. As shown in Figure 6.5 there is less variation in the active suspension displacement but with a larger average amount of suspension movement.

- 55 -
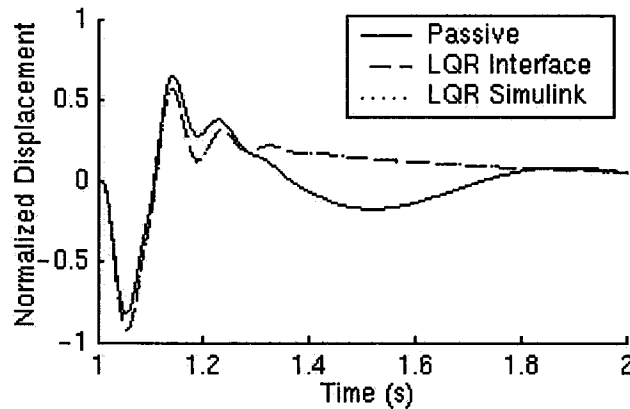
Figure 6.5: Suspension displacement[†]

6.2.1.2 Eigen Analysis

The following two tables summarize the passive and fully-active system in regards to their eigenvalues, damping ratios and natural frequencies. For this research these values correspond to when the vehicle is in static equilibrium. Notice that the active suspension significantly increases the system damping for the first eigenvalue that represents the sprung mass vibration mode while slightly decreasing the damping of the unsprung mass mode. This corresponds to the body movement becoming 'stiffer' and the unsprung mass becoming 'softer'.

Passive Suspension		
Natural Frequency (rad/s)	Damping Ratio	Eigenvalues
8.88	0.256	-2.27 ± 8.59i
68.9	0.241	-16.6 ± 66.8i

Table 6.0: Eigen analysis of the passive system

Although the sprung mass mode is overdamped for the active suspension, the damping ratio depends on the values used for the Q and R weighting matrices since it is these values that determine the numerical value of the LQR feedback gain and hence the system eigenvalues. For example when changing the Q matrix to Q=diag[1e7 100 100 1e8] the system is no longer overdamped since system damping becomes 0.749 and 0.239.

LQR Suspension		
Natural Frequency (rad/s)	Damping Ratio	Eigenvalues
n/a	>1	-2.09
n/a	>1	-39.4
67.3	0.212	-14.3 ± 65.8i

Table 6.1: Eigen analysis of the LQR fully-active system

6.2.1.3 Frequency Response

To generate frequency response plots a linear model is required and since this quarter car model is inherently linear these graphs are especially valuable. To explore the influence of the weighting matrices on the system response, the following systems are shown in Figure 6.6 to 6.8.

[†]*Notice: the two active responses are nearly indistinguishable from one another.*

1) LQR A: Q=diag[1e8 100 100 1e8] & R=[1]

2) LQR B: Q=diag[1e8 100 100 100] & R=[10]

3) LQR C: Q=diag[1e9 100 100 1e8] & R=[1]

4) LQR D: Q=diag[1e6 100 1e4 2e8] & R=[0.1]

5) LQR E: Q=diag[100 100 1e4 2e9] & R=[0.1]

In taking LQR A to be the nominal setting, LQR B decreases the force output of the active actuator and weights the unsprung mass displacement less. LQR C weights the sprung mass velocity even more heavily and the last two systems reverse the trend by putting most of the emphasis on decreasing the unsprung mass motion with more available actuator force.
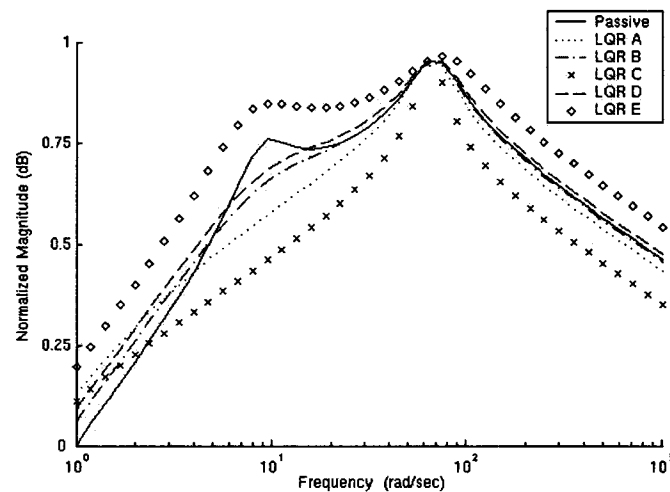
Figure 6.6: Sprung mass vertical acceleration

Figure 6.6 confirms the existence of the sprung mass acceleration 'invariant point' in the quarter car model when tire damping is neglected. As outlined by Williams {48}, invariant points exist in the quarter car where at a certain input frequency certain responses are only functions of the sprung and unsprung mass and the tire spring rate. At these frequencies, the response is independent of the suspension force and so an active element will not have any influence. Williams {48} states that for the sprung mass acceleration, the invariant point occurs at the wheel hop frequency as confirmed above. Since only the response near the sprung mass resonant frequency is necessary for ride improvements significant gains in ride are still achievable with the inclusion of an active element.

Another interesting feature of this response is that at extremely low input frequencies (below the sprung mass natural frequency) the fully-active LQR system has a response greater than the passive system. This however is not a significant drawback since it occurs for such low frequencies. In a typical driving situation, to excite these frequencies would require one to drive extremely slowly over a large road disturbance.

Near the sprung mass resonant frequency, all the active systems, except for LQR E, significantly decrease the sprung mass acceleration. In the mid frequency range LQR D and LQR E show worse than passive performance since their weighting is geared towards the unsprung mass motion. The system that

- 57 -

shows the most improvement in ride is LQR C which is expected since it is the system most weighted towards decreasing the sprung mass velocity.

For the tire response the behaviour around the unsprung mass natural frequency is most important since it is this region that directly affects the tire movement. As expected, in Figure 6.7 only LQR D and LQR E reduces the dynamic tire forces at this frequency since they are the only algorithms weighted towards the unsprung mass motion. The other systems demonstrate a deterioration in tire grip at this frequency with the situation reversing for frequencies around the sprung mass natural frequency.
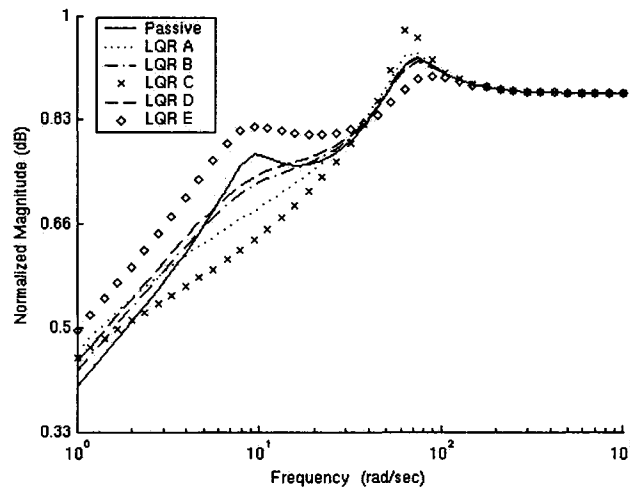
Figure 6.7: Tire dynamic force

For suspension displacement, Figure 6.8 shows that for systems weighted towards ride the suspension space is smaller than the passive suspension near the sprung mass resonance and greater at higher frequencies. For the systems weighted towards handling, the converse occurs. The second invariant point predicted by Williams {48} is for the suspension deflection and it occurs at a road input frequency of:

$$W = \frac{k_t}{\sqrt{(m_{sprng} + m_{unsprng})}}$$

(6.3)

For the parameters used the equation predicts W=5.30rad/s and is confirmed in Figure 6.8 where all the system responses intersect at this frequency.
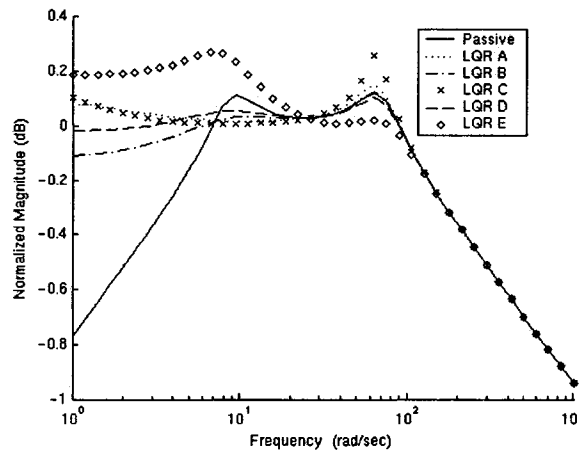
Figure 6.8: Suspension displacement

- 58 -

6.2.2 S & G Model

Since it is generally thought that the idealized combination of S & G damping yields the theoretically best achievable results for semi-active damping, it is compared with semi-active damping to gauge the performance of the switch controller. The following parameters are used for the semi-active models and unless labelled, the results displayed are for linear vehicle models.

Skyhook damping coefficient: 1.29kNs/m

Ground-hook damping coefficient: 1.29kNs/m

Semi-active high damping coefficient: 1.29kNs/m

Semi-active low damping coefficient: 0Ns/m

For the semi-active suspension, frequency response plots do not capture the switching between high and low damping by the controller since they only plot the response for either high or low damping. As a result these graphs do not accurately show the dynamics of this system and so will not be considered; only time domain results are shown.

6.2.2.1 Time Domain Simulation

As expected the S & G damping model performs better than the more realistic switch algorithm as shown in Figure 6.9 to 6.11. Despite this, the response of the semi-active switch controller approximates the response of the theoretically ideal S & G damping algorithm reasonably well. Hence the results are encouraging as they indicate that the semi-active switch controller performs fairly well for a semi-active suspension.
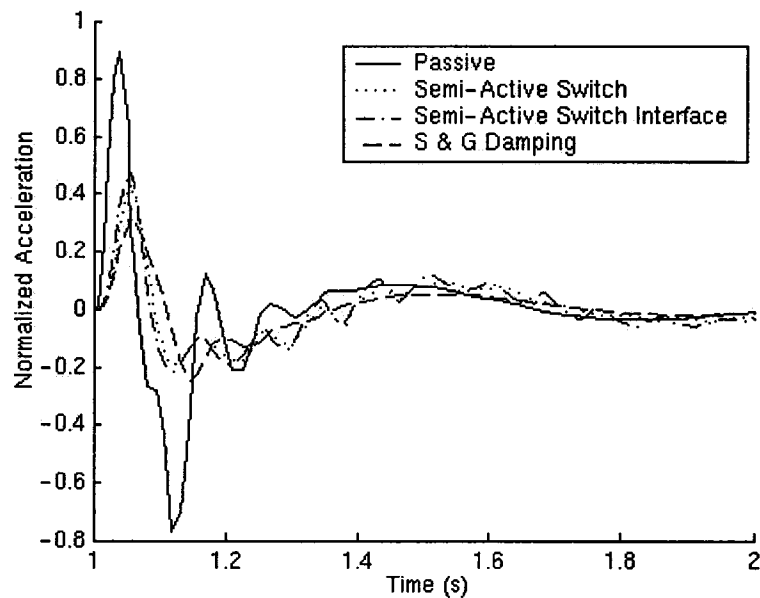
Figure 6.9: Sprung mass vertical acceleration[†]

[†]Notice: the two semi- active responses are nearly indistinguishable from one another.
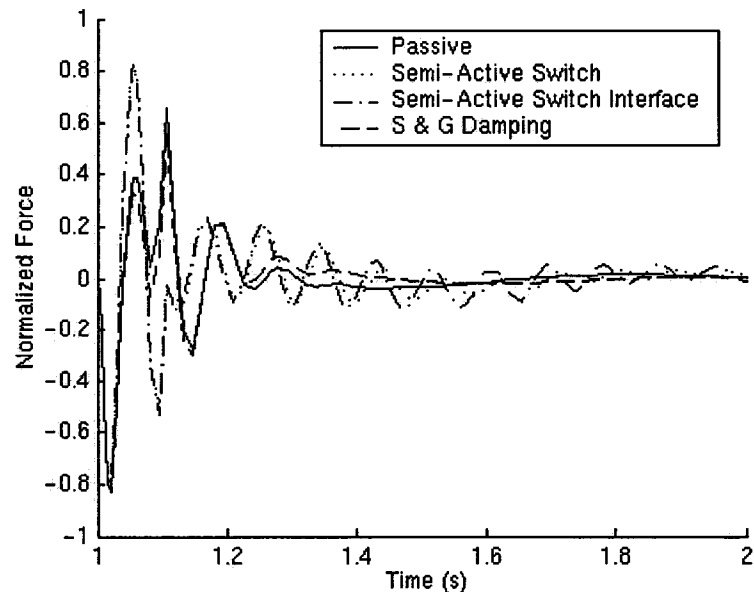
Figure 6.10: Tire dynamic force[†]
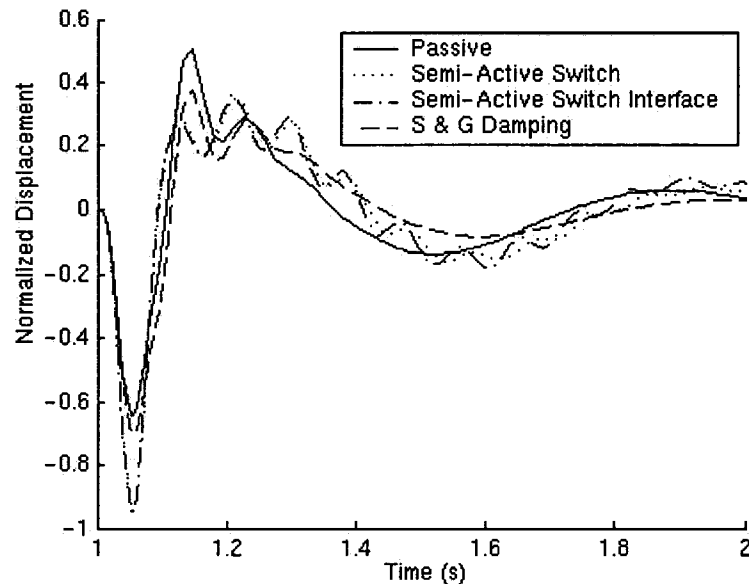
Figure 6.11: Suspension displacement[†]

6.2.3 Fully-Active versus Semi-Active

6.2.3.1 Time Domain Simulation

The time domain response of the semi-active suspension in Figure 6.9 to 6.11 rivals the performance of the fully-active suspension in Figure 6.3 to 6.5. At first this relative performance may seem puzzling, however with closer inspection an explanation is brought to light. The speed bump road profile suits semi-active damping very well since for most of the road disturbance the semi-active damper is switched off. This is expected because as the tire climbs and descends the speed bump the wheel attains a velocity greater than the sprung mass. As a result the semi-active suspension during the manoeuvre is ultra soft which is ideal for ride.

This theory is further confirmed in Figure 6.12 to 6.14 where a sine wave (amplitude of 5cm with a frequency of 2Hz) is used as the input. Without changing the controller settings, the semi-active response is much less impressive compared to the fully-active system than it was for the bump input. In other words, for this input where switching takes places continuously the performance of the semi-active controller is less impressive than it is for the bump response.
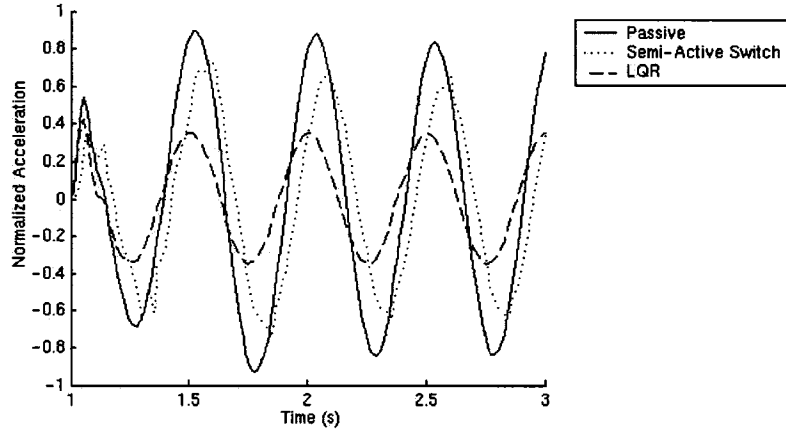
Figure 6.12: Sprung mass vertical acceleration

Unlike with the speed bump, here both the fully-active and semi-active suspension simultaneously decrease the sprung mass acceleration, the dynamic tire force and the suspension displacement. These results are consistent with the frequency response plots that suggest the same performance for this input frequency. Hence the LQR active system performance relative to the passive and semi-active suspension seems dependant on the input used for the road.
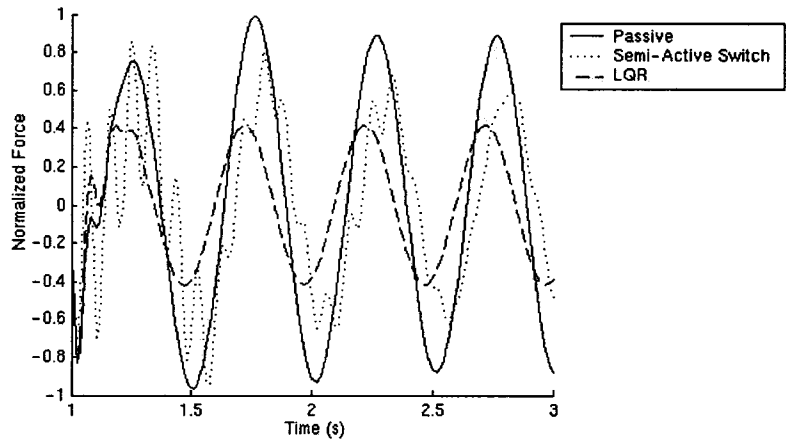
Figure 6.13: Tire dynamic force

- 61 -
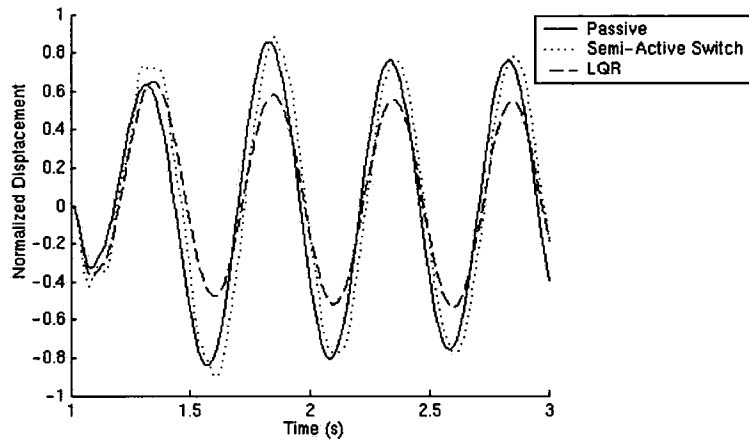
Figure 6.14: Suspension displacement

The relative power requirements of the active element for the semi-active and fully-active system are shown in Figure 6.15. These results do not account for friction, nonlinearities of the mounting bushings or other nonlinear effects within the active element and so should be taken as a preliminary indicator. As adopted by Karnopp et al. {26}, power greater than zero is dissipative when using equation 3.68.

The responses indicate that the power of the semi-active element is never less than zero, confirming that the control algorithm works as intended since the actuator does not consume power- it only dissipates it. On the other hand the LQR suspension spends more time supplying power to the vehicle than it does absorbing it.
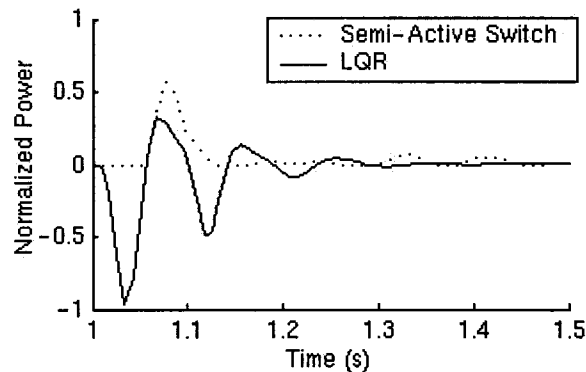
Figure 6.15: Power consumption of active element
while traveling over speed bump

A shortcoming of the tire model used is that it cannot directly simulate the tire lifting off the ground because the road profile is applied to the end of the tire spring and so the tire is constrained to be in contact with the road. At best with this tire model, tire lift off can be monitored.

Assuming no gravity and spring preload or pre-compression exists, when the unsprung mass moves up more than the road the tire will lose contact with the ground. In reality when a vehicle is at rest the weight of the vehicle compresses the tire which creates an internal preload force in the tire. This internal force pushes the tire against the road and gives the tire the ability to expand up to the amount that it was initially compressed. Now when the wheel unit moves up greater than the road, this internal tire force

- 62 -

expands the tire and so lift off does not necessarily occur. Hence the difference between the movement of the wheel and the road must be greater than the static compression of the tire for lift off to occur. Expressed mathematically the condition for tire lift off is when the function TL is greater than zero, where:

$$TL = z_u - z_{road} - ss \geq 0 \qquad (6.4)$$

Within ADAMS the static deflection of the quarter car model is 1.53cm when gravity is turned on; this is confirmed with equation 6.5.

$$ss = \frac{(m_{sprng} + m_{usprng})g}{k_t} \qquad (6.5)$$

$$ss = 1.53cm$$
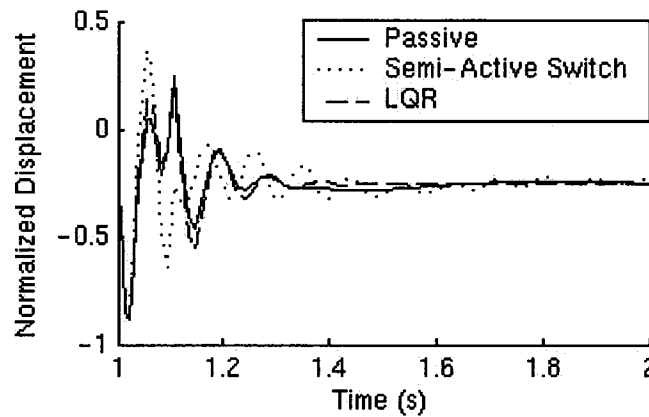
Figure 6.16: Tire lift off tracking function TL

Equation 6.4 is evaluated and plotted in Figure 6.16 for the speed bump input. Although all three systems exhibit lift off, the fully-active and semi-active suspension system show the most. When looking at the sine wave input no lift off occurs, however as with the speed bump input, the active systems exhibit a greater tendency towards lift off than the passive suspension.

6.2.3.2 Eigen Analysis

The switching controller turns the semi-active system into two distinct models: when the damping force is on and when it is off. As a result the linear model is described by each of these two states separately in Table 6.2 and 6.3.

Semi-Active Suspension, High Damping		
Natural Frequency (rad/s)	Damping Ratio	Eigenvalues
8.75	0.282	-2.47 ± 8.39i
69.9	0.413e-3	-0.289 ± 69.9i

Table 6.2: Eigen analysis of semi-active damping when damping is on

Even with damping on the system differs from the passive and LQR fully-active suspension since here the generated active force is the damping coefficient times the absolute velocity of the sprung mass (rather than the strut velocity). When switched high the semi-active system increases the damping of the sprung mass mode and decreases the damping of the unsprung mass mode compared to the passive

- 63 -

suspension. On the other hand, compared to LQR, at high damping the semi-active system has less damping for both the sprung and unsprung modes of vibration.

Semi-Active Suspension, Low Damping		
Natural Frequency (rad/s)	Damping Ratio	Eigenvalues
8.74	0	$0 \pm 8.74i$
69.9	0	$0 \pm 69.9i$

Table 6.3: Eigen analysis of semi-active damping when damping is off

Since there is no passive damper included in this system, when the controller switches to low there is no damping in the entire model. Although this is not realistic, the objective is to compare a 'theoretical best' semi-active suspension with a fully-active suspension.

6.2.4 Kalman Filter

6.2.4.1 Time Domain Simulation

To execute the Kalman filter, matrices describing the noise characteristics of the sensors and process are required. Since this is strictly a virtual study this information is lacking and so sample values are taken from Roh et al. {38}. The noise matrices adopted are:

Q_n=[5.06e-4]

R_n=diag[4.76e-4 0.25]

For this model, it is assumed that the sprung mass acceleration and the suspension displacement are the measured sensor variables. A plot of the true versus estimated states for the four state variables is shown in Figure 6.17 to 6.20 using the speed bump as the road input. The estimator is generally very good in its approximation of the states, although there are some differences in the initial stages of the run.
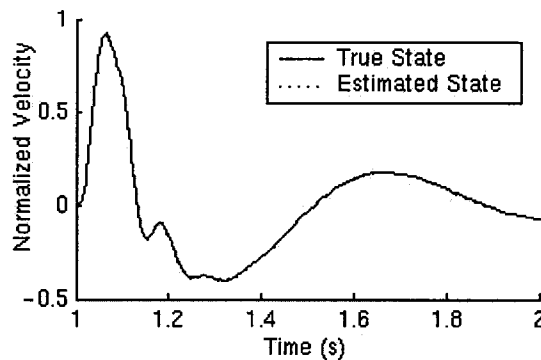
Figure 6.17: Sprung mass velocity[†]

[†]Notice: the two responses are nearly indistinguishable from one another.

- 64 -
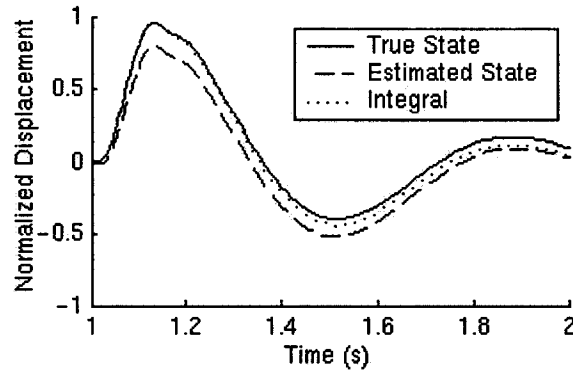
Figure 6.18: Sprung mass displacement
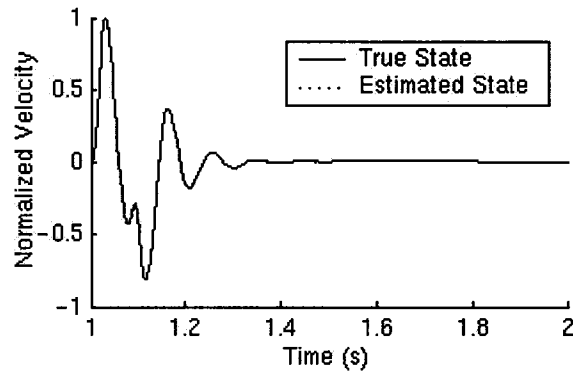
Figure 6.19: Unsprung mass velocity[†]
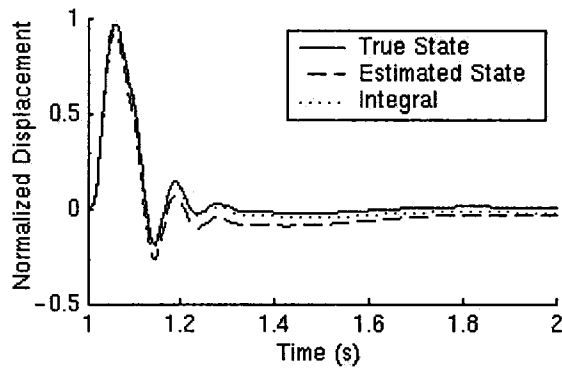
Figure 6.20: Unsprung mass displacement[†]

To better attain an estimate of the absolute displacement of the sprung and unsprung mass, the estimated absolute velocity of each mass is integrated and plotted in Figure 6.18 and 6.20 ('Integral' series name). This series produces a better estimate than the Kalman filter and hence may be used in conjunction with the state estimated velocities.

6.3 Lumped Mass Full Car Model

6.3.1 Fully-Active Suspension

Here the Q and R diagonal weight matrices are:

Q=diag[8e9 100 1e10 100 1e10 100 1e5 1e8 1e5 1e8 1e5 1e8 1e5 1e8]

R=diag[6e-2 6e-2 6e-2 6e-2]

- 65 -

With respect to the quarter car model, here the R matrix value is smaller meaning more actuator force is used. In addition, the sprung mass vertical velocity is the heaviest weighted followed by the body pitch and roll velocity then the unsprung mass displacement and finally the unsprung mass velocity. The corresponding states are listed in Appendix A.

6.3.1.1 Time Domain Simulation

A more aggressive LQR controller is used with this model so that a significant improvement in ride is achieved in Figure 6.21 to 6.23. The initial peaks of the passive suspension response are all but eliminated while also settling more quickly for the fully-active system. However the LQR does see a high frequency, low amplitude fluctuation long after the disturbance is encountered as if the system damping is small.

Figure 6.21: Sprung mass vertical acceleration[†]
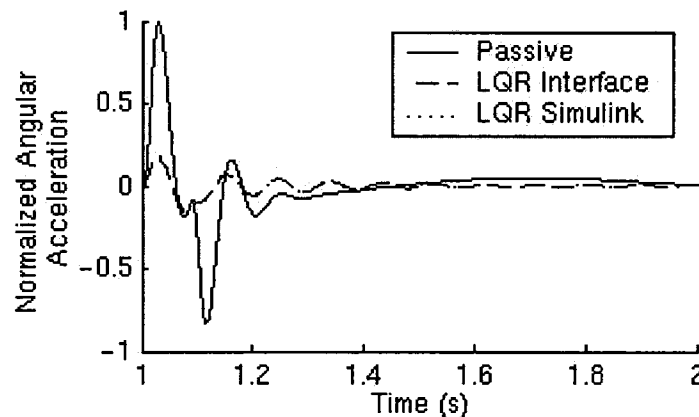
Figure 6.22: Sprung mass roll acceleration[†]
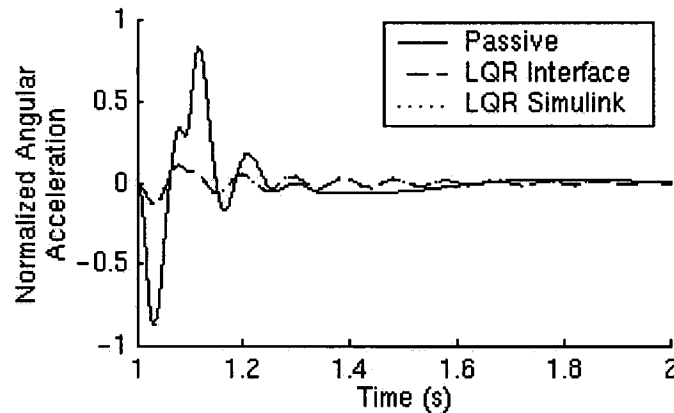
Figure 6.23: Sprung mass pitch acceleration[†]

The increased ride comfort comes at a cost of decreased tire holding capability. Shown in Figure 6.24, LQR demonstrates an increased amount of tire fluctuation compared to the passive suspension. This translates to a larger variation of the tire contact patch and directly affects the longitudinal road /tire grip. However this result is not a disaster since the vehicle is traveling straight and lateral tire force production is not needed. This does indicate however that during this disturbance there will be a loss of longitudinal tire grip and so wheel spin and tire lift off is more likely to occur.

These findings cannot be extended to the realm of handling; in other words these results do not imply that active suspension worsens the handling characteristics of the vehicle. This is a ride study and so the tire forces shown are not indicative of how the system behaves in a handling manoeuvre (consisting of both road disturbance inputs and inertial body forces, i.e. braking on a rough surface with potholes). Since the roll motion is drastically reduced, the active suspensions will decrease the lateral load transfer. As discussed in the introduction, this leads to greater lateral tire forces which increase handling.
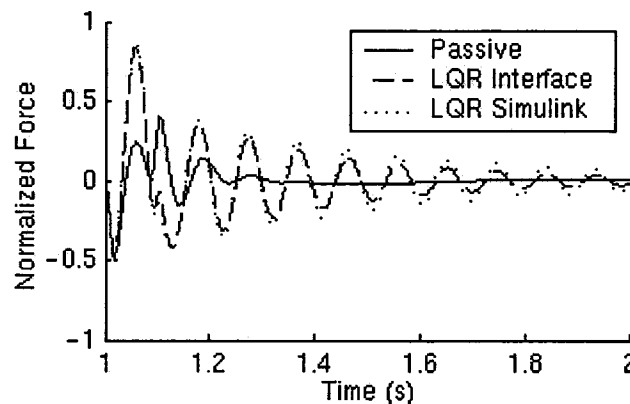
Figure 6.24: Tire dynamic force of corner 11

As Figure 6.25 demonstrates, the LQR algorithm applies a positive force for more than half of the disturbance. Based on the sign convention adopted in Chapter 3, this translates to a downward force on the sprung mass and an upward force on the unsprung mass. This is expected since the sprung mass will have a tendency to move up as it traverses up the bump and so needs a downward force to stabilize it. Although the

- 67 -

unsprung mass has the same tendency to move up and requires a downward force for stabilization, suppressing the sprung mass motion is a higher priority since that is how the controller is weighted.
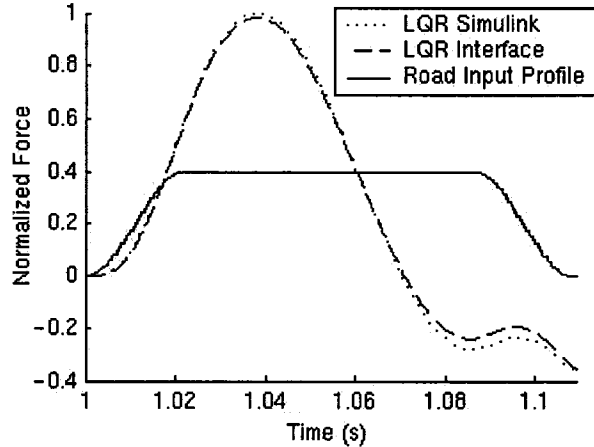
Figure 6.25: Active control force of corner 11

As a result, the active force increases the unsprung mass displacement according to Figure 6.26. In essence, the suspension becomes actively soft by pulling the sprung and unsprung mass in together to reduce the body movement. The cost of this is the deterioration in the tire forces.
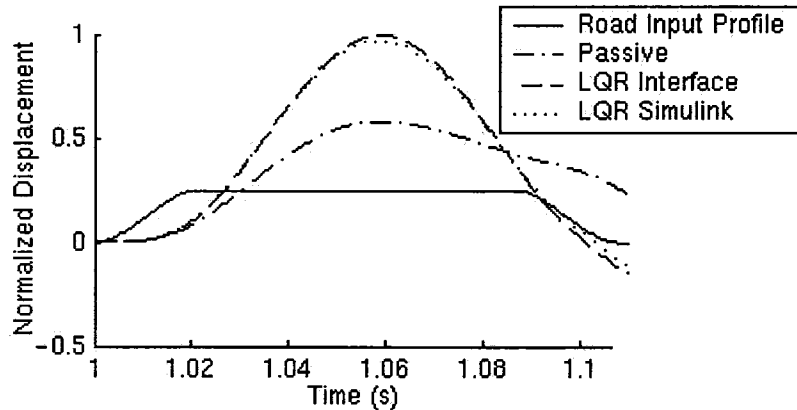
Figure 6.26: Unsprung mass displacement of corner 11

A shortcoming of the LQR controller is that in its current form the weighting matrices do not directly control the sprung mass acceleration. As shown in Figure 6.27, the sprung mass velocity of the active suspension is effectively maintained at zero due to the large bias in the Q matrix. However in certain situations, the controller's quest to drive the velocity to zero may increase the body acceleration due to the tendency to immediately and sharply drive the velocity to zero. In other words, to keep acceleration low may at times require a gradual reduction in system velocity, something that this controller does not consider.

- 68 -
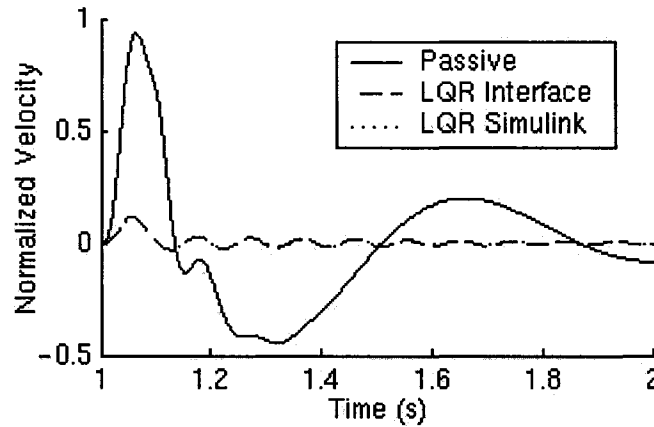
Figure 6.27: Sprung mass vertical velocity[†]
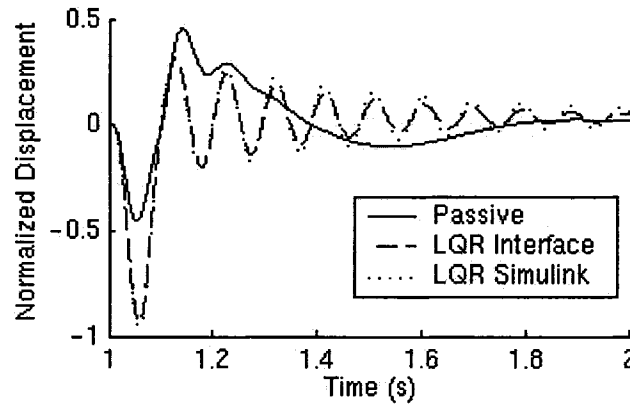
Figure 6.28: Suspension displacement of corner 11[†]

This full car model, unlike the previous quarter car model, is inherently nonlinear due to the two rotational degrees of freedom of the body. Despite this, high correlation is observed between the linearized version of the vehicle and the corresponding nonlinear interface model for both the passive and active systems. The differences that are seen are probably due to a combination of the slight nonlinearity of the full car model and the effects of interfacing ADAMS with Simulink.

6.3.1.2 Eigen Analysis

Passive Suspension		
Natural Frequency (rad/s)	Damping Ratio	Eigenvalues
5.67	0.198	-1.13 ± 5.56i
9.00	0.260	-2.34 ± 8.70i
11.9	0.495	-5.90 ± 10.4i
68.8	0.242	-16.6 ± 66.8i
69.7	0.233	-16.2 ± 67.7i
69.9	0.335	-23.4 ± 65.8i
73.3	0.312	-22.9 ± 69.6i

Table 6.4: Eigen analysis of the passive system

[†]Notice: the two active responses are nearly indistinguishable from one another.

- 69 -

LQR Suspension		
Natural Frequency (rad/s)	Damping Ratio	Eigenvalues
n/a	>1	-0.696
n/a	>1	-9.90e-2
n/a	>1	-0.132
66.2	2.80e-2	-1.90 ± 66.2i
67.7	6.00e-2	-4.10 ± 67.6i
70.2	2.80e-2	-1.95 ± 70.2i
73.0	0.372	-27.1 ± 67.8i
n/a	>1	-505
n/a	>1	-841
n/a	>1	-1.11e3

Table 6.5: Eigen analysis of the LQR fully-active system

Table 6.4 and 6.5 show that once again LQR significantly increases the damping associated with the body modes of vibration while decreasing the damping of the unsprung mass vibration. This change in damping may account for the decrease in sprung mass motion and the increase in unsprung mass motion (with respect to the passive system) for the time domain simulation.

Curiously the three dominant eigenvalues of the LQR system have a damping ratio of one, indicating that their modes are overdamped and so have no associated vibration. The dominant eigenvalues of the passive suspension become more positive real and more negative real (the eigenvalues that are overdamped). This illustrates that although LQR guarantees closed-loop stability, it does not make any provisions regarding the level of stability of the resulting system.

Although not shown, the eigen analysis attained from within ADAMS (with the tire spring included) is exactly the same as that shown in Table 6.4.

6.3.1.3 Frequency Response

Figure 6.29 to 6.31 plot the frequency response of the sprung mass acceleration as contributed from each corner of the vehicle. Significant reduction in body acceleration is achieved by properly tuning the LQR controller for ride, most importantly in the region of the sprung mass natural frequency. With this model, invariant points exist at the wheel hop frequency for all three body accelerations as a result of using a simplified vehicle model.
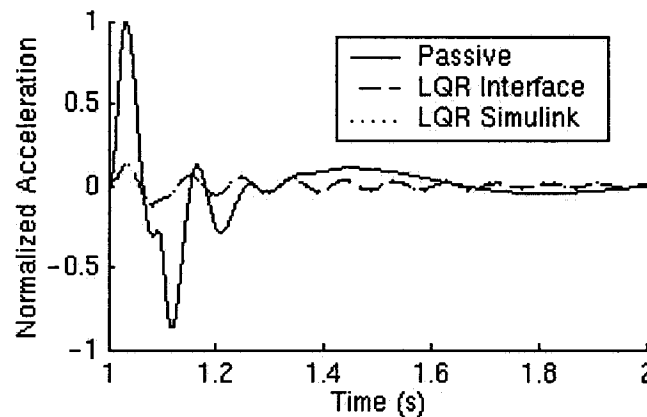
- 70 -
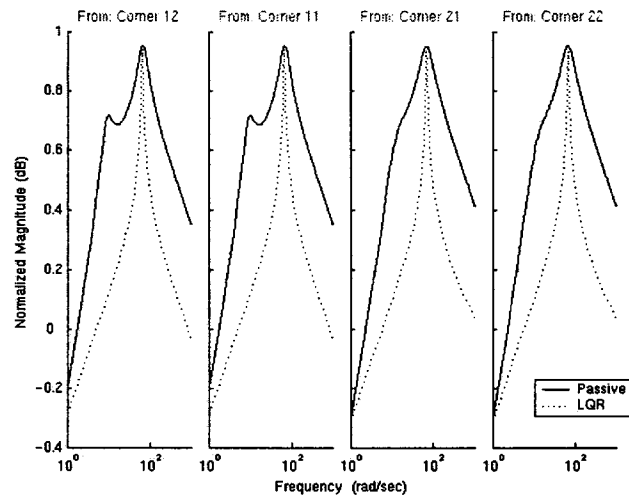
Figure 6.29: *Sprung mass vertical acceleration*
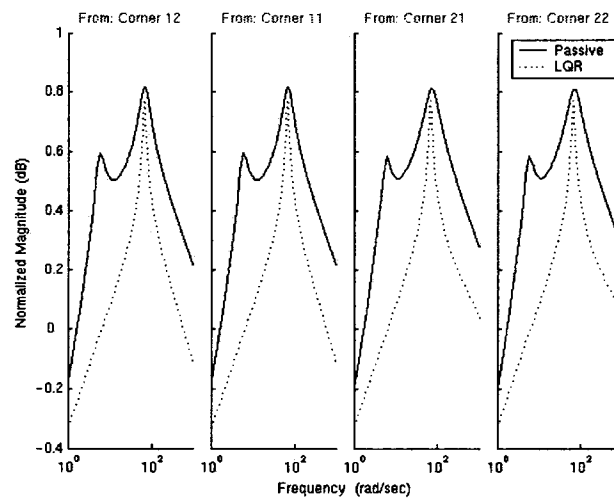
Figure 6.30: *Sprung mass roll acceleration*
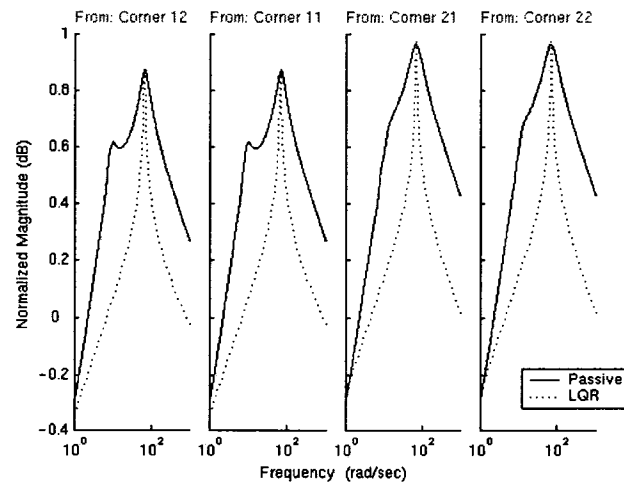
Figure 6.31: *Sprung mass pitch acceleration*

The LQR algorithm when tuned for ride yields a larger deviation in the tire forces at the wheel hop frequency, while decreasing the tire force deviation for low frequency road inputs. In essence, favourable

- 71 -

results are attained near the sprung mass natural frequency, both in terms of ride and traction. The invariant point for the suspension rattle space is also present in the full car model as shown in Figure 6.33. This measure mimics the response of the tire dynamic force, suggesting that the increase in suspension movement near the unsprung mass natural frequency is the cause of the degradation in tire force.
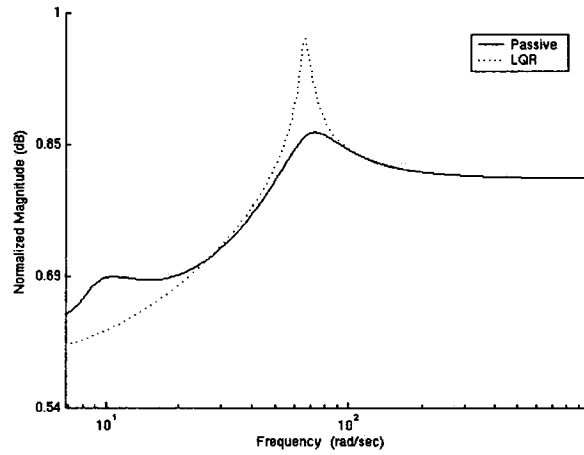
Figure 6.32: Tire dynamic force of corner 11

In considering these frequency response plots, along with the eigen analysis of the passive and the active systems an explanation of the responses can be forged. Since LQR reduces the damping associated with the unsprung mass while increasing the damping of the sprung mass, the sprung mass sees less acceleration and more tire force movement than the passive system, while the unsprung mass experiences the reverse.
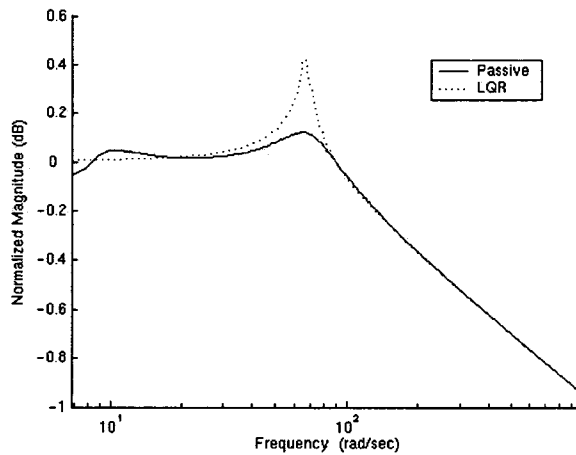
Figure 6.33: Suspension displacement of corner 11

6.3.2 Fully-Active versus Semi-Active

For the models shown in this section the following parameters are used. Unless labelled, the results displayed are for models created entirely in Matlab.

Semi-active high damping coefficient: 1.29kNs/m

Semi-active low damping coefficient: 0Ns/m

6.3.2.1 Time Domain Simulation

With the more aggressive controller than that used for the quarter car model, the fully-active system performs much better than the semi-active suspension in increasing ride comfort. This is demonstrated in Figure 6.34 to 6.36 where body acceleration is drastically reduced by the fully-active suspension. The semi-active suspension is successful in that it also makes significant gains over the passive suspension in reducing the acceleration levels. Most impressive is its pitch acceleration response, which rivals the fully-active suspension.

Since the linear and nonlinear models are almost identical in their response, only the linear model responses are shown.
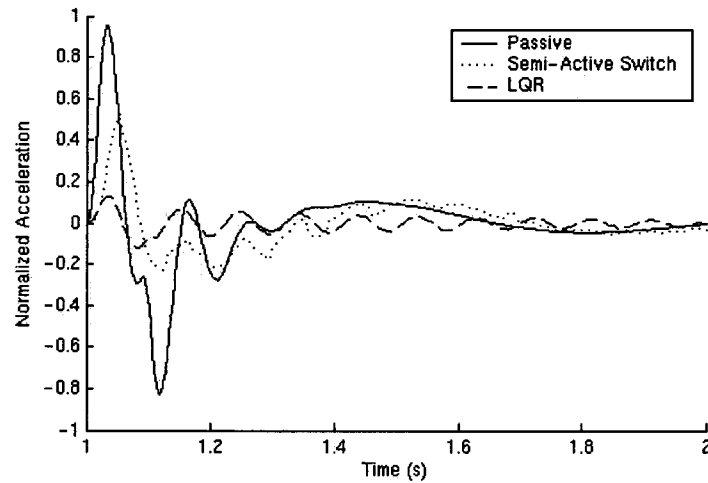
Figure 6.34: Sprung mass vertical acceleration
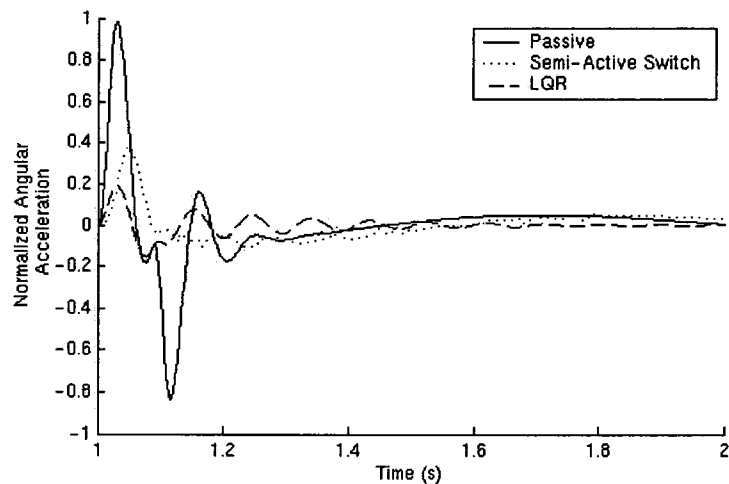
Figure 6.35: Sprung mass roll acceleration

- 73 -
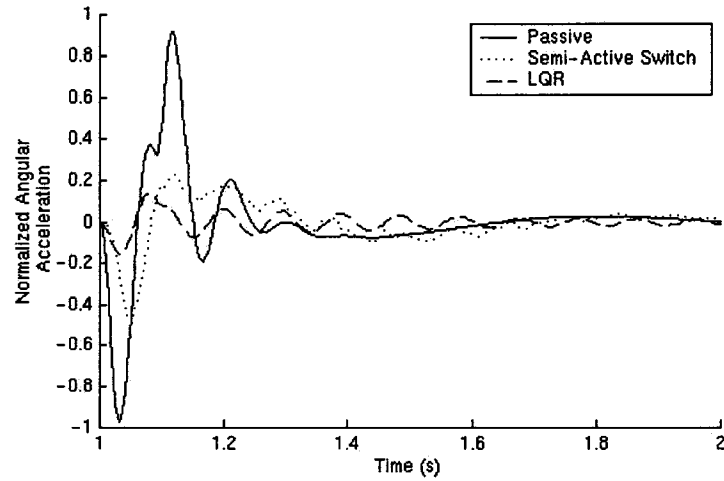
Figure 6.36: Sprung mass pitch acceleration

Figures 6.37 and 6.38 demonstrate that the semi-active system is better than the fully-active system in conserving tire grip and reducing the suspension working space. Even though the semi-active system has significantly less damping than the fully-active system, it demonstrates less unsprung mass oscillatory behaviour.
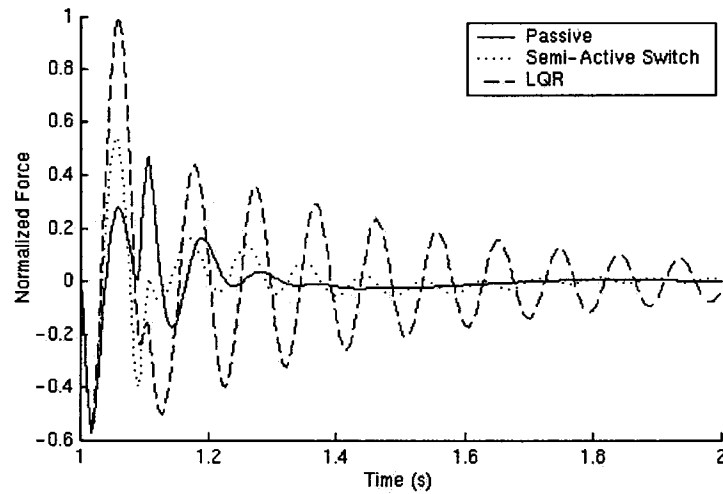
Figure 6.37: Tire dynamic force of corner 11

- 74 -
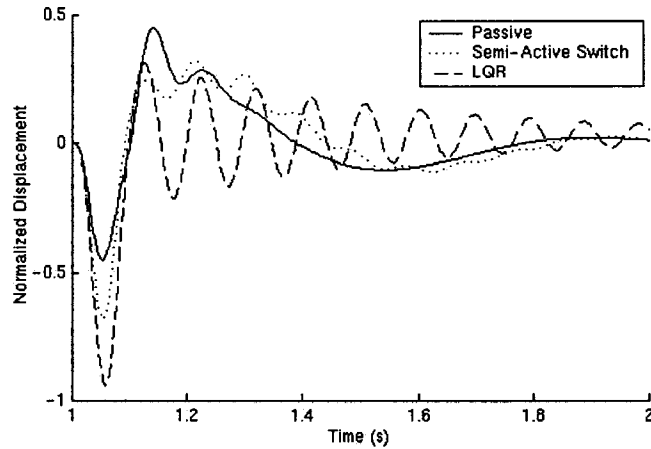
Figure 6.38: Suspension displacement of corner 11
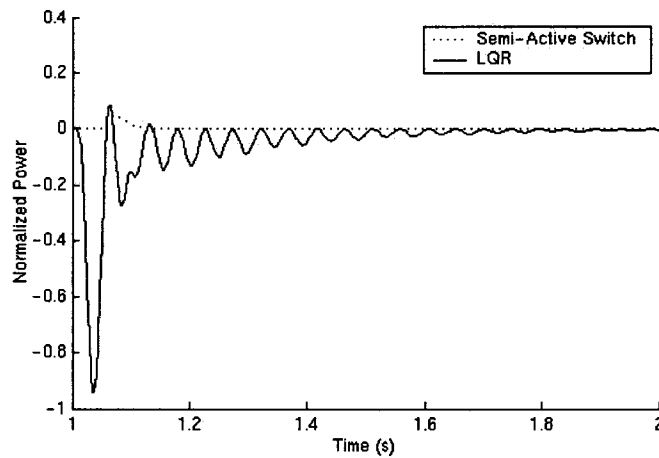
*Figure 6.39: Power consumption of active element
while traveling over speed bump, corner 11*

The power consumed by the fully-active system is significantly greater than that dissipated by the semi-active damper. The response of the LQR element is also much more oscillatory than the quarter car model; this is attributed to the weights used. As expected the fully-active system requires more power than semi-active damping during the speed bump disturbance.
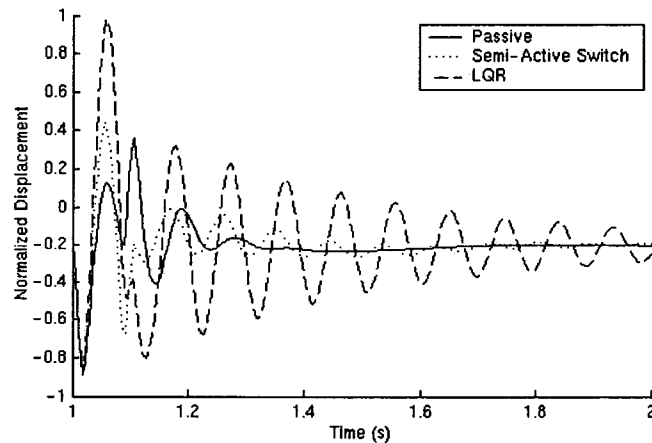
Figure 6.40: Tire lift off tracking function TL of corner 11

- 75 -

Although tire lift off (Figure 6.40) occurs for the passive suspension, significantly more occurs for both fully-active and semi-active systems. This is in accordance with the response of Figure 6.38 which indicates that both active systems increase wheel movement.

6.3.2.2 Eigen Analysis

When switched to high damping, Table 6.6 indicates that the behaviour of the body vibration modes (the first three eigenvalues listed) are similar to the body modes of the passive system, but with slightly more damping. However, for the remaining modes that deal with the unsprung mass, the semi-active and the passive system differ substantially, since the semi-active skyhook algorithm drastically reduces the modal damping. These results indicate that when switched to high damping, the semi-active system should slightly improve the sprung mass movement at the expense of the unsprung mass motion.

Semi-Active Suspension, High Damping		
Natural Frequency (rad/s)	Damping Ratio	Eigenvalues
5.62	0.218	-1.23 ± 5.49i
8.86	0.286	-2.54 ± 8.49i
11.3	0.522	-5.90 ± 9.65i
69.9	8.90e-4	-6.20e-2 ± 69.9i
69.9	4.26e-3	-0.298 ± 69.9i
73.7	8.16e-3	-0.602 ± 73.7i
73.7	9.40e-4	-6.90e-2 ± 73.7i

Table 6.6: Eigen analysis of semi-active damping when damping is on

Semi-Active Suspension, Low Damping		
Natural Frequency (rad/s)	Damping Ratio	Eigenvalues
5.62	0	0 ± 5.62i
8.86	0	0 ± 8.86i
11.3	0	0 ± 11.3i
69.9	0	0 ± 69.9i
69.1	0	0 ± 69.1i
73.7	0	0 ± 73.7i
73.8	0	0 ± 73.8i

Table 6.7: Eigen analysis of semi-active damping when damping is off

6.3.3 Kalman Filter

The required dimensions for the noise co-variance matrices for the quarter car model differ from those for this model, and so the matrices used for the quarter car are extended to construct this Kalman filter. The matrices used are:

Q_n=diag[5.06e-4 5.06e-4 5.06e-4 5.06e-4]

R_n=diag[4.76e-4 4.76e-4 4.76e-4 4.76e-4 4.76e-4 4.76e-4 4.76e-4 4.76e-4 0.25 0.25 0.25 0.25 0.25 0.25]

6.3.3.1 Time Domain Simulation

In contrast to the Kalman filter implemented for the quarter car model, with the full car model it is assumed that sensors measure the sprung mass acceleration and velocity and the strut relative velocity and displacement. The estimator is generally very good in finding the true states; sample results are shown in Figure 6.41 to 6.44, however it has difficulty in estimating the displacement of the cabin body (Figure 6.42). As demonstrated with the quarter car model, a better estimate of the displacement can be found by integrating the corresponding velocity state estimate instead of using the Kalman response.
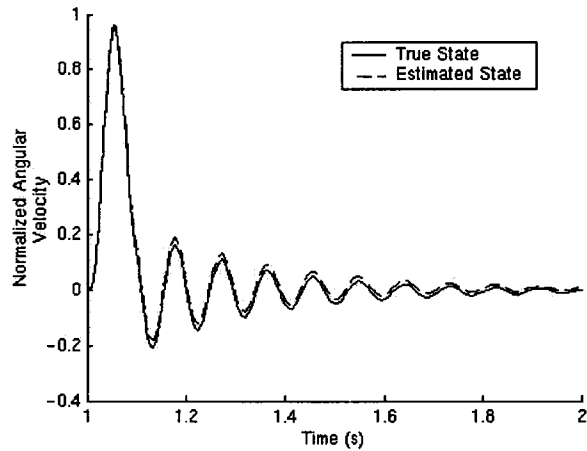
Figure 6.41: Angular pitch velocity[†]
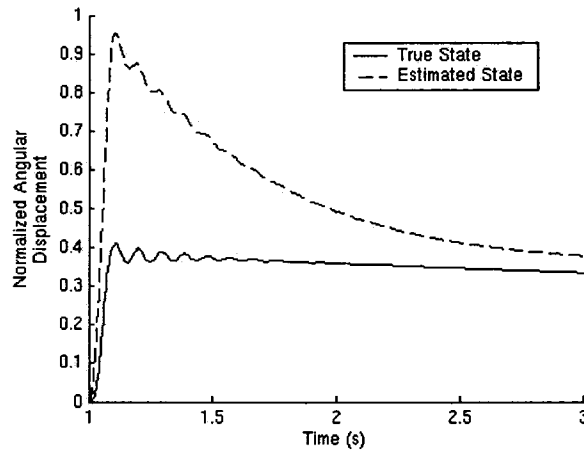
Figure 6.42: Angular pitch displacement
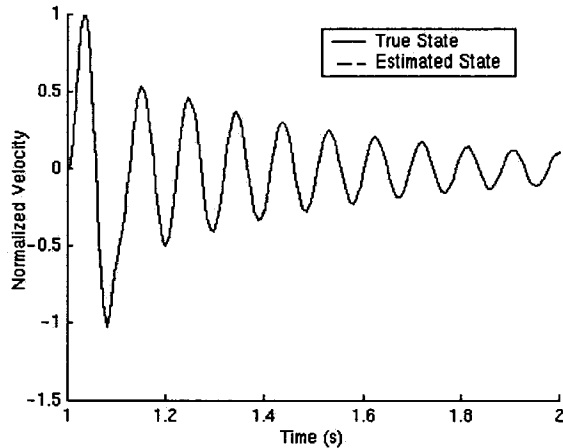
Figure 6.43: Velocity of corner 11[†]
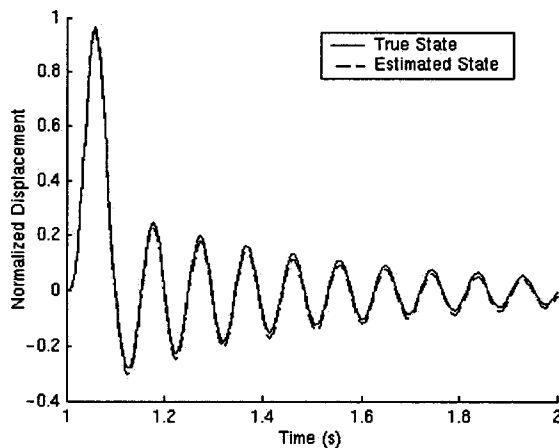
Figure 6.44: Displacement of corner 11[†]

6.4 Iltis Quarter Car Model

6.4.1 Fully-Active Suspension

The LQR controller is largely weighted towards decreasing the sprung mass velocity (first number in the Q matrix below) and then decreasing the wheel displacement. Unless otherwise stated, the values below are used for the results of the LQR system that follow. The corresponding state variables are listed in Appendix A.

Q=diag[5e9 100 100 1e4]

R=[1e-2]

The Iltis model is inherently very nonlinear due to its kinematic suspension that introduces rotational degrees of freedom and due to its variable rate springs and dampers. As a result, significant differences are seen between the linearized equations of motions solved entirely in Simulink and interfacing the nonlinear ADAMS model with the Simulink controller. During linearization, the nonlinear spring and damper are assigned a constant stiffness value by linearizing their force generation equation about a specific configuration (called the set–point).

[†]*Notice: the two active responses are nearly indistinguishable from one another.*

- 78 -

The simplification is significant since the more the linear model deviates from the set-point configuration the more it will differ from the behaviour of the nonlinear model. This especially holds true for the Iltis model since some of its force producing elements vary with its input to the fourth order. Nonetheless, comparing the nonlinear and linear models is a useful exercise in gauging the degree to which these nonlinearities influence the response.

6.4.1.1 Time Domain Simulation
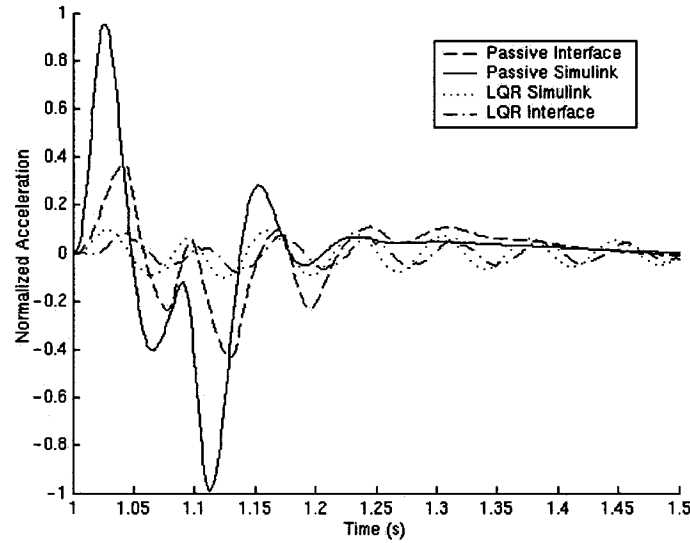
Figure 6.45: Sprung mass vertical acceleration

Figure 6.45, 6.48 and 6.49 show a significant difference between the response of the linear passive Simulink model and the nonlinear passive interface model. It appears as though the linear version has stiffer spring and damper rates than the nonlinear Iltis model, since the nonlinear passive model sees smaller cabin acceleration with greater tire force fluctuation. To confirm this theory the strut spring is linearized and compared to its original nonlinear form, which is:

$$F_s = -4.0092 \times 10^6 + (2.8397 \times 10^7)x - (6.7061 \times 10^7)x^2 + (5.2796 \times 10^7)x^3 \qquad x \text{ in } [m] \qquad (6.6)$$

The derivative is taken and evaluated at the strut length when the vehicle is in static equilibrium ($x_0 = 0.42896m$). The result is the linear spring rate.

$$\left.\frac{\partial F_s}{\partial x}\right|_{x_0} = 2.8397 \times 10^7 - 2(6.7061 \times 10^7)x + 3(5.2796 \times 10^7)x^2 \qquad (6.7)$$

$$k_s = \left.\frac{\partial F_s}{\partial x}\right|_{x_0} = 8.48kN/m$$

This result is then used in the following equation that defines the new linear spring force, where $F_s(x_0)$ is the new spring preload at the set-point (427N):

$$F_{lnr} = \left.\frac{\partial F_s}{\partial x}\right|_{x_0} \Delta x + F_s(x_0) \qquad (6.8)$$

- 79 -

In graphing and comparing the force generated by the linear and the nonlinear spring in Figure 6.46, for a certain range of spring length the linear spring generates a greater negative force (spring in compression) than its nonlinear version. When reviewing the results from Figure 6.49, the spring length stays within the range of 0.43m and 0.45m. In other words for the majority of the simulation the linear version generates more force than its nonlinear counterpart. A less significant cause for the response differences is from the linearization of the rotational degrees of freedom, as discussed in Chapter 4.
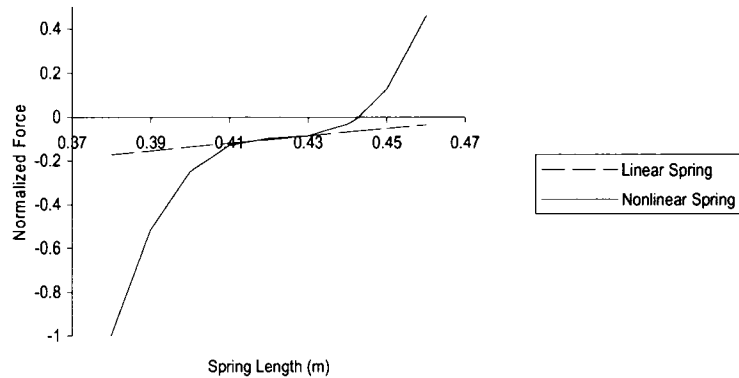
Figure 6.46: Force produced for the linear and nonlinear spring
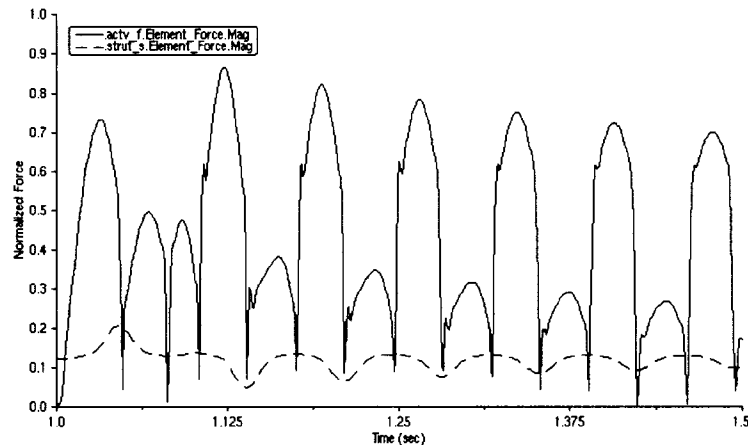
Figure 6.47: Force magnitude (absolute) of the passive nonlinear spring and the active element

In contrast to the passive system, the linear and nonlinear versions of the fully-active system have an extremely similar response. The reason is that the active element produces forces much greater than the passive elements (more than an order of magnitude greater) as seen in Figure 6.47. Here the active element force is the solid line series and the nonlinear passive spring force is the dashed series. The addition of the active element makes the differences caused by linearizing the spring force element almost insignificant.

Furthermore, although the active system drastically reduces the body acceleration, a small fluctuation in acceleration is seen after the disturbance is encountered. This characteristic was also seen in the full car lumped mass response.

- 80 -
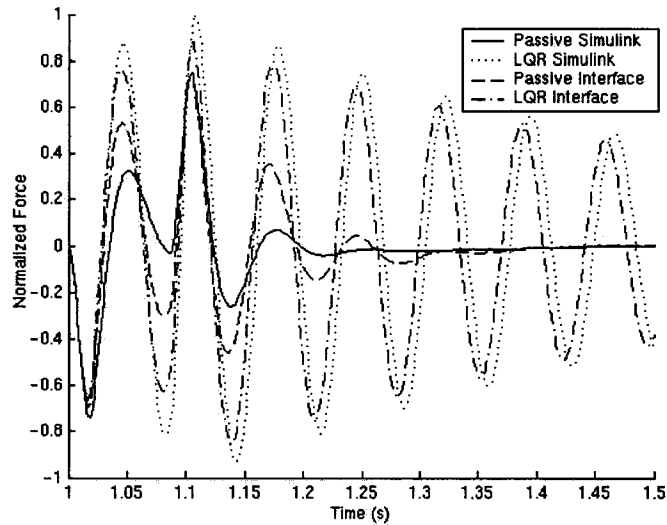
Figure 6.48: Tire dynamic force

The tire forces in Figure 6.48 are consistent with previous results which show that the active system increases the force fluctuation for an aggressive controller. In addition the nonlinear passive interface model sees more change in tire force than the linear passive system since the nonlinear springs tend to generate less resistive suspension force.
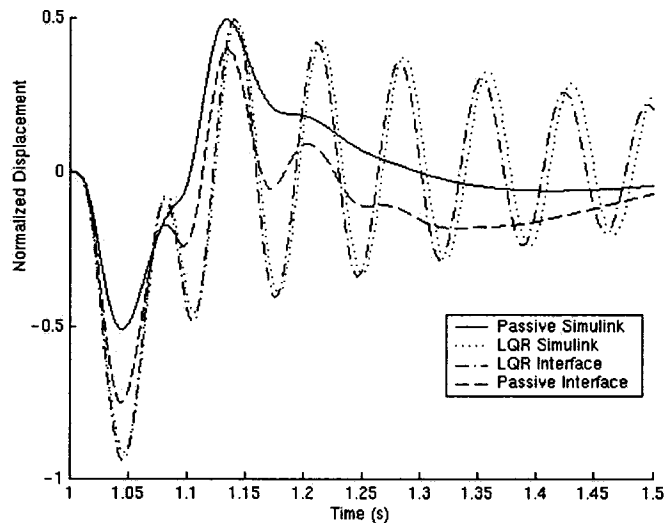
Figure 6.49: Suspension displacement

6.4.1.2 Eigen Analysis

The linear equations of motion synthesized by the static export and gravity export methods yield remarkably similar results. Although these models are created using two different processes, their resulting eigenvalues, natural frequency and damping rates are nearly identical (Table 6.8 and 6.9). Why this is the case is not known, a deeper knowledge of the algorithm used by ADAMS to linearize the system is needed. It was expected that the linear system resulting from the static export process would be noticeably stiffer since gravity and spring preload are not included during its linearization.

Because the eigenvalues of these two systems are essentially identical, they yield identical responses, not only in time domain and frequency response but also in their production of the LQR gain and Kalman filter. Hence in the interest of space the results of only one of these two systems will be shown.

Passive Suspension		
Natural Frequency (rad/s)	Damping Ratio	Eigenvalues
10.1	0.556	-5.64 ± 8.43i
85.9	0.363	-31.2 ± 79.1i

Table 6.8: Eigen analysis of the passive system, static export method

Passive Suspension		
Natural Frequency (rad/s)	Damping Ratio	Eigenvalues
10.1	0.560	-5.65 ± 8.36i
85.8	0.363	-31.2 ± 79.1i

Table 6.9: Eigen analysis of the passive system, gravity export method

Table 6.10 is an eigen analysis conducted within ADAMS using the complete nonlinear model (tire spring included). These values are thought to be more accurate than those generated from the static export and gravity export method since linearization is done once without rebuilding the tire spring within Simulink. Nonetheless all three linearization methods produce a linear model that is essentially the same.

Passive Suspension		
Natural Frequency (rad/s)	Damping Ratio	Eigenvalues
10.1	0.559	-5.64 ± 8.37i
85.8	0.363	-31.2 ± 79.1i

Table 6.10: Eigen analysis of the passive system, from ADAMS linearization

Yet again the fully-active suspension changes the eigenvalue of the sprung mass vibration (first row of Table 6.8, 6.9 and 6.10) to being overdamped with the dominant eigenvalue moving closer to positive real. At the same time the eigenvalue representing the unsprung mass vibration gets less damping in the active linear model.

At first the change of the sprung mass eigenvalue to becoming more positive real may seem alarming as it indicates that the system response is closer to becoming unbounded and unstable. However this dominant eigenvalue is also overdamped, meaning that when its associated natural frequency is excited the response will not be oscillatory. Hence, even though the eigenvalue is more positive real for the active system, because it is overdamped it will probably never be actually excited.

LQR Suspension		
Natural Frequency (rad/s)	Damping Ratio	Eigenvalues
n/a	>1	-7.50e-2
87.2	2.30e-2	-2.04 ± 87.2i
n/a	>1	-1.33e3

Table 6.11: Eigen analysis of the LQR fully-active system, static export method

6.4.1.3 Frequency Response
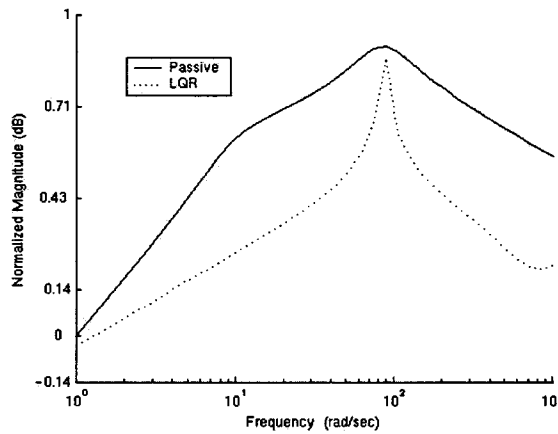
Figure 6.50: Sprung mass vertical acceleration
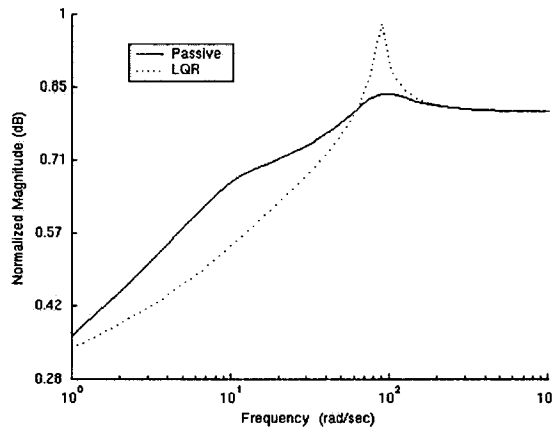
Figure 6.51: Tire dynamic force

Remnants of the invariant point from the previous two vehicle models exist in the Iltis frequency response plots (Figure 6.50 to 6.52). For example, for the sprung mass acceleration the gap between the active and passive system tends to close drastically in the range of the wheel hop. At the same time an invariant point is present for the suspension displacement and the tire force response since at a particular frequency the active system has no effect on the system response, regardless of the LQR gain used.

Encouragingly, the body acceleration is reduced throughout the frequency range, particularly for frequencies around the sprung mass resonance. These responses also confirm that for this manoeuvre, an increase in ride comes at a cost of greater vehicle suspension displacement at the wheel hop frequency,

- 83 -

translating to greater tire forces. Although the system now includes a kinematic suspension, the system behaviour for the most part mimics that of the lumped mass vehicles.
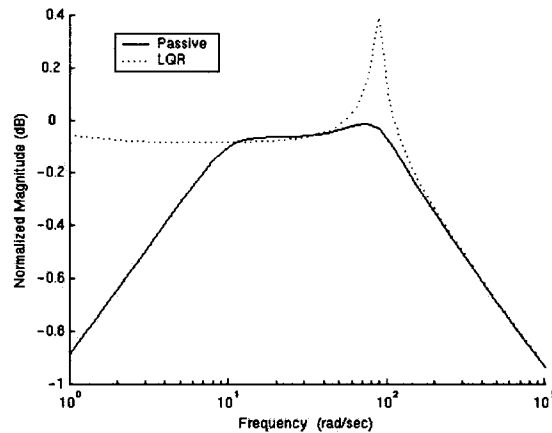
Figure 6.52: Suspension displacement

6.4.2 Fully-Active versus Semi-Active

For the models shown in this section, the following parameters are used for the semi-active switch.

High damping coefficient: 30kNs/m

Low damping coefficient: 0Ns/m

6.4.2.1 Time Domain Simulation

Because of the significant differences between the linear and nonlinear vehicle models, only the interfacing systems are analyzed in this section.
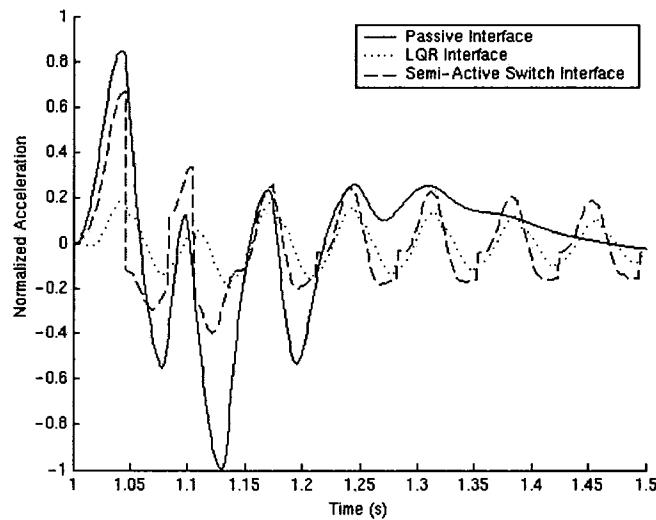
Figure 6.53: Sprung mass vertical acceleration

Both the semi-active and fully-active systems decrease the body acceleration while substantially increasing the tire normal forces and the suspension displacements. The discrete changes in the body acceleration of the semi-active system are produced by the instantaneous switching of the controller between high and low damping. This occurs because the switching algorithm does not consider the

detrimental effects of instantaneously switching between high and low damping on the sprung mass acceleration; for this a more sophisticated algorithm is required.
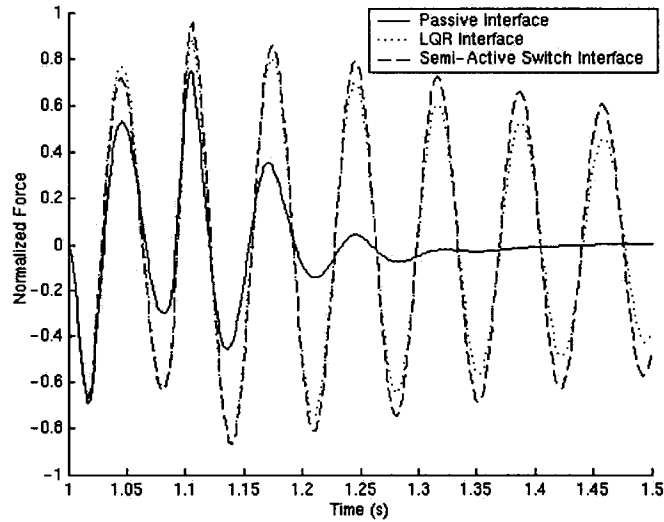
Figure 6.54: Tire dynamic force

Although at times it is slightly dissipative (Figure 6.56), the fully-active system is mostly absorptive of power in its attempt to decrease cabin movement. On the other hand the semi-active system is only dissipative and reaches magnitudes far smaller than its fully-active counterpart. As Figure 6.57 indicates, both active systems increase the tendency for tire lift.
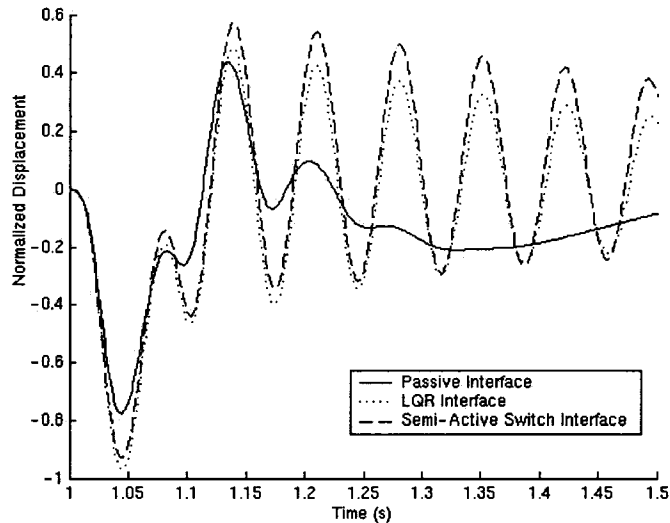
Figure 6.55: Suspension displacement

- 85 -
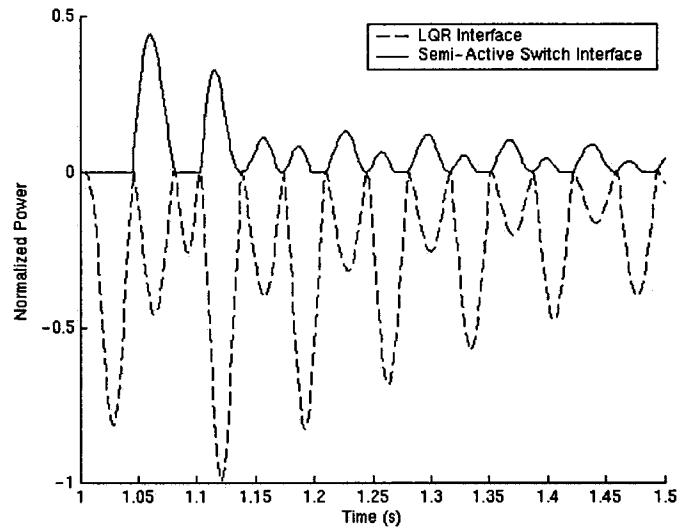
Figure 6.56: Power consumption of active element while traveling over speed bump
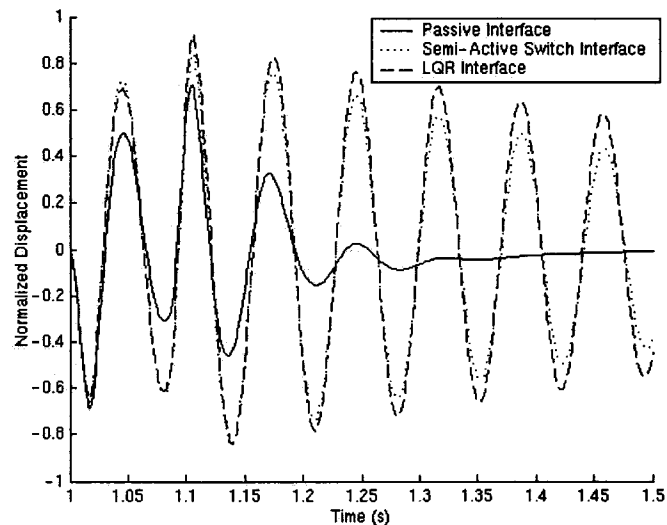
Figure 6.57: Tire lift off tracking function TL

6.4.2.2 Eigen Analysis

Table 6.12 suggests that when damping is on, the sprung mass mode of vibration becomes overdamped while the unsprung mass mode damping, relative to the passive system, is significantly reduced. The system is overdamped when switched high because of the excessively large damping coefficient used for this model. However, as shown in Figure 6.58, being overdamped does not significantly influence the vehicle response during the bump disturbance since the controller is mostly switched off during this time. Instead, its influence is greatest after the disturbance, when the E.C.U. is switched to high damping.

- 86 -

Semi-Active Suspension, High Damping		
Natural Frequency (rad/s)	Damping Ratio	Eigenvalues
n/a	>1	-1.83
n/a	>1	-52.2
89.2	1.30e-2	-1.19 ± 89.2i

Table 6.12: Eigen analysis of semi-active damping when damping is on, static export method

Semi-Active Suspension, Low Damping		
Natural Frequency (rad/s)	Damping Ratio	Eigenvalues
9.69	0	0 ± 9.69i
89.9	0	0 ± 89.9i

Table 6.13: Eigen analysis of semi-active damping when damping is off, static export method
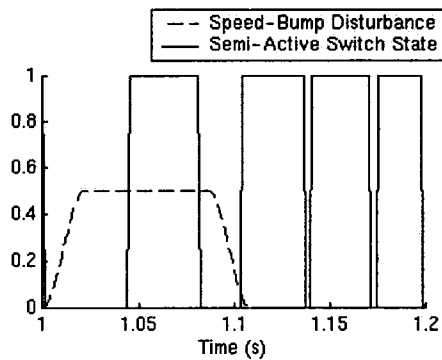
Figure 6.58: State of the semi-active switch and the road disturbance versus time (state 1- high damping, state 0- low damping)

6.4.3 Kalman Filter

The noise matrices used for the Kalman filter are:

Q_n=[5.06e-4]

R_n=diag[4.76e-4 0.25 0.25]

The weight matrices (with the corresponding state variables listed in Appendix A) used for the LQR controller are:

Q=diag[5e9 100 100 1e4]

R=[1e-2]

6.4.3.1 Time Domain Simulation

Displayed in Figure 6.59 to 6.62 are the results of using the nonlinear interface quarter car model with the Kalman filter and the LQR controller. When assuming that the sensor measures are the sprung mass velocity and acceleration, and the suspension displacement, the performance of the filter is not as good as with the previous vehicle models. A reason may be that the Kalman filter design is based on the constant eigenvalue linear vehicle model. However in the results below the state estimator is used with the nonlinear version of the vehicle with changing eigenvalues, suggesting that the filter may not be optimal for this nonlinear model. Nonetheless, reasonable state estimates are produced by the filter, and these drive the

- 87 -

estimate error to zero with time. Improved performance may be attained by using a different set of sensor measurements.
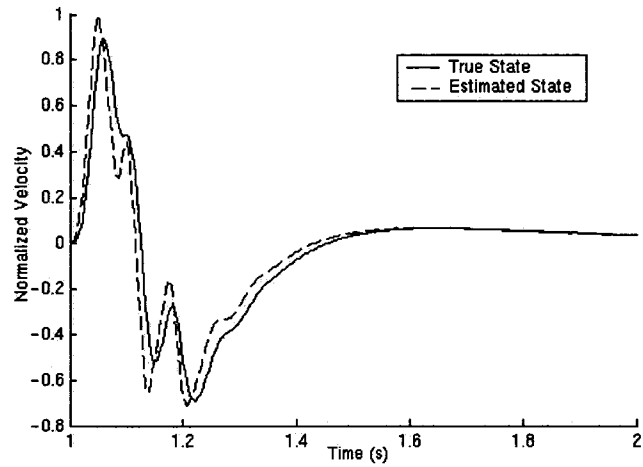
Figure 6.59: Sprung mass velocity
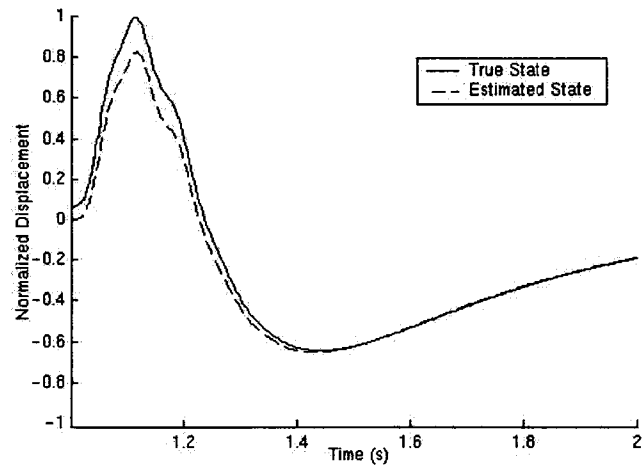
Figure 6.60: Sprung mass displacement
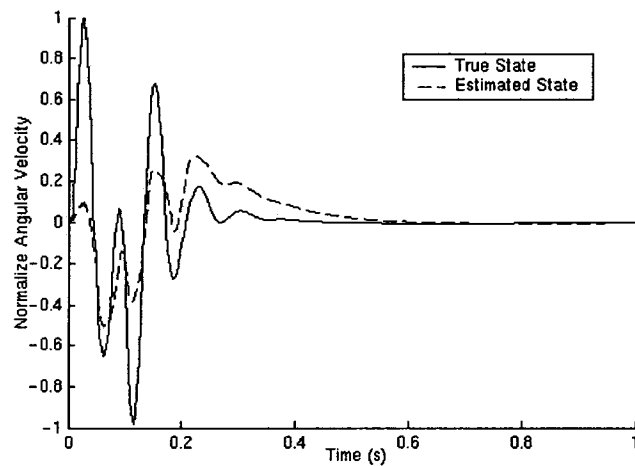
Figure 6.61: Lower control arm angular velocity

Figure 6.62: Lower control arm angular displacement

6.5 Iltis Full Car Model

6.5.1 Fully-Active Suspension

In remaining consistent with the previous models, here the states that are the most to least weighted are the sprung mass: pitch velocity, pitch displacement, roll velocity, roll displacement and vertical velocity. The bounce mode is not weighted as much since studies have shown that pitch and roll motions are more bothersome to passengers. Here the Q and R weight matrices are diagonal matrices and unless otherwise stated, the matrices below are used for the LQR results. The corresponding state variables are listed in Appendix A.

Q=diag[1 1 1 1 1 1 1 1e9 1e9 1 1 1 1 2e9 1e9 1 1 1e9 1]

R=diag[4e-2 4e-2 4e-2 4e-2]

6.5.1.1 Time Domain Simulation

As with the quarter car Iltis, the passive nonlinear and linear model show significant differences in their response for Figure 6.63 to 6.65. Like the quarter car Iltis, this is attributed to the stiffness difference between the linear and nonlinear passive springs. The linear model tends to have greater acceleration initially but then generally sees less than the nonlinear version after the disturbance. A reason may be that as the strut changes in length with time, the nonlinear elements generate both greater and smaller forces than their linear version. This would change the relative stiffness of the two models as time proceeds.

The fully-active suspension is most effective in reducing the acceleration peaks of the sprung mass acceleration at the expense of introducing a low amplitude high frequency acceleration response later on in time for the vertical and roll acceleration.

Figure 6.63: Sprung mass vertical acceleration
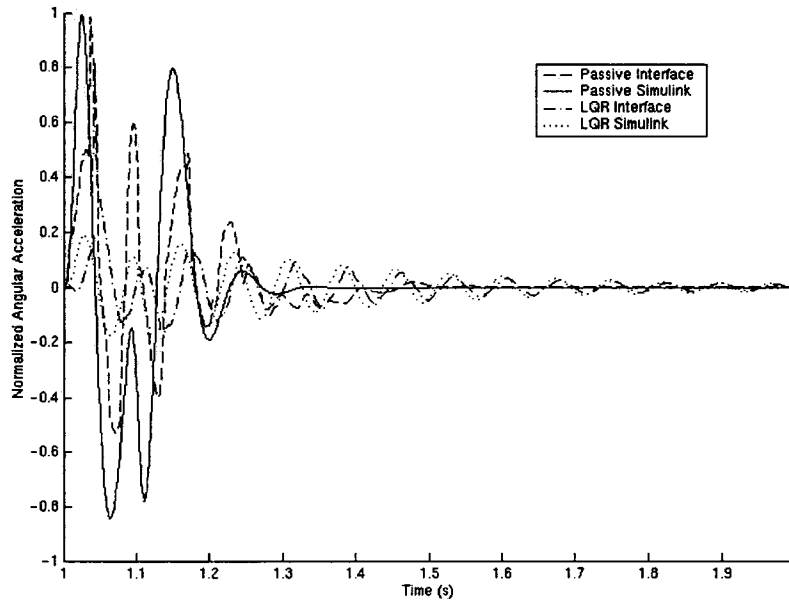
Figure 6.64: Sprung mass roll acceleration

- 90 -
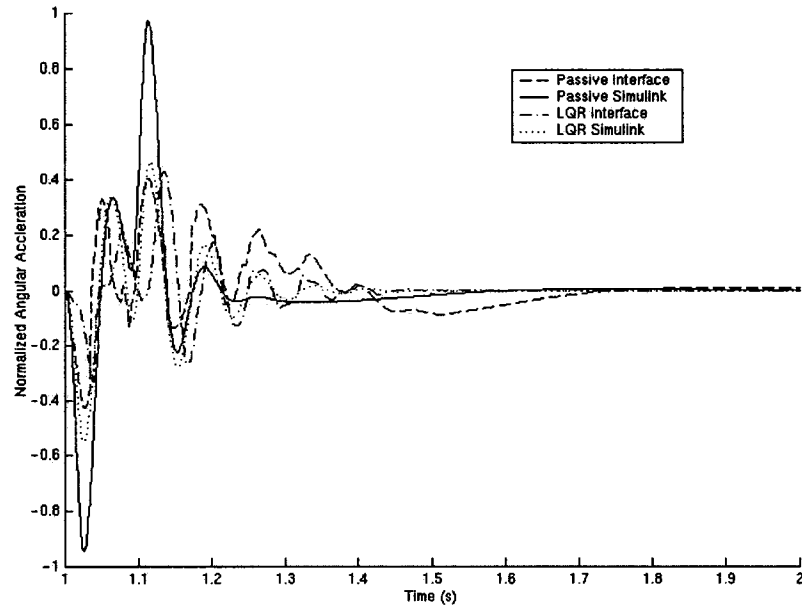
Figure 6.65: Sprung mass pitch acceleration

For the responses in Figure 6.66 and 6.67, the linearized Simulink LQR model sees greater tire force and suspension movement than its nonlinear version, even though the behaviour of these two models is similar for the cabin acceleration responses. Regardless of this, both systems demonstrate deterioration in tire normal force and suspension movement compared to the passive systems. The aggressive LQR optimal gain that delivers a significant control force, even when the states of the system are low, is thought to contribute to the oscillatory response after the disturbance is encountered.
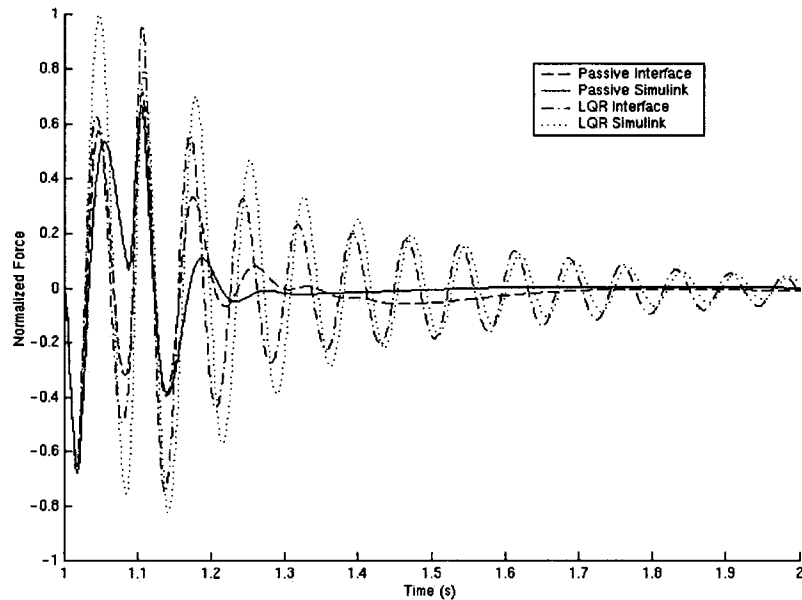
Figure 6.66: Tire dynamic force of corner 11

Like the full car lumped mass model, the active Iltis systems decrease the roll movement of the sprung mass (Figure 6.64). This shows that despite the increase in tire force fluctuation (a result of the road bump input), during a handling manoeuvre with just body inertial inputs, the active systems would better

- 91 -

preserve the change in normal force on the tires due to a decrease in mass transfer. This leads to an increase in lateral tire forces which indicates an increase in handling.
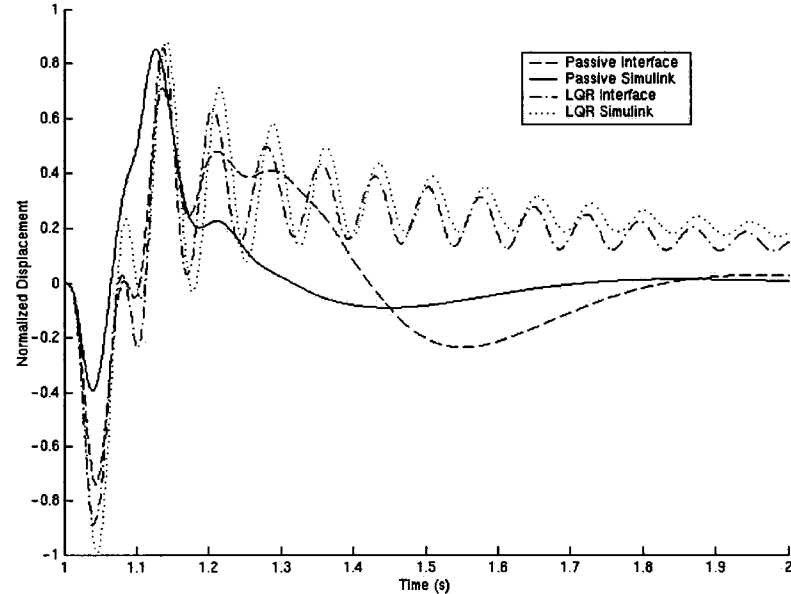
Figure 6.67: Suspension displacement of corner 11

6.5.1.2 Eigen Analysis

Unlike the full car lumped mass model, the Iltis cabin body is free to translate in the x and y direction and rotate about the z-axis. Hence the full car Iltis has three free modes of vibration, meaning that it is completely unconstrained in three directions and so in theory should have three zero eigenvalues. These eigenvalues are shown in the first three rows of Table 6.14, 6.15 and 6.16. They are not exactly zero, but are in the order of 10^{-7} to 10^{-9} with some having positive real components. Even when linearized directly by ADAMS (Table 6.16), the free mode eigenvalues are not exactly zero as a result of numerical error.

Because the free mode eigenvalues of the static export and gravity export models have positive real components, they are slightly unstable. However, all is not lost because the positive real components are of such low order that the linear models still behave reasonably and can still be used to create the E.C.U. This feature cannot be circumvented unless the models are constrained in these free directions- but this would produce a less realistic model.

These tables also demonstrate that all three linearization methods match quite closely, further proving that the static and gravity export linearization procedures yield similar linear models. When these two models are extended to active suspension they yield identical results once more.

- 92 -

Passive Suspension		
Natural Frequency (rad/s)	Damping Ratio	Eigenvalues
0.162	-1.36e-8	2.19e-9 ± 0.161i
0.162	7.35e-8	-1.20e-8 ± 0.162i
0.167	-3.76e-8	6.29e-9 ± 0.167i
8.87	0.492	-4.36 ± 7.72i
10.0	0.561	-5.64 ± 8.32i
n/a	>1	-11.4
n/a	>1	-45.4
71.7	0.347	-24.9 ± 67.2i
85.8	0.360	-30.9 ± 80.0i
86.8	0.363	-31.5 ± 80.6i
89.1	0.346	-31.1 ± -84.4i

Table 6.14: Eigen analysis of the passive system, static export method

Passive Suspension		
Natural Frequency (rad/s)	Damping Ratio	Eigenvalues
0.163	-1.55e-7	2.50e-8 ± 0.161i
0.162	9.04e-7	-1.47e-7 ± 0.162i
0.167	1.94e-7	-3.25e-8 ± 0.167i
8.54	0.511	-4.37 ± 7.34i
n/a	>1	-9.76
10.0	0.563	-5.64 ± 8.27i
n/a	>1	-46.8
71.8	0.348	-25.0 ± 67.3i
85.8	0.360	-30.9 ± 79.9i
86.8	0.363	-31.5 ± 80.8i
90.0	0.346	-31.1 ± 84.4i

Table 6.15: Eigen analysis of the passive system, gravity export method

Passive Suspension		
Natural Frequency (rad/s)	Damping Ratio	Eigenvalues
5.10e-02	4.32e-8	-2.20e-9 ± 5.10e-2i
5.14e-02	2.35e-8	-1.21e-9 ± 5.14e-2i
5.29e-02	1.39e-8	-7.33e-10 ± 5.29e-2i
8.54	0.512	-4.37 ± 7.33i
n/a	>1	-9.71
10.0	0.564	-5.64 ± 8.26i
n/a	>1	-46.9
71.8	0.348	-24.9 ± 67.3i
85.8	0.360	-30.9 ± 80.0i
86.8	0.363	-31.5 ± 80.8i
89.9	0.346	-31.1 ± 84.4i

Table 6.16: Eigen analysis of the passive system, ADAMS linearization

For this vehicle the LQR changes the eigenvalues of the passive system the same way in which the eigenvalues are changed by the previous three vehicle models. Damping is both increased and decreased while the dominant eigenvalues of the LQR suspension are closer to being positive real than the passive

version. It is these changes that contribute to the difference in the behaviour between the passive and fully-active suspension systems.

LQR Suspension		
Natural Frequency (rad/s)	Damping Ratio	Eigenvalues
0.162	7.24e-5	-1.17e-5 ± 0.161i
0.163	2.81e-6	-4.56e-7 ± 0.162i
0.177	7.16e-5	-1.20e-5 ± 0.167i
n/a	>1	-0.660
n/a	>1	-0.850
n/a	>1	-1.08
84.9	0.177	-14.9 ± 83.6i
85.2	0.163	-13.9 ± 84.1i
85.6	3.60e-2	-3.08 ± 85.6i
89.9	0.346	-31.1 ± 84.4i
n/a	>1	-156
n/a	>1	-171
n/a	>1	-886

Table 6.17: Eigen analysis of the LQR fully-active system, static export method

In looking more closely at Table 6.17, with the LQR gain included in the system, the free modes of vibration still exist (listed as the first three eigenvalues). With the LQR algorithm these eigenvalues, that previously had positive real components for the passive suspension, are now slightly negative. This is because, so long as the LQR is solvable, it guarantees system stability regardless if the original plant is stable or not.

6.5.1.3 Frequency Response

As shown earlier the linear version of the Iltis model is somewhat different than the nonlinear response. Hence the following frequency response plots hold less accuracy since they are based on the linear models. Nonetheless, looking at these graphs is a valuable exercise, as it lends insight into the system behaviour for a range of input frequencies.

The LQR system is effective in reducing the body acceleration for road frequencies within the region of the sprung and unsprung mass natural frequency and also for frequencies greater than the unsprung mass natural frequency. For bounce, roll and pitch acceleration the system exhibits an invariant point at the unsprung mass natural frequency. The roll acceleration invariant point is not as strong since at this frequency a small improvement is seen with the fully-active system.

These invariant points for the sprung mass acceleration do not negate the value of fully-active suspension. To improve ride, reduction in system acceleration for frequencies near the sprung mass natural frequency is required- not at the higher frequency of the unsprung mass. Furthermore, Hrovat {31} reported that these invariant points disappear when tire damping is considered, regardless of how small a value is used.

For the weighting matrices selected, there is a cross over point between the passive and the fully-active suspension, below this point the active system generates more body acceleration than the passive

- 94 -

system. This crossover occurs below the sprung mass natural frequency for all three body acceleration responses. However the location of these crossover points are dependant on the values of the weighting matrices and so are not invariant points.
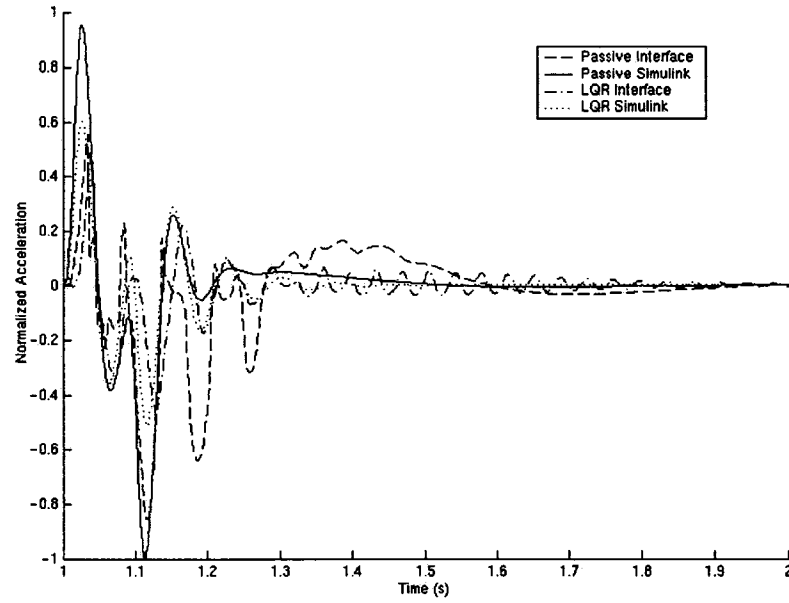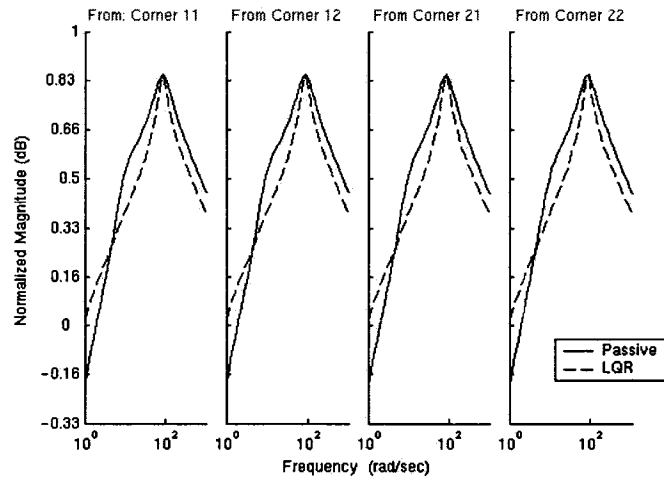

Figure 6.68: Sprung mass vertical acceleration
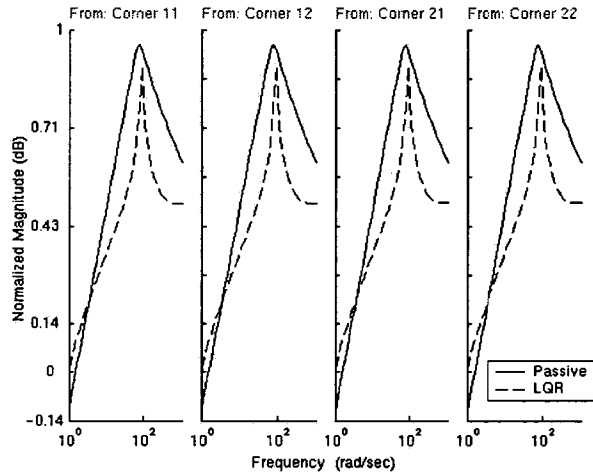
Figure 6.69: Sprung mass roll acceleration
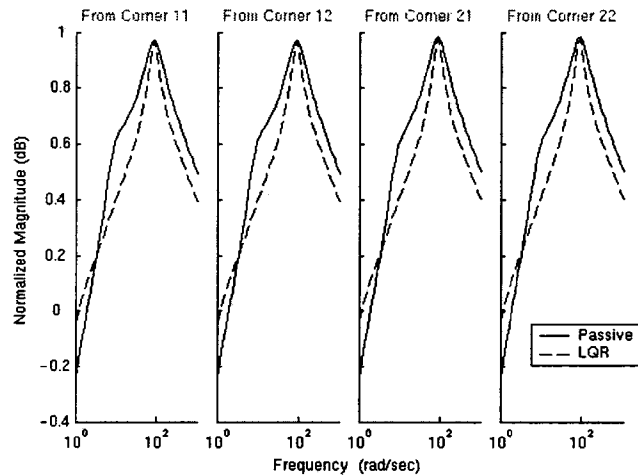
Figure 6.70: Sprung mass pitch acceleration

- 95 -

Once more the linear frequency response shows that the active suspension deteriorates the tire contact forces (Figure 6.71) in the wheel hop region while strengthening it in the unsprung mass resonant region. This response is in accordance with the suspension displacement response which shows a similar pattern. These responses are consistent with the previous models since here the LQR system changes the system eigenvalues the same way it alters the eigenvalues of the previous vehicle models.
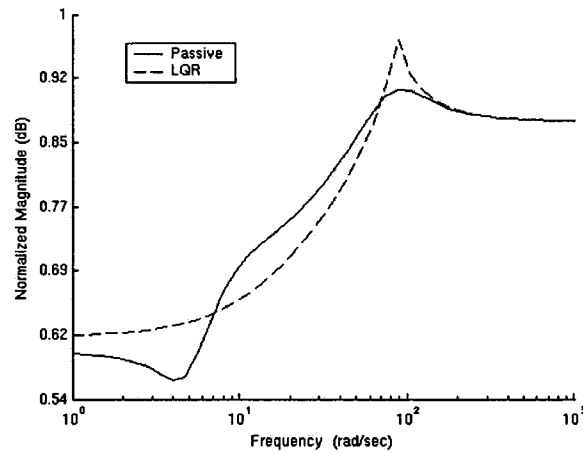
Figure 6.71: Tire dynamic force of corner 11
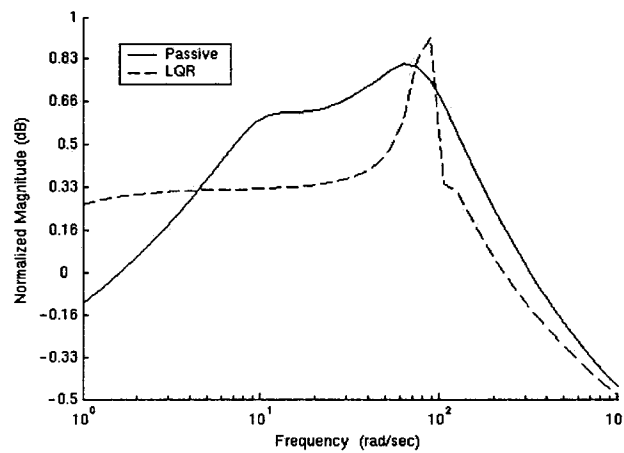
Figure 6.72: Suspension displacement of corner 11

Based on these results, a variable frequency dependant LQR gain may be worthwhile. For frequencies near the sprung mass resonance, the LQR could be switched to improve ride and near the wheel hop the controller could be weighted to improve the tire forces.

6.5.2 Fully-Active versus Semi-Active

For the models in this section, the following parameters are used.

Semi-active high damping coefficient: 7kNs/m

Semi-active low damping coefficient: 0Ns/m

Semi-active passive damper coefficient: 2.5kNs/m

6.5.2.1 Time Domain Simulation

In comparing the nonlinear passive, semi-active and fully-active systems in Figure 6.73 to 6.75, the performance of the semi-active system seems impressive. For the most part it follows the response of the passive system while reducing the acceleration peaks of the body. Also for the weighting matrices used, the LQR algorithm reduces the body acceleration relative to both the semi-active and passive systems. There are instances however where the fully-active system has a worse than passive performance as in Figure 6.75.

It should also be mentioned that the performance of the LQR algorithm is even more impressive when looking at the velocity response of the sprung mass. The fully-active system almost immediately reaches and fluctuates about zero velocity, even when even using a smaller feedback controller gain. In other words the controller is better at reducing the sprung mass velocity than it is at reducing the system acceleration.

Figure 6.73: Sprung mass vertical acceleration
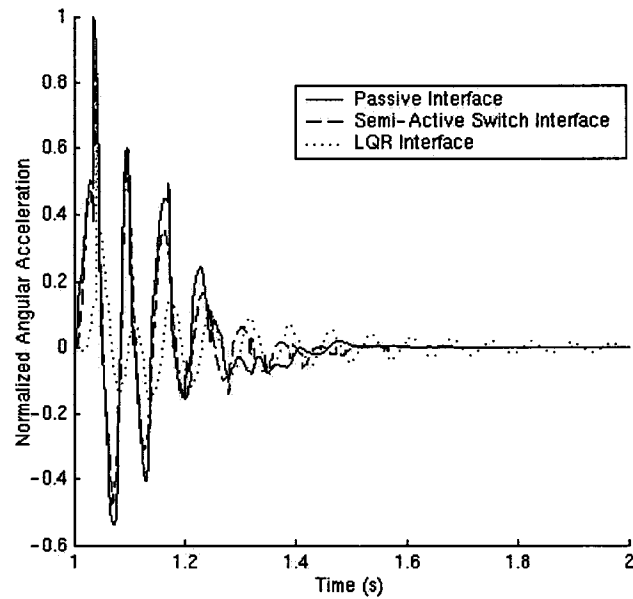
Figure 6.74: Sprung mass roll acceleration
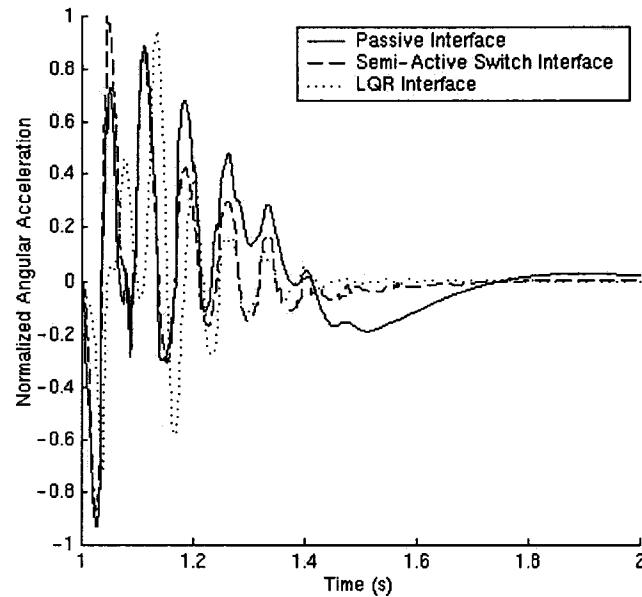
Figure 6.75: Sprung mass pitch acceleration

Similar to the quarter car Iltis response, well after the disturbance the full car sees large suspension and tire force fluctuations while the passive suspension has next to none (Figure 6.76 and 6.77). These fluctuations are caused by the attempts of the controller to stabilize the movements of the sprung mass that has a large inertia. Furthermore these continued oscillations may also be a result of the low damping associated with the unsprung mass as seen in Table 6.17.

- 98 -
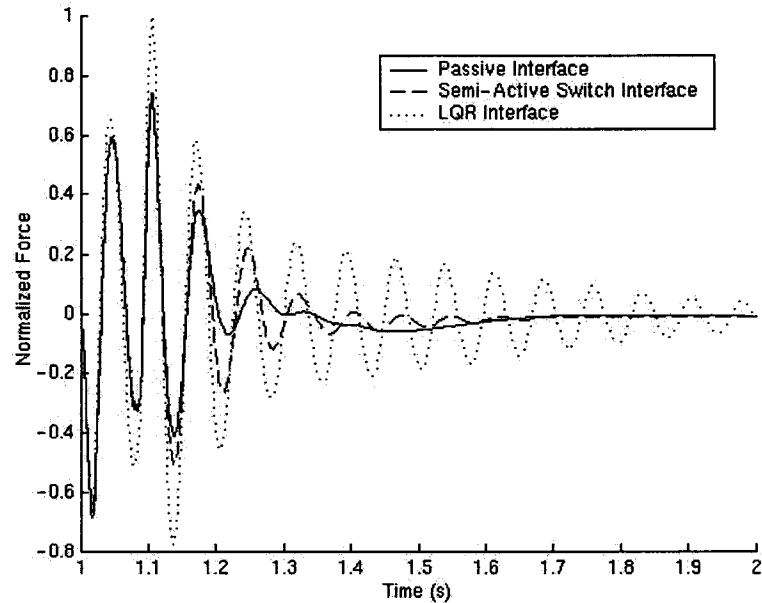
Figure 6.76: Tire dynamic force of corner 11
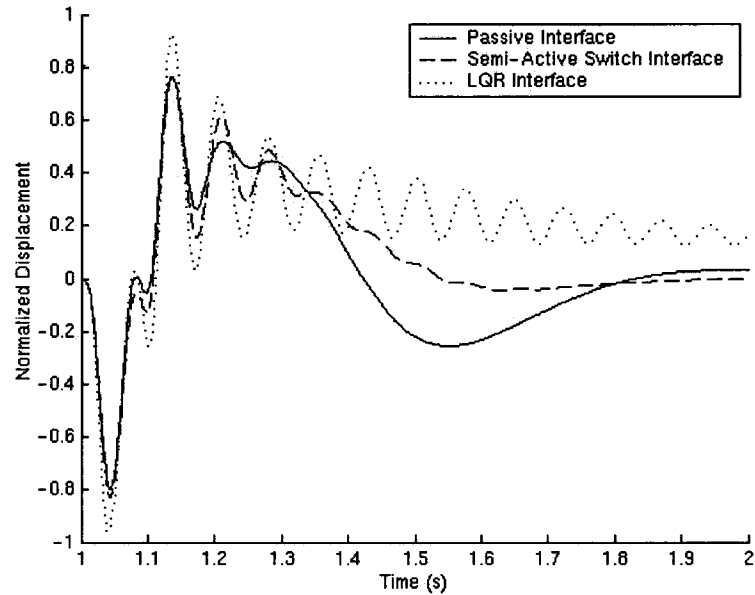
Figure 6.77: Suspension displacement of corner 11

As Figure 6.78 shows, the fully-active system consumes more power than the semi-active damper dissipates. The oscillatory behaviour of the fully-active system is also extended to the power consumption of the active element since the actuator continues to demand power well after the speed bump has been passed. Curiously a large impulsive peak in power is dissipated by the fully-active system ($t \approx 1.04s$) which is not present in the other vehicle models. This is most likely due to a numerical anomaly from the numerical solver in integrating the system equations.
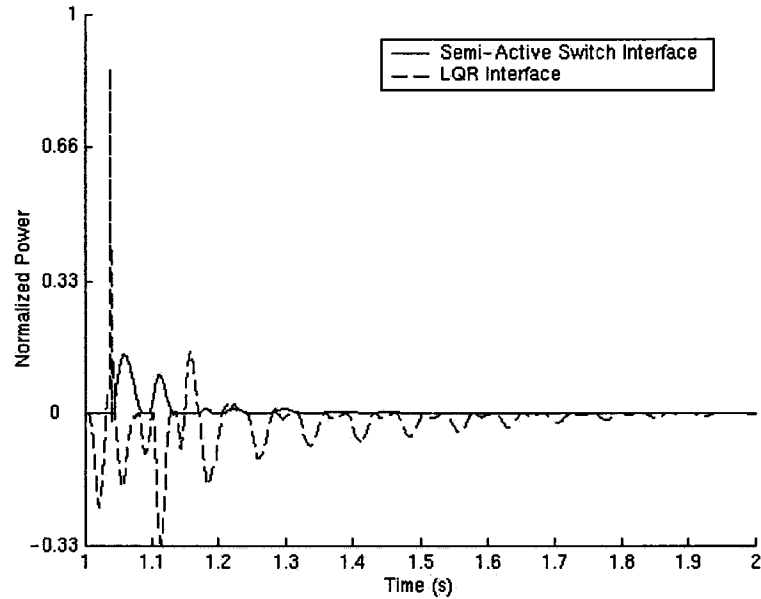
Figure 6.78: Power consumption of active element while traveling over speed bump, corner 11
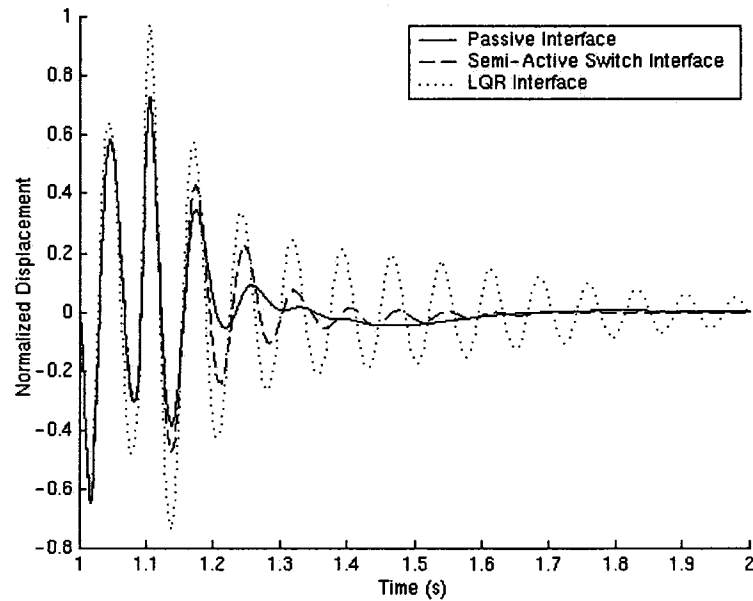
Figure 6.79: Tire lift off tracking function TL of corner 11

6.5.2.2 Eigen Analysis

Unlike the previous semi-active models, passive strut dampers are included in the semi-active system for the full car nonlinear Iltis model. This is because without any passive dampers present, for the speed bump manoeuvre, the ADAMS model becomes unstable and the suspension 'snaps'. This occurs because while encountering the speed bumps, the semi-active switch controller is most often switched to zero damping; i.e. no suspension damping is initially present. As a result, suspension displacements that become too large for the vehicle to withstand are produced before the system can react.

- 100 -

Also, because the semi-active damper delivers a force proportional to the absolute sprung mass velocity, changing the low state of the switch to a non-zero damping coefficient has little effect. This is because the sprung mass, which has an initial zero velocity, takes time to accumulate a vertical velocity for this disturbance and so during the bump its velocity is extremely small. As a result an extremely low force would still be applied during this time and instabilities in the ADAMS model would still be present. If instead a random road profile were used, this issue would not exist due to the continuous switching of the controller throughout the disturbance.

Semi-Active Suspension, High Damping		
Natural Frequency (rad/s)	Damping Ratio	Eigenvalues
0.161	-5.34e-8	8.62e-9 ± 0.161i
0.162	5.13e-5	-8.35e-6 ± 0.162i
0.167	-3.16e-8	-5.29e-9 ± 0.167i
8.63	0.134	-1.16 ± 8.55i
9.70	0.818	-7.93 ± 5.58i
18.2	0.243	-4.45 ± 17.7i
88.2	8.65e-2	-7.63 ± 89.9i
89.4	9.33e-2	-8.35 ± 89.0i
89.9	8.59e-2	-7.72 ± 89.6i
89.9	8.45e-2	-7.60 ± 89.7i

Table 6.18: Eigen analysis of semi-active damping when damping is on, static export method

When compared to the passive suspension, the semi-active suspension in its low damping mode (Table 6.19), has a much smaller damping associated with the last four eigenvalues. These eigenvalues represent the unsprung mass natural frequency modes of vibration. Also the system here, unlike the passive system, has no modes of vibration that are overdamped; in fact the system at this state has significantly lower damping than the passive system. When compared to the fully-active system, the semi-active system in its high damping mode generally demonstrates less damping for both the sprung and unsprung mass modes of vibration.

Semi-Active Suspension, Low Damping		
Natural Frequency (rad/s)	Damping Ratio	Eigenvalues
0.161	-3.09e-9	4.99e-10 ± 0.161i
0.162	1.78e-8	-2.89e-9 ± 0.162i
0.167	-8.52e-9	1.42e-9 ± 0.167i
8.54	0.116	-0.990 ± 8.49i
9.68	0.130	-1.25 ± 9.58i
18.2	0.244	-4.45 ± 17.7i
89.4	8.41e-2	-7.52 ± 89.0i
89.4	9.33e-2	-8.35 ± 89.0i
89.9	8.45e-2	-7.60 ± 89.7i
90.0	8.59e-2	-7.74 ± 89.7i

Table 6.19: Eigen analysis of semi-active damping when damping is off, static export method

6.5.3 Kalman Filter

The weight matrices used for the LQR controller are:

Q=diag[1 1 1 1 1 1 1 1 1e9 1e9 1 1 1 1 2e9 1e9 1 1 1e9 1]

R=diag[0.5 0.5 0.5 0.5]

The noise matrices used for the Kalman filter are:

Q_n=diag[5.06e-4 5.06e-4 5.06e-4 5.06e-4]

R_n=diag[4.76e-4 4.76e-4 4.76e-4 0.25 0.25 0.25 0.25]

6.5.3.1 Time Domain Simulation

In evaluating the Kalman filter, results are shown for the linearized vehicle from the gravity export method rather than the nonlinear ADAMS model. Also, here the assumed sensor measures are the sprung mass vertical, pitch and roll velocities along with the four suspension velocities. In practice the strut velocity can easily be measured directly or indirectly (by first measuring its displacement with an L.V.D.T. and then passing the signal through a filtered derivative).

Some typical results comparing the true versus estimated states for certain measures are shown in Figure 6.80 to 6.83. Notice that the Kalman filter is very good at estimating the states for the body movement but not as good for the unsprung motion. For a more realistic response, more realistic matrices representing the sensor noise are required.

Figure 6.80: Angular pitch velocity[†]

Figure 6.81: Angular pitch position

[†]*Notice: the two responses are nearly indistinguishable from one another.*

Figure 6.82: Angular velocity of corner 11
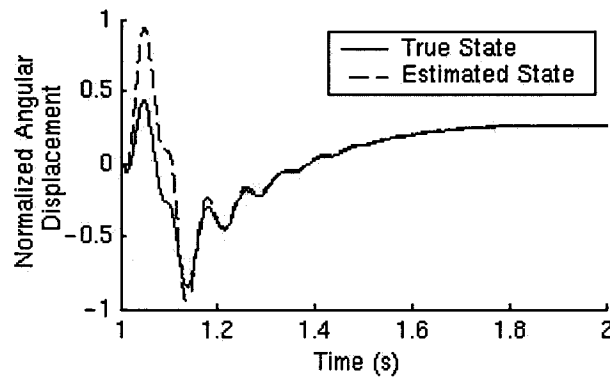
Figure 6.83: Angular displacement of corner 11

6.6 Iltis Full Car Model with Bushings

6.6.1 Passive Suspension

6.6.1.1 Time Domain Simulation

In adding bushings to the suspension, the system response is altered in magnitude while roughly keeping the same response pattern (Figure 6.84 to 6.88). The interface model without the bushings tends to see higher sprung mass acceleration than the interface model with bushings. On the other hand the linearized versions of these two models are almost exactly the same in their response, indicating that the linearization process minimizes the influence of the bushings on the resulting linear model.
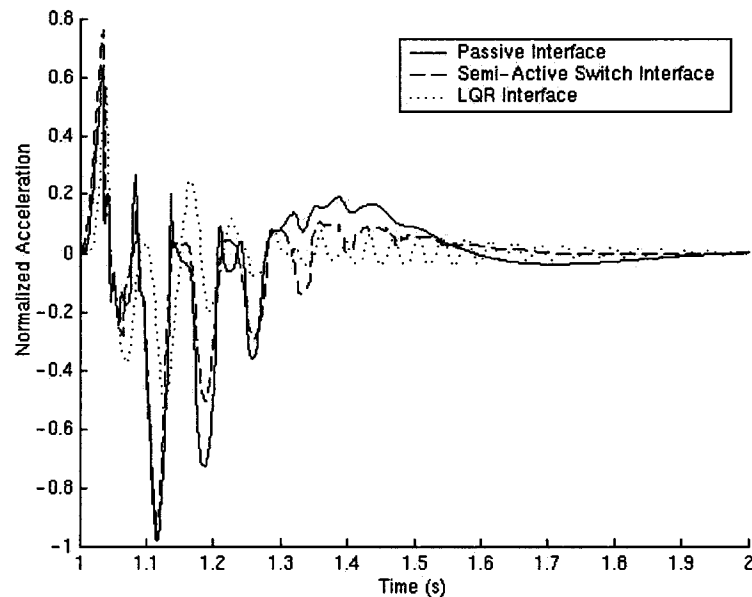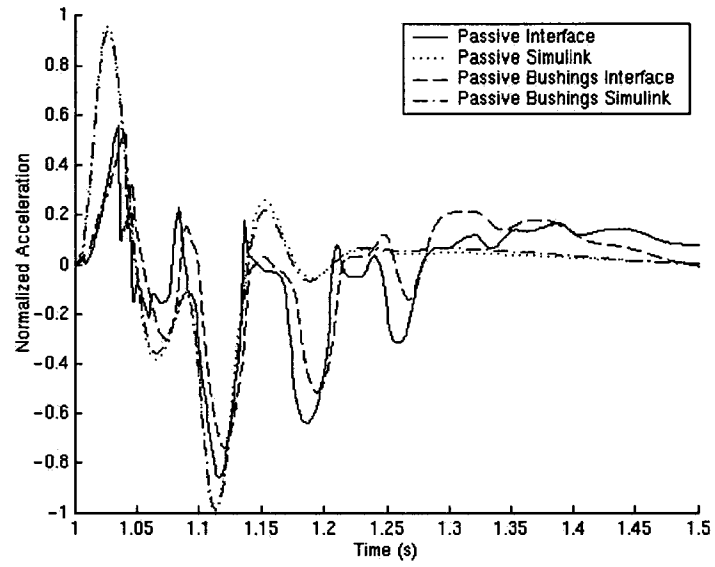
Figure 6.84: Sprung mass vertical acceleration
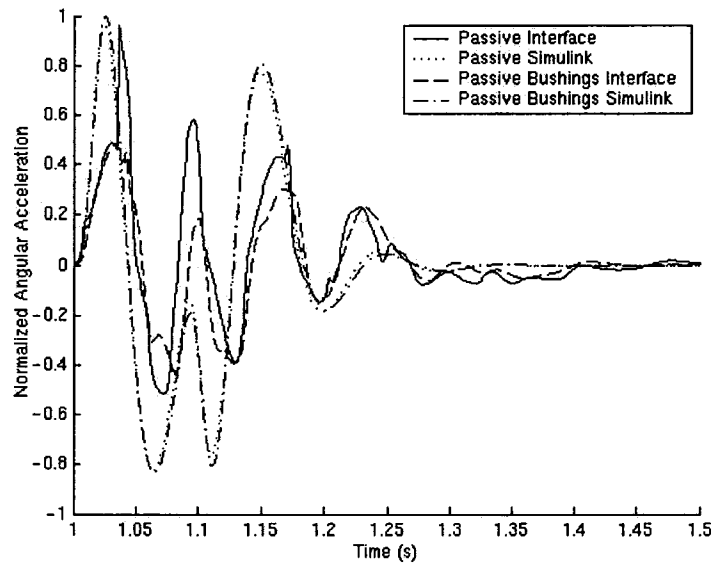
Figure 6.85: Sprung mass roll acceleration

- 104 -
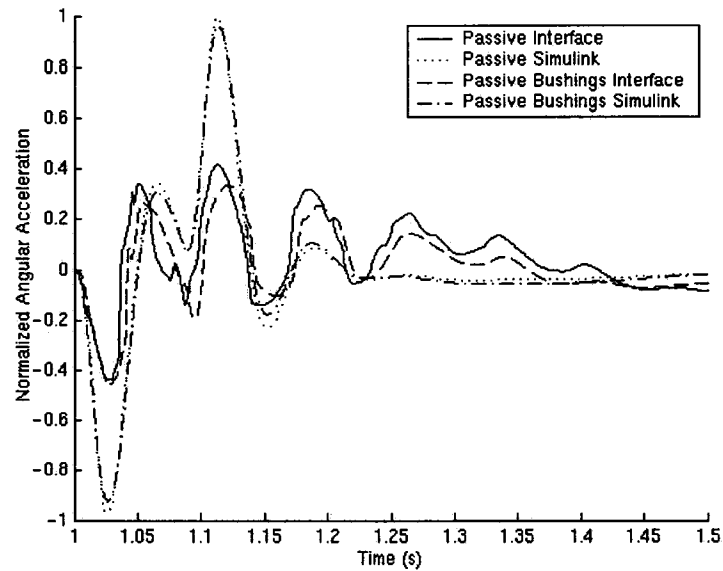
Figure 6.86: Sprung mass pitch acceleration
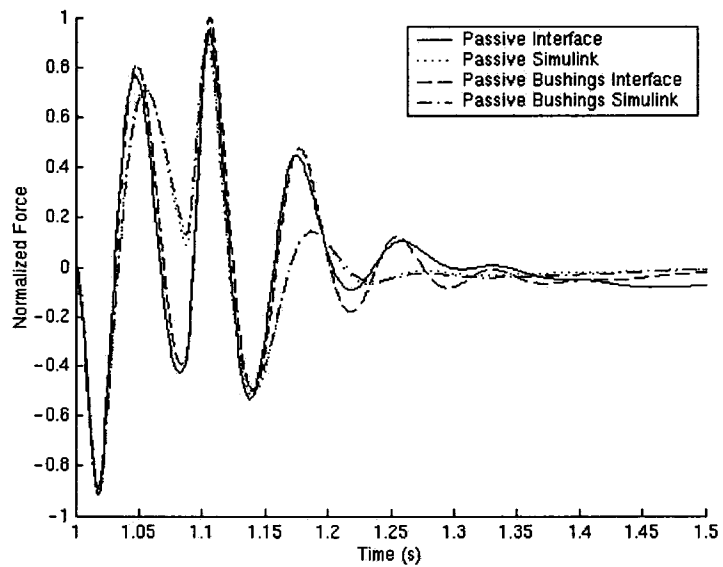
Figure 6.87: Tire dynamic force of corner 11

For the tire force and suspension movement (Figure 6.87 and 6.88 respectively) there is a negligible difference between the linear models that have and don't have bushings and a significant difference between their nonlinear versions. The nonlinear system with bushings behaves as though its suspension is softer than the system without bushings. This makes sense since although the bushings are extremely stiff, they are less stiff than a suspension without bushings (as though bushings of infinite stiffness are used).

- 105 -

Figure 6.88: Suspension displacement of corner 11

6.6.2 Passive versus Fully-Active Suspension

The weights used for both the linear and nonlinear models are:

Q=diag[1 1 1 1 1 1 1 1 1 1 1 1 1 1 1 1 1 1 1 1 1e8 1e6 1 1 1e8 1e8 2e8 1e8 1 1 1 1 1 1 1 1 1 1 1 1 1

1 1 1 1 1 1 1 1 1 1 1 1 1 1 1 1 1 1 1 1 1 1 1 1 1 1 1 1 1 1 1 1 1 1 1 1]

R=diag[0.5 0.5 0.5 0.5]

These matrices are tuned by optimizing the response of the nonlinear interface model and is weighted towards decreasing body velocity like the previous models. The corresponding state variables are listed in Appendix A.

6.6.2.1 Time Domain Simulation

As Figure 6.89 to 6.93 shows, the active nonlinear system is consistently better than the passive system in ride, but the active linear model is not as effective compared to the linear passive model. The linear active suspension is probably less effective since it is very different from its original nonlinear version. As a result the LQR controller is not simultaneously optimal for both linear and nonlinear models.

- 106 -

Figure 6.89: Sprung mass vertical acceleration
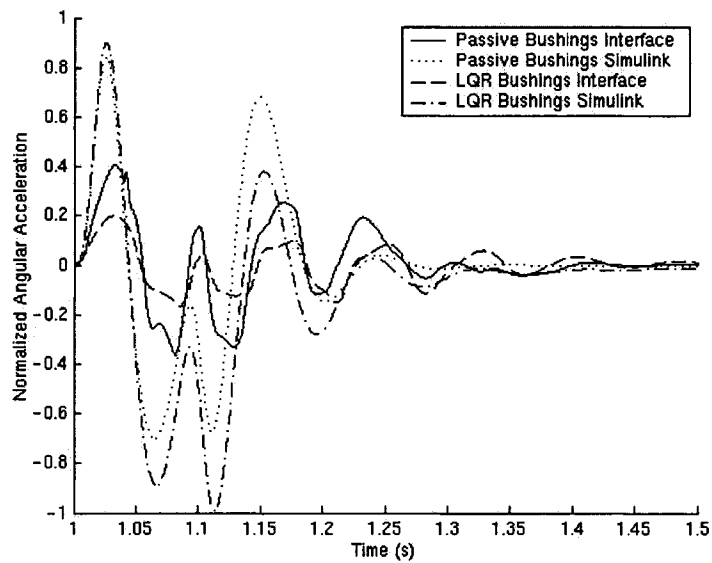
Figure 6.90: Sprung mass roll acceleration

- 107 -
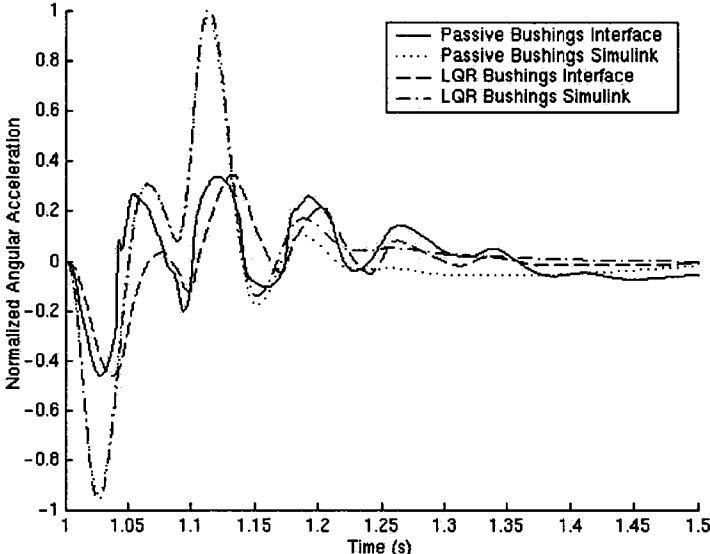
Figure 6.91: Sprung mass pitch acceleration
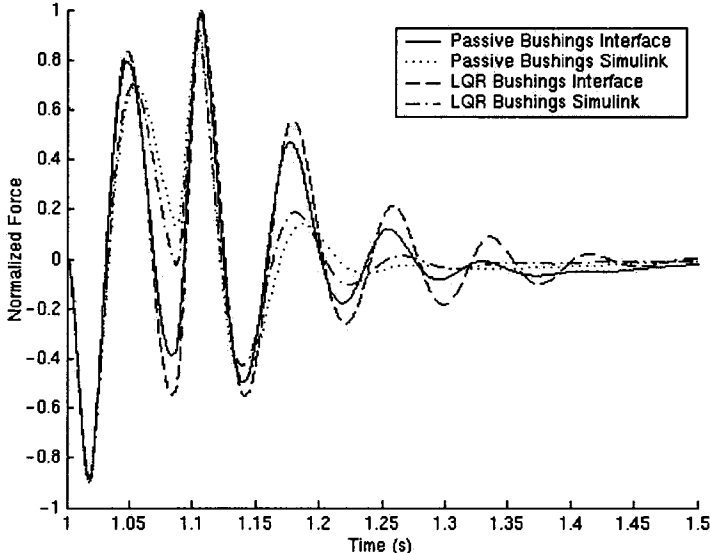
Figure 6.92: Tire dynamic force of corner 11
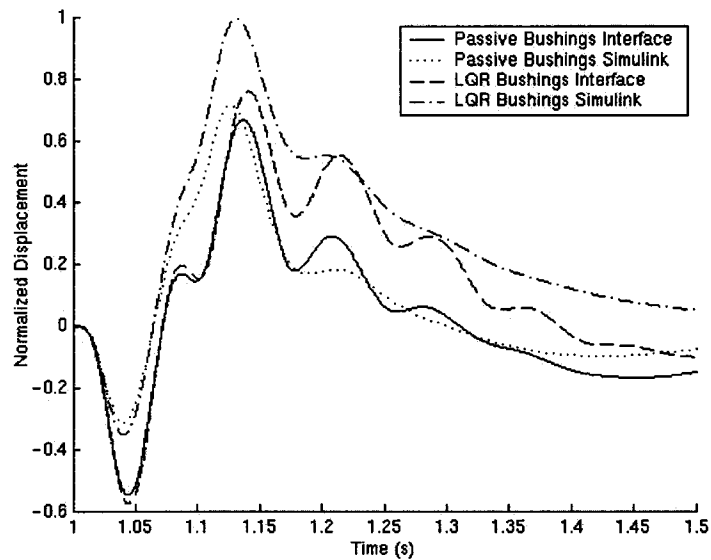
Figure 6.93: Suspension displacement of corner 11

6.6.3 Eigen Analysis

Table 6.20 to 6.22 are the eigen analysis for the passive and fully-active suspension system with bushings. One of the main objectives of adding bushings in the full vehicle model is to see if the LQR will solve a system with a large number of degrees of freedom (38) and if the interface between ADAMS and Simulink can cope with having to exchange a larger number of variables. As expected the computing time to solve the LQR gain and the solve time of the interface model is somewhat longer than the models without bushings, but is still reasonable.

The eigenvalues of the passive suspension without bushings are roughly preserved when the bushings are added; they are listed as the first eleven eigenvalues in Table 6.20 and 6.21. The remaining eigenvalues are from the bushings that add high frequency components to the vehicle.

The original eigenvalues are even identifiable with the LQR system of Table 6.22; they also correspond to the first eleven entries. LQR again slightly changes the value of the free body eigenvalues so that their real components are negative and also changes the system damping, most notably the sprung mass modes of vibration are increased.

Passive Suspension		
Natural Frequency (rad/s)	Damping Ratio	Eigenvalues
0.161	-6.25e-9	1.01e-9 $\pm$ 0.161i
0.162	4.46e-8	-7.24e-9 $\pm$ 0.162i
0.167	-2.05e-8	3.43e-9 $\pm$ 0.167i
9.86	0.420	-4.14 $\pm$ 8.94i
11.2	0.481	-5.39 $\pm$ 9.83i
n/a	>1	-17.0
n/a	>1	-40.4
70.9	0.364	-25.9 $\pm$ 66.1i
87.1	0.349	-30.5 $\pm$ 81.6i
88.2	0.352	-31.0 $\pm$ 82.6i
90.8	0.334	-30.3 $\pm$ 85.6i
228	7.25e-2	-16.6 $\pm$ 228i
229	7.10e-2	-16.3 $\pm$ 229i
235	7.05e-2	-16.6 $\pm$ 234i
251	8.64e-2	-21.7 $\pm$ 250i
299	0.130	-39.0 $\pm$ 296i
300	0.124	-37.4 $\pm$ 298i
304	0.114	-34.6 $\pm$ 301i
304	0.123	-37.3 $\pm$ 301i
342	0.347	-118 $\pm$ 320i
342	0.349	-119 $\pm$ 320i
356	0.341	-121 $\pm$ 334i
367	0.296	-108 $\pm$ 350i
414	0.212	-87.7 $\pm$ 405i
419	0.212	-88.9 $\pm$ 409i
433	0.234	-101 $\pm$ 420i
438	0.239	-104 $\pm$ 425i
1.12e3	0.569	-639 $\pm$ 922i
1.12e3	0.571	-642 $\pm$ 923i
1.13e3	0.574	-647 $\pm$ 924i
1.13e3	0.575	-650 $\pm$ 925i
1.14e3	0.412	-472 $\pm$ 1.04e3i
1.14e3	0.411	-471 $\pm$ 1.04e3i
1.14e3	0.412	-472 $\pm$ 1.04e3i
1.15e3	0.421	-486 $\pm$ 1.05e3i
1.57e3	0.850	-1.34e3 $\pm$ 828i
1.57e3	0.856	-1.35e3 $\pm$ 813i
1.57e3	0.855	-1.34e3 $\pm$ 816i
1.57e3	0.857	-1.35e3 $\pm$ 812i

Table 6.20: Eigen analysis of the passive suspension, static export method

Passive Suspension		
Natural Frequency (rad/s)	Damping Ratio	Eigenvalues
n/a	>1	-13.4
n/a	>1	-43.9
5.10e-2	7.41e-8	-3.78e-9 ± 5.10e-2i
5.14e-2	2.01e-8	1.03e-9 ± 5.14e-2i
5.29e-2	9.68e-8	-5.12e-9 ± 5.29e-2i
9.34	0.445	-4.16 ± 8.36i
10.9	0.494	-5.39 ± 9.47i
71.1	0.358	-25.6 ± 66.4i
86.7	0.346	-30.0 ± 81.4i
87.8	0.348	-30.6 ± 82.3i
90.5	0.331	-29.9 ± 85.3i
227	7.55e-2	-17.2 ± 227i
228	7.41e-2	-16.9 ± 227i
233	7.38e-2	-17.2 ± 232i
249	9.09e-2	-22.6 ± 248i
300	0.127	-38.1 ± 297i
301	0.121	-36.5 ± 299i
304	1.20	-36.6 ± 302i
304	0.111	-33.6 ± 302i
341	0.349	-119 ± 319i
341	0.348	-119 ± 319i
354	0.340	-120 ± 333i
364	0.293	-106 ± 348i
410	0.214	-87.5 ± 400i
414	0.213	-88.3 ± 404i
428	0.236	-101 ± 416i
434	0.244	-106 ± 420i
1.58e3	0.856	-1.35e3 ± 815i
1.57e3	0.855	-1.35e3 ± 816i
1.57e3	0.854	-1.34e3 ± 818i
1.57e3	0.849	-1.34e3 ± 830i
1.12e3	0.570	-640 ± 922i
1.13e3	0.572	-643 ± 923i
1.13e3	0.574	-648 ± 924i
1.13e3	0.576	-651 ± 925i
1.14e3	0.413	-472 ± 1.04e3i
1.15e3	0.412	-472 ± 1.04e3i
1.15e3	0.412	-472 ± 1.04e3i
1.15e3	0.422	-487 ± 1.05e3i

Table 6.21: Eigen analysis of the passive system, ADAMS linearization

- 111 -

LQR Suspension		
Natural Frequency (rad/s)	Damping Ratio	Eigenvalues
1.42e3	3.74e-5	-6.04e-6 ± 0.161i
1.62e3	2.17e-6	-3.53e-7 ± 0.162i
1.67e3	5.06e-5	-8.46e-6 ± 0.167i
n/a	>1	-5.55
9.95	0.849	-8.44 ± 5.26i
11.2	0.764	-8.57 ± 7.24i
76.4	0.230	-18.2 ± 74.2i
86.8	0.347	-30.1 ± 81.5i
87.8	0.349	-30.7 ± 82.4i
90.8	0.334	-30.3 ± 85.6i
n/a	>1	-107
228	7.17e-2	-16.4 ± 228i
229	7.10e-2	-16.3 ± 229i
235	7.05e-2	-16.6 ± 234i
251	8.65e-2	-21.7 ± 250i
299	0.129	-38.6 ± 297i
300	0.124	-37.4 ± 298i
304	0.114	-34.6 ± 302i
304	0.122	-37.2 ± 302i
342	0.347	-119 ± 321i
342	0.348	-119 ± 321i
355	0.341	-121 ± 334i
369	0.292	-108 ± 353i
414	0.212	-87.7 ± 405i
418	0.212	-88.8 ± 409i
433	0.233	-101 ± 421i
438	0.239	-104 ± 425i
1.12e3	0.569	-639 ± 922i
1.12e3	0.571	-642 ± 923i
1.13e3	0.574	-647 ± 924i
1.13e3	0.575	-650 ± 925i
1.14e3	0.412	-472 ± 1.04e3i
1.14e3	0.411	-471 ± 1.04e3i
1.14e3	0.412	-472 ± 1.04e3i
1.15e3	0.421	-486 ± 1.05e3i
1.57e3	0.850	-1.34e3 ± 827i
1.57e3	0.856	-1.35e3 ± 812i
1.57e3	0.855	-1.35e3 ± 816i
1.57e3	0.857	-1.35e3 ± 812i

Table 6.22: Eigen analysis of the LQR fully-active system, static export method

6.7 Solve Mode Performance

Table 6.23 is a summary of the results attained from either solving the interface system using the discrete or continuous mode. The discrete mode is always dependable since it finds a solution all the time with reasonable solve times. The continuous mode however has difficulty in solving the more complicated models, either not being able to find a solution or producing a response that is not correct. When it is able to solve correctly however, it has run times quicker than its discrete mode counterpart. To get a smooth response for the discrete mode, the communication interval was set to 1ms/cycle.

Model	System	Discrete Mode	Continuous Mode
Quarter Car Lumped Mass	Passive, u=0	Solves	Solves
	LQR	Solves	Solves
	LQG	Solves	Solves
	Semi-Active	Solves	Solves
Full Car Lumped Mass	Passive, u=0	Solves	Solves
	LQR	Solves	Solves
	LQG	Solves	Solves
	Semi-Active	Solves	Solves
Quarter Car Iltis	Passive, u=0	Solves	Solves
	LQR	Solves	High frequency noise response
	LQG	Solves	Crashes when executed- does not solve
	Semi-Active	Solves	Solves
Full Car Iltis	Passive, u=0	Solves	Solves
	LQR	Solves	Solves incorrectly - high frequency, high amplitude response
	LQG	Solves	Does not solve
	Semi-Active	Solves	Solves extremely slow
Full Car Iltis with Bushings	Passive, u=0	Solves	Crashes, does not solve, extremely slow
	LQR	Solves	Too slow, does not solve

Table 6.23: Summary of the solver methods used

7 CONCLUSIONS AND RECOMMENDATIONS
7.0 Conclusions

Two software suites were used with one another to model and evaluate active suspension systems for various vehicle models. A quarter and full car model have both been created for a lumped mass vehicle and for the Bombardier Iltis utility truck. For each vehicle model, a fully-active and semi-active system has been implemented for comparison with a passive suspension. One of the requirements of the LQR system is knowledge of all the system states. So that one does not have to use a sensor to measure every state variable in a vehicle, a Kalman filter was used with the E.C.U. Finally, bushings were added to the full car Iltis model to evaluate its effect on the surrounding systems.

This research focused on the ride characteristics of the vehicle by evaluating the system when disturbed by either a vertical speed bump or a sine wave. Hence these conclusions cannot be directly extended to the handling behaviour of the vehicle; for that a different simulation environment is needed. Here the fully-active control algorithm made use of the linear quadratic regulator while the semi-active suspension adopted the switching law developed by Karnopp et al. {26}. The controller was created in Matlab/Simulink while the vehicle was modeled and simulated using various methods.

For the lumped mass vehicle, the models were attained one of three ways: 1. linear vehicle derived from analytical equations and implemented in Simulink, 2. linear vehicle modeled partially by ADAMS and exported to Simulink for completion or 3. vehicle modeled in ADAMS and solved in its nonlinear form by software interfacing. For the Bombardier Iltis vehicle, the models were produced by one of the three methods: 1. linear vehicle produced thru the static export method, 2. linear vehicle produced thru the gravity export method or 3. vehicle modeled in ADAMS and solved in its nonlinear form by software interfacing.

Software Interface

Interfacing ADAMS with Simulink to simulate a multi-domain system proved successful. The link was able to exchange a large number of variables with reasonable run times, providing the user a convenient arena to conduct such studies. The discrete solve mode was able to find the system response for all simulations conducted while the continuous solve mode was only successful in solving simple systems.

- 114 -

Fully-Active Control

In implementing the LQR algorithm, a significant increase in ride performance was attained at the expense of the wheel movement. The active system increased the suspension movement, the tire dynamic force and the tire lift off tendency relative to the passive suspension. In addition the fully-active system was able to decrease the sprung mass acceleration by as much as 87% but increase the tire forces by as much as 75% relative to the passive suspension. These results were consistent with the eigen analysis that indicated that the LQR, when weighted towards ride, increased the damping of the sprung mass vibration mode, while reducing the damping of the unsprung mass mode.

As shown in the frequency response plots, a shortcoming of the controller was its inability to simultaneously increase the ride performance, at the sprung mass natural frequency and decrease the tire force fluctuation at the unsprung mass natural frequency. As demonstrated with the quarter car model, the algorithm was able to achieve both goals, but only by using two separate sets of weighting matrices.

With the quarter car model, the system had a significantly better relative performance for the sine wave input than it did for the bump input. This seemed to indicate that the controller was less effective in dealing with discrete disturbances than in dealing with continuous disturbances, suggesting that a different control algorithm be used for different road disturbances.

Semi-Active Control

The performance of the semi-active suspension was for the most part intermediate to that of the passive and fully-active suspension. Its design was extremely well suited to dealing with the discrete bump disturbance since it switched to low damping during most of the disturbance, an ideal situation for ride in this case. This system was able to decrease the sprung mass acceleration relative to the passive suspension by as much as 50% while increasing the tire forces by as much as 45%. However, at the same time, the controller was unable to switch between high and low damping without disturbing the body acceleration. For that, a more sophisticated switch algorithm is needed.

Nonetheless, with the savings in energy over the full-active suspension combined with a more sophisticated controller, this system has the potential of approaching the performance of the fully-active suspension without the complicated hardware.

Static Export Method versus Gravity Export Method

The static export and gravity export procedures, developed to attain proper linear plant models for the Iltis, produced essentially identical model responses both in the time and frequency domain. This similarity existed despite the fact that the role of gravity differed in the two procedures. When the entire vehicle was constructed within ADAMS and the eigenvalues of the passive system was attained, they were found to be essentially identical to those produced from these two methods. This further validated these two procedures.

- 115 -

Linear versus Nonlinear

For the lumped mass vehicle models, the linear and nonlinear versions were very similar in their behaviour with the differences being attributed to the linearization of their rotational degrees of freedom.

However, a different scenario emerged for the Iltis vehicles. For the passive suspension, the linear and nonlinear versions differed significantly in their behaviour. This was shown to be caused by the linearization of the nonlinear force elements that produced substantially stiffer linear elements. However these differences became insignificant for the fully-active version since the active force element generated forces much greater than the passive elements. As a result the linear and nonlinear models were more similar in their behaviour.

Lumped Mass Model versus Iltis

Common response patterns, features and behaviour were noticed among the different vehicle models. Although the lumped mass vehicles did not have a working kinematic suspension, they were still able to demonstrate the same fundamental responses as the more complicated Iltis utility truck. These results confirm the value of these simplified lumped mass vehicles and their suitability for performing preliminary studies of a vehicle's behaviour.

Handling Performance

It is difficult to conclude how the active systems affect handling since the simulations conducted are for ride studies. There are two competing measures that each indicates opposite tendencies: the tire dynamic force and the body roll movement. For the road bump input, the active systems increase the fluctuation in tire forces while decreasing the roll movement of the body.

It is suggested that the increase in tire force fluctuations are a result of using the active systems with the bump road input. This is because to preserve ride, the fully-active systems reacts to the bump by pulling the sprung and unsprung mass in together and the semi-active system switches to low damping. With a different road input profile, the active systems would certainly react differently.

Hence if one were to imagine how this system would behave while turning a corner on a smooth surface, one could say that the active systems would only act to decrease the body roll of the vehicle. It would thus behave like an active anti-roll bar system[†] with the ability of changing the relative roll stiffness between the front and rear suspensions. Having the ability of changing the relative roll stiffness between the front and rear suspensions gives the added handling performance, as proven in TRW's ARC system. The reason is that it achieves a more balanced vehicle that has neither a tendency for understeer or oversteer-this increases the directional stability envelope of the car.

With these arguments in mind, it is the opinion of the author that the active systems would increase the handling of the vehicle during cornering.

[†]*Notice: An anti-roll bar promotes greater variations in left to right tire forces (than a passive system) when correcting roll, i.e. they put additional force on the outside tire and takes away force from the inside tire. The effect leads to a decrease in tire lateral grip with a reduction in body roll. This is why passenger vehicles usually only have front anti-roll bars to promote understeer rather than oversteer.*

Kalman Filter

In using the Kalman filter to estimate and feed the states into the LQR controller, a slight deterioration in system performance was observed. However, with better noise matrix descriptions and a deeper investigation into what is best to measure with sensors, a better performance of the filter should be seen. Nonetheless, the state estimator proved to be a worthy technique of implementing the LQR algorithm without having to measure all the system states.

Suspension Bushings

Adding bushings to the passive full car Iltis model changed the vehicle behaviour as though the suspension was now softer. However, these differences were not as prominent when the linear versions of the vehicle were considered- it is unclear how linearization affects the suspension bushing influence, but it seemed to minimize it. Also, with the fully-active suspension, since the response is dominated by the large forces from the active element, the bushings did not alter the vehicle behaviour significantly. With the addition of the bushings, the degrees of freedom of the model were increased dramatically and yet the LQR algorithm was still solvable and the ADAMS/Simulink interface was able to exchange the increased number of variables reasonably well.

7.1 Recommendations

Vehicle Model

Increasing the vehicle model complexity for an increase in accuracy would be a worthwhile exercise. Two features of importance are the passenger seating and the powertrain. In this way a more accurate picture of the acceleration levels felt by the occupants, including the influence of the engine would be attained.

To further explore the properties of the invariant points for the frequency response of the system, tire damping should be included. This would confirm the comments by Hrovat {31} that these invariant points disappear when tire damping is considered. It is an important feature as it limits the effectiveness of active suspension around the frequency of its existence.

To evaluate the influence of the nonlinear rotational degrees of freedom of the Iltis model, the nonlinear force elements of its ADAMS model should be replaced with linear rates. In this way differences between the nonlinear ADAMS model and its corresponding linearized version would only be attributed to the linearization of the rotation terms of the sprung mass and suspension. Comparison of these two models would also shed light on the spring influence on the Iltis models.

Instead of driving the models by motion, one could instead use spindle forces as the input, similar to what is used on road test simulation durability rigs. The input data could be found from on road data acquisition testing for various road grades and vehicle manoeuvres. In this way, the static export and gravity export procedures could be avoided altogether in finding the linear model version since a virtual model of the tire would not be needed. More information on this topic is found in {2}, {24}.

Controller

As discovered in the frequency response plots, the LQR controller is limited in its ability of simultaneously increasing ride performance at low input frequencies and preserving tire forces at high frequencies. A more sophisticated controller is recommended for use, one that is able to determine the input frequency and adjust the optimal gain accordingly. A possible solution might be in using a modified LQR algorithm that uses weighting matrices that are a function of the unsprung mass oscillation frequency or road input frequency. It is not know if such a controller currently exists but would be worth investigating.

Nonlinear control may also be valuable in being able to find a better compromise (than the LQR) between the body and wheel motion during a bump disturbance. For implementation in a real vehicle, the controller should have two modules, one for ride response and one for handling. The two can then be weighted against each other to find a better compromise between ride and handling.

An LQR control algorithm with the cost function as a function of the sprung mass acceleration would allow the user to directly control the body acceleration rather than the body velocity. This would inevitably lead to a better acceleration response of the vehicle, which is the primary measure in evaluating ride quality.

The switch algorithm chosen approximated the ideal skyhook damper and so demonstrated the advantages of increased ride but with an increase in wheel movement. Algorithms that approximate the combination of a skyhook and ground-hook damper exist, and so would give a better performance in both ride and handling. Implementing such an algorithm should be considered for future studies. Also a more sophisticated switch controller that accounts for the discrete changes in body acceleration, when switching between high and low damping is needed.

ADAMS/Controls

One valuable feature in ADAMS/Controls would be the option of exporting linear time variable state-space matrices to Simulink. This would increase the accuracy of the linear model but at the same time increase the computational demands since it would entail linearizing the ADAMS model and updating the matrices at a specific time rate. However the result would be a linear model with eigenvalues that change according to the vehicle configuration. The LQR algorithm could then be continuously updated based on these linear plant matrices to produce an LQR gain that would continue to be optimal with time.

To further improve ADAMS/Controls, motions of any kind should be able to be passed between the software programs regardless if they are a driving motion or not. Currently, it is not possible to pass forces from ADAMS to Simulink. Although for this study this feature was not needed, it may become important in other work and should be considered. In addition, motion should be able to be captured in the input state space matrix when linearizing and exporting the system to Simulink. This would avoid having to follow the static export and gravity export methods to attain a suitable linear plant model.

Miscellaneous

Future work should incorporate a hydraulic model into the active system. Although this may be done empirically and implemented in Simulink, the natural progression from this project would be to create the system in a third program and interface it with the vehicle model and the E.C.U. This would have the advantage of being able to perform preliminary simulations before prototyping, with the aim of tuning and optimizing the system parameters beforehand. Due to the characteristics of hydraulic systems, it is expected that its addition would significantly change the system performance from what has been shown in this study. A potential software program to use is Easy5, it is able to link directly to both ADAMS and Simulink.

Due to its increased presence in production vehicles, an active anti-roll bar system could be simulated using the same techniques developed in this study. Systems similar to both BMW's Dynamic Drive and TRW's ARC could be evaluated and compared with a fully-active and semi-active system before deciding on which system to implement. However, in evaluating this system a handling analysis would be more valuable since that is the arena in which this system functions.

Using a random road input taken from real world vehicle testing would be valuable in further understanding the behaviour of active systems. With this input, a more complete picture of active suspension would emerge.

Handling studies should be conducted for various manoeuvres to obtain a complete picture of the capabilities of active suspension. This would require using a more sophisticated tire model such as the Calspan model or the Magic Formula tire model. Although tire models today are empirical in nature, enough published data exists so that track testing would not be necessary for its virtual implementation. ADAMS/Car would be a suitable software to use for this.

REFERENCES

Textbooks

1. A. Anderson, J.B. Moore, "Linear Optimal Control", Prentice Hall, New Jersey, 1971.

2. W.B. Ferry, "Combining Virtual simulation and Physical Vehicle Test Data to Optimize Automotive Durability Testing", M.A.Sc. Thesis, University of Windsor, 2002.

3. T.D. Gillespie, "Fundamentals of Vehicle Dynamics", Society of Automotive Engineers International, Warrendale, PA, 1992.

4. M.S. Grewal, A.P. Andrews, "Kalman Filtering- Second Edition", John Wiley & Sons Inc., New York, 2001.

5. D.J. Inman, "Engineering Vibration-Second Edition", Prentice Hall Inc., New Jersey, 2001.

6. D.E. Kirk, "Optimal Control Theory", Prentice-Hall, New Jersey, 1970.

7. W. Kortum, R.S. Sharp (eds.), "Multibody Computer Codes in Vehicle System Dynamics", Swets & Zeitlinger Inc., Amsterdam, 1993.

8. H. Kwakernakk, R. Sivan, "Linear Optimal Control Systems", John Wiley & Sons Inc., New York, 1972.

9. E.B. Lee, L. Markus, "Foundations of Optimal Control Theory", John Wiley & Sons Inc., New York, 1967.

10. D. Mcloy, H.R. Martin, "The Control of Fluid Power", John Wiley & Sons Inc., New York, 1973.

11. Mechanical Dynamics Incorporated (MDI), "Getting Started using ADAMS/Controls", ADAMS/Controls Electronic User's Guide, Mechanical Dynamics Incorporated, 2002.

12. Mechanical Dynamics Incorporated (MDI), "Using ADAMS/Solver", ADAMS/Solver Online Electronic User's Guide, Mechanical Dynamics Incorporated, 2002.

13. J.S. Meditch, "Stochastic Optimal Linear Estimation and Control", McGraw Hill, New York, 1969.

14. H.E. Merritt, "Hydraulic Control Systems", John Wiley & Sons Inc., New York, 1967.

15. B. P. Minaker, "Active Geometry Suspension for Road Vehicles", Ph.D. Thesis, Queen's University, 2001.

16. N.D. Naidu, "Optimal Control Systems", CRC Press, London, 2002.

17. P.E. Nikravesh, "Computer-Aided Analysis of Mechanical Systems", Prentice Hall, New Jersey, 1988.

18. K. Ogata, "Modern Control Engineering- Third Edition", Prentice Hall, New Jersey, 1997.

19. H. Rahnejat, "Multi-Body Dynamics- Vehicles, Machines and Mechanisms", Professional Engineering Publishing, London, 1998.

20. A.A. Shabana, "Computational Dynamics – Second Edition", John Wiley and Sons Inc., 2001.

21. A.A. Shabana, "Dynamics of Multibody Systems", John Wiley and Sons Inc., New York, 1989.

22. B.H. Tongue, "Principles of Vibration- Second Edition", Oxford University Press, New York, 2002.

23. J.Y. Wong, "Theory of Ground Vehicles – Second Edition", John Wiley & Sons Inc., New York, 1993.

24. C. Wood, "Integrated Durability Analysis of a Vehicle through Virtual Simulation", M.A.Sc. Thesis, University of Windsor, 2003.

Papers

25. M. Bouazara, M.J. Richard, "An Optimization Method Designed to Improve 3-D Vehicle Comfort and Road Holding Capability through the use of Active and Semi-Active Suspensions", European Journal of Mechanics and Solids, Vol. 20, pp. 509-520, 2001.

26. D. Karnopp, M.J. Crosby, R.A. Harwood, "Vibration Control using Semi-Active Force Generators", Journal of Engineering for Industry, Vol. 96, pp. 619-626, 1974.

27. D. Danesin, P. Vercellone, F. Mastronardi, M. Fenoglio, A. Fornero, M. Velardocchia, "Vehicle Dynamics with Real Time Damper Systems", 16th European ADAMS User Conference, Conference Proceedings, 2001.

28. J.Z. Feng, F. Yu, Y.X. Zhao, G. Xu, "Design of a Bandwidth-limited Active Suspension Controller for Off-Road Vehicle Based on the Co-Simulation Technology", SAE Paper No. 2004-01-1067.

29. B. Harris, D. Negrut, "ADAMS Theory in a Nutshell", Department of Mechanical Engineering, The University of Ann Arbor Michigan, 2001.

30. A.S. Haycock, "Modelling and Control of Automotive Suspension Systems", Rover Group Limited, pp. 926-931, U.K.

31. D. Hrovat, "Survey of Advanced Suspension Developments and Related Optimal Control Applications", Automatica, Vol. 33, pp. 1781-1817, 1997.

32. A. Jansson, M. Yahiaoui, C. Richards, "Running Combined Multibody Hydraulic System Simulations within ADAMS", 1998 International ADAMS User Conference, 1998.

33. A.W. McCormac, D.M. Hanna, R.J. Anderson, J.E. Tragenza, "Terrain Previewing for an Active Suspension System", Suffield Memorandum No. 1432, Defence Research Establishment Suffield, Ralston, Alberta.

34. T. Merker, G. Girres, O. Thriemer, "Active Body Control (ABC) The DaimlerChrysler Active Suspension Damping System", SAE Paper No. 2002-21-0054.

35. F. Oueslati, S. Sankar, "A Class of Semi-Active Suspension Schemes for Vehicle Vibration Control", Journal of Sound and Vibration, Vol. 3, pp. 391-411, 1994.

36. N.V. Orlandea, "ADAMS Theory and Applications", Advanced Vehicle Systems Dynamics Proceedings of the Third ICTS Seminar, Swets and Zeitlinger, Lisse., pp. 121-166, 1986.

37. A. Pinkos, E. Shtarkman, T. Fitzgerald, "An Actively Damped Passenger Car Suspension System with Low Voltage Electro-Rheological Magnetic Fluid", SAE Paper No. 930268.

38. H.S. Roh, Y. Park, "Stochastic Optimal Preview Control of an Active Vehicle Suspension", Journal of Sound and Vibration, Vol. 220, pp. 313-330, 1999.

39. K. Sharma, D.A. Crolla, D.A. Wilson, "The Design of a Fully Active Suspension System Incorporating a Kalman Filter for State Estimation", IEE Control, Conference Publication No. 389, Vol. 1, pp. 344-349, 1994.

40. R.S. Sharp, "The Application of Multi-Body Computer Codes to Road Vehicle Dynamics Modelling Problems", Proceedings of the Institution of Mechanical Engineers, Vol. 208, pp. 55-61, 1993.

41. V.N. Sohoni, J. Whitesell, "Automatic Linearization of Constrained Dynamical Models", Transactions of the ASME, Vol. 108, pp. 300-304, 1986.

42. H.D. Taghirad, E. Esmalzadeh, "Automobile Passenger Comfort Assured Through LQG/LQR Active Suspension", Journal of Vibration and Control, 1997.

43. A.G. Thompson, "An Active Suspension with Optimal Linear State Feedback", Vehicle System Dynamics, Vol. 5, pp. 187-203, 1976.

44. J.E. Tregenza, "Operator's Manual and Technical Reference Manual for the Active Iltis", Dynamics Laboratory Report No. DL/DRES/91/100, Department of Mechanical Engineering, Queen's University, Kingston, Canada, 1991.

45. J.E. Tregenza, "State of the Art Review Active Suspension Evaluation Program", Dynamics Laboratory Report No. DL/DRES/89/1, Department of Mechanical Engineering, Queen's University, Kingston, Canada, 1989.

46. M. Valasek, M. Novak, Z. Sika, O. Vaculin, "Extended Ground-Hook – New Concept of Semi-Active Control of Truck's Suspension", Vehicle System Dynamics, Vol. 27, pp 289-303, 1997.

47. G.N. Villec, "Cosimulation of an Automotive Control System using ADAMS and Xmath", International ADAMS User Conference, 1998.

48. R.A. Williams, "Automotive Active Suspensions, Part 1:Basic Principles", IMechE, Vol. 211, pp 415-426, 1997.

49. P.G. Wright, D.A. Williams, "The Application of Active Suspension to High Performance Road Vehicles", IMechE, C239/84, pp 23-28, 1984.

50. P.G. Wright, D.A. Williams, "The Case for an Irreversible Active Suspension System", SAE Paper No. 890081, 1993.

A.A.0 Quarter Car Model
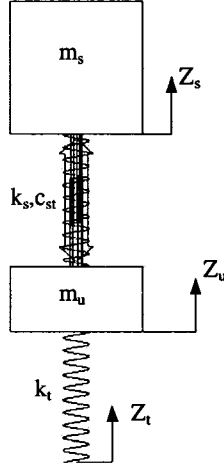
Figure A.0: Quarter car model

Tire Force

$$F_t = k_t (Z_u - Z_t) \tag{A.0}$$

Suspension Force

$$F_{sc} = k_s (Z_s - Z_u) + c_{st} (\dot{Z}_s - \dot{Z}_u) \tag{A.1}$$

Equations of Motion

$$m_s \ddot{Z}_s = -F_{sc} - F_u \tag{A.2}$$

$$m_u \ddot{Z}_u = F_{sc} + F_u - F_t \tag{A.3}$$

State Variables

$$x = (\dot{Z}_s, Z_s, \dot{Z}_u, Z_u)^T$$

State-Space Form

$$\dot{x} = Ax + B_1 u + B_2 w \tag{A.4}$$

where:

$$A = \begin{bmatrix} \dfrac{-c_{st}}{m_u} & \dfrac{-k_s}{m_s} & \dfrac{c_{st}}{m_s} & \dfrac{k_s}{m_s} \\ 1 & 0 & 0 & 0 \\ \dfrac{c_{st}}{m_u} & \dfrac{k_s}{m_u} & \dfrac{-c_{st}}{m_u} & \dfrac{-(k_s + k_t)}{m_u} \\ 0 & 0 & 1 & 0 \end{bmatrix}, B_1 = \begin{bmatrix} -\dfrac{1}{m_s} \\ 0 \\ \dfrac{1}{m_u} \\ 0 \end{bmatrix}, B_2 = \begin{bmatrix} 0 \\ 0 \\ \dfrac{k_t}{m_u} \\ 0 \end{bmatrix}$$

- 123 -
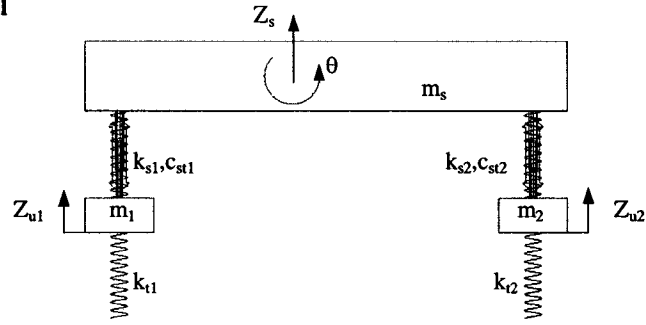
A.A.1 Half Car Model

Figure A.1: Half car model

Tire Forces

Front

$$F_{t1} = k_{t1}(Z_{u1} - Z_{t1})$$
(A.5)

Rear

$$F_{t2} = k_{t2}(Z_{u2} - Z_{t2})$$
(A.6)

Suspension Forces

Front

$$F_{sc1} = k_{s1}(Z_s - l_f \sin\theta - Z_{u1}) + c_{st1}(\dot{Z}_s - l_f \dot{\theta}\cos\theta - \dot{Z}_{u1})$$
(A.7)

Rear

$$F_{sc2} = k_{s2}(Z_s + l_r \sin\theta - Z_{u2}) + c_{st2}(\dot{Z}_s + l_r \dot{\theta}\cos\theta - \dot{Z}_{u2})$$
(A.8)

Equations of Motion

$$m_s \ddot{Z}_s = -F_{sc1} - F_{sc2} - u_1 - u_2$$
(A.9)

$$I_y \ddot{\theta} = l_f F_{sc1} - l_r F_{sc2} + l_f u_1 - l_r u_2$$
(A.10)

$$m_1 \ddot{Z}_{uf} = F_{sc1} + u_1 - F_{t1}$$
(A.11)

$$m_2 \ddot{Z}_{ur} = F_{sc2} + u_2 - F_{t2}$$
(A.12)

State Variables

$$x = (\dot{Z}_{u1}, Z_{u1}, \dot{Z}_{u2}, Z_{u2}, \dot{Z}_s, Z_s, \dot{\theta}, \theta)^T$$

State-Space Form

$$\dot{x} = Ax + B_1 u + B_2 w$$
(A.13)

- 124 -

where:

$$A = \begin{bmatrix} -\dfrac{c_{st1}}{m_1} & -\dfrac{(k_{s1}+k_{t1})}{m_1} & 0 & 0 & \dfrac{c_{st1}}{m_1} & \dfrac{k_{s1}}{m_1} & -\dfrac{l_f c_{st1}}{m_1} & -\dfrac{l_f k_{s1}}{m_1} \\[2mm] 1 & 0 & 0 & 0 & 0 & 0 & 0 & 0 \\[2mm] 0 & 0 & -\dfrac{c_{st2}}{m_2} & -\dfrac{(k_{s2}+k_{t2})}{m_2} & \dfrac{c_{st2}}{m_2} & \dfrac{k_{s2}}{m_2} & \dfrac{l_r c_{st2}}{m_2} & \dfrac{l_r k_{s2}}{m_2} \\[2mm] 0 & 0 & 1 & 0 & 0 & 0 & 0 & 0 \\[2mm] \dfrac{c_{st1}}{m_s} & \dfrac{k_{s1}}{m_s} & \dfrac{c_{st2}}{m_s} & \dfrac{k_{s2}}{m_s} & -\dfrac{(c_{st1}+c_{st2})}{m_s} & -\dfrac{(k_{s1}+k_{s2})}{m_s} & \dfrac{(l_f c_{st1}-l_r c_{st2})}{m_s} & \dfrac{(k_{s1}l_f - k_{s2}l_r)}{m_s} \\[2mm] 0 & 0 & 0 & 0 & 1 & 0 & 0 & 0 \\[2mm] -\dfrac{l_f c_{st1}}{I_y} & \dfrac{-l_f k_{s1}}{I_y} & \dfrac{c_{st2}l_r}{I_y} & \dfrac{k_{s2}l_r}{I_y} & \dfrac{(l_f c_{st1}-l_r c_{st2})}{I_y} & \dfrac{(l_f k_{s1}-l_r k_{s2})}{I_y} & -\dfrac{(l_f^2 c_{st1}+l_r^2 c_{st2})}{I_y} & -\dfrac{(l_f^2 k_{s1}+l_r^2 k_{s2})}{I_y} \\[2mm] 0 & 0 & 0 & 0 & 0 & 0 & 1 & 0 \end{bmatrix}$$

$$B_1 = \begin{bmatrix} \dfrac{1}{m_1} & 0 \\[2mm] 0 & \dfrac{1}{m_2} \\[2mm] 0 & 0 \\[2mm] -\dfrac{1}{m_s} & -\dfrac{1}{m_s} \\[2mm] 0 & 0 \\[2mm] \dfrac{l_f}{I_y} & -\dfrac{l_r}{I_y} \\[2mm] 0 & 0 \end{bmatrix}, \quad B_2 = \begin{bmatrix} \dfrac{1}{m_1} & 0 \\[2mm] 0 & \dfrac{1}{m_2} \\[2mm] 0 & 0 \\[2mm] 0 & 0 \\[2mm] 0 & 0 \\[2mm] 0 & 0 \\[2mm] 0 & 0 \end{bmatrix}$$
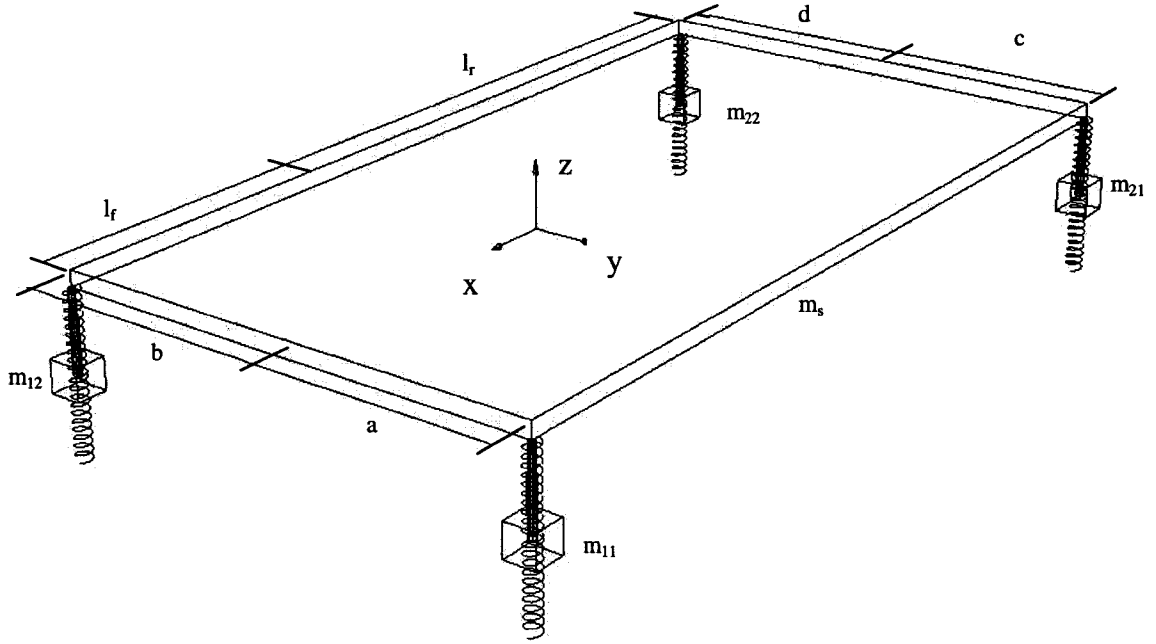
- 125 -

A.A.2 Full Car Model

Figure A.2: Full car model

Tire Forces

Front

$$F_{t11} = k_{t11}(Z_{u11} - Z_{t11})$$ (A.14)

$$F_{t12} = k_{t12}(Z_{u12} - Z_{t12})$$ (A.15)

Rear

$$F_{t21} = k_{t21}(Z_{u21} - Z_{t21})$$ (A.16)

$$F_{t22} = k_{t22}(Z_{u22} - Z_{t22})$$ (A.17)

Suspension Forces

Front

$$F_{sc11} = k_{s11}(Z_s - l_f\sin\theta + a\sin\varphi - Z_{u11}) + c_{st11}(\dot{Z}_s - l_f\dot{\theta}\cos\theta + a\dot{\varphi}\cos\varphi - \dot{Z}_{u11})$$ (A.18)

$$F_{sc12} = k_{s12}(Z_s - l_f\sin\theta - b\sin\varphi - Z_{u12}) + c_{st12}(\dot{Z}_s - l_f\dot{\theta}\cos\theta - b\dot{\varphi}\cos\varphi - \dot{Z}_{u12})$$ (A.19)

Rear

$$F_{sc21} = k_{s21}(Z_s + l_r\sin\theta + c\sin\varphi - Z_{u21}) + c_{st21}(\dot{Z}_s + l_r\dot{\theta}\cos\theta + c\dot{\varphi}\cos\varphi - \dot{Z}_{u21})$$ (A.20)

$$F_{sc22} = k_{s22}(Z_s + l_r\sin\theta - d\sin\varphi - Z_{u22}) + c_{st22}(\dot{Z}_s + l_r\dot{\theta}\cos\theta - d\dot{\varphi}\cos\varphi - \dot{Z}_{u22})$$ (A.21)

Equations of Motion

$$m_s\ddot{Z}_s = -F_{sc11} - F_{sc12} - F_{sc21} - F_{sc22} - u_{11} - u_{12} - u_{21} - u_{22}$$ (A.22)

$$I_y\ddot{\theta} = l_f F_{sc11} + l_f F_{sc12} - l_r F_{sc22} - l_r F_{sc21} + l_f u_{11} + l_f u_{12} - l_r u_{21} - l_r u_{22}$$ (A.23)

$$I_x\ddot{\varphi} = -aF_{sc11} + bF_{sc12} + dF_{sc22} - cF_{sc21} - au_{11} + bu_{12} - cu_{21} + du_{22}$$ (A.24)

- 126 -

$$m_{11}\ddot{Z}_{11} = F_{sc11} + u_{11} - F_{t11} \tag{A.25}$$

$$m_{12}\ddot{Z}_{12} = F_{sc12} + u_{12} - F_{t12} \tag{A.26}$$

$$m_{21}\ddot{Z}_{21} = F_{sc21} + u_{21} - F_{t21} \tag{A.27}$$

$$m_{22}\ddot{Z}_{22} = F_{sc22} + u_{22} - F_{t22} \tag{A.28}$$

State Variables

$$x = (\dot{Z}_s, Z_s, \dot{\phi}, \phi, \dot{\theta}, \theta, \dot{Z}_{u12}, Z_{u12}, \dot{Z}_{u11}, Z_{u11}, \dot{Z}_{u21}, Z_{u21}, \dot{Z}_{u22}, Z_{u22})^T$$

State-Space Form

$$\dot{x} = Ax + B_1 u + B_2 w \tag{A.29}$$

where:

$$A = \begin{bmatrix}
A_{1,1} & A_{1,2} & A_{1,3} & A_{1,4} & A_{1,5} & A_{1,6} & A_{1,7} & A_{1,8} & A_{1,9} & A_{1,10} & A_{1,11} & A_{1,12} & A_{1,13} & A_{1,14} \\
1 & 0 & 0 & 0 & 0 & 0 & 0 & 0 & 0 & 0 & 0 & 0 & 0 & 0 \\
A_{3,1} & A_{3,2} & A_{3,3} & A_{3,4} & A_{3,5} & A_{3,6} & A_{3,7} & A_{3,8} & A_{3,9} & A_{3,10} & A_{3,11} & A_{3,12} & A_{3,13} & A_{3,14} \\
0 & 0 & 1 & 0 & 0 & 0 & 0 & 0 & 0 & 0 & 0 & 0 & 0 & 0 \\
A_{5,1} & A_{5,2} & A_{5,3} & A_{5,4} & A_{5,5} & A_{5,6} & A_{5,7} & A_{5,8} & A_{5,9} & A_{5,10} & A_{5,11} & A_{5,12} & A_{5,13} & A_{5,14} \\
0 & 0 & 0 & 0 & 1 & 0 & 0 & 0 & 0 & 0 & 0 & 0 & 0 & 0 \\
A_{7,1} & A_{7,2} & A_{7,3} & A_{7,4} & A_{7,5} & A_{7,6} & A_{7,7} & A_{7,8} & A_{7,9} & A_{7,10} & A_{7,11} & A_{7,12} & A_{7,13} & A_{7,14} \\
0 & 0 & 0 & 0 & 0 & 0 & 1 & 0 & 0 & 0 & 0 & 0 & 0 & 0 \\
A_{9,1} & A_{9,2} & A_{9,3} & A_{9,4} & A_{9,5} & A_{9,6} & A_{9,7} & A_{9,8} & A_{9,9} & A_{9,10} & A_{9,11} & A_{9,12} & A_{9,13} & A_{9,14} \\
0 & 0 & 0 & 0 & 0 & 0 & 0 & 0 & 1 & 0 & 0 & 0 & 0 & 0 \\
A_{11,1} & A_{11,2} & A_{11,3} & A_{11,4} & A_{11,5} & A_{11,6} & A_{11,7} & A_{11,8} & A_{11,9} & A_{11,10} & A_{11,11} & A_{11,12} & A_{11,13} & A_{11,14} \\
0 & 0 & 0 & 0 & 0 & 0 & 0 & 0 & 0 & 0 & 1 & 0 & 0 & 0 \\
A_{13,1} & A_{13,2} & A_{13,3} & A_{13,4} & A_{13,5} & A_{13,6} & A_{13,7} & A_{13,8} & A_{13,9} & A_{13,10} & A_{13,11} & A_{13,12} & A_{13,13} & A_{13,14} \\
0 & 0 & 0 & 0 & 0 & 0 & 0 & 0 & 0 & 0 & 0 & 0 & 1 & 0
\end{bmatrix}$$

$$A_{1,1} = -\frac{(c_{st11}+c_{st12}+c_{st22}+c_{st21})}{m_s}$$

$$A_{1,2} = -\frac{(k_{s11}+k_{s12}+k_{s22}+k_{s21})}{m_s}$$

$$A_{1,3} = -\frac{(ac_{st11}-bc_{st12}-dc_{st22}+cc_{st21})}{m_s}$$

$$A_{1,4} = \frac{(-ak_{s11}+bk_{s12}+dk_{s22}-ck_{s21})}{m_s}$$

$$A_{1,5} = \frac{(l_f c_{st11}+l_f c_{st12}-l_r c_{st22}-l_r c_{st21})}{m_s}$$

$$A_{1,6} = \frac{(l_f k_{s11}+l_f k_{s12}-l_r k_{s22}-l_r k_{s21})}{m_s}$$

$$A_{1,7} = \frac{c_{st12}}{m_s}$$

$$A_{1,8} = \frac{k_{s12}}{m_s}$$

$$A_{1,9} = \frac{c_{st11}}{m_s}$$

$$A_{1,10} = \frac{k_{s11}}{m_s}$$

$$A_{1,11} = \frac{c_{st21}}{m_s}$$

$$A_{1,12} = \frac{k_{s21}}{m_s}$$

$$A_{1,13} = \frac{c_{st22}}{m_s}$$

$$A_{1,14} = \frac{k_{s22}}{m_s}$$

$$A_{3,1} = \frac{-c_{st11}a+c_{s12}b+c_{s22}d-c_{st21}c}{I_x}$$

$$A_{3,2} = \frac{-ak_{s11}+bk_{s12}+dk_{s22}-ck_{s21})}{I_x}$$

$$A_{3,3} = \frac{-c_{st11}a^2-b^2 c_{st12}-d^2 c_{st22}-c^2 c_{st21}}{I_x}$$

$$A_{3,4} = \frac{(-a^2 k_{s11}-b^2 k_{s12}-d^2 k_{s22}-c^2 k_{s21})}{I_x}$$

$$A_{3,5} = \frac{(al_f c_{st11}-bl_f c_{st12}+dl_r c_{st22}-cl_r c_{st21})}{I_x}$$

$$A_{3,6} = \frac{(al_f k_{s11}-bl_f k_{s12}+dl_r k_{s22}-cl_r k_{s21})}{I_x}$$

$$A_{3,7} = \frac{-bc_{st12}}{I_x}$$

$$A_{3,8} = \frac{-bk_{s12}}{I_x}$$

$$A_{3,9} = \frac{ac_{st11}}{I_x}$$

$$A_{3,10} = \frac{ak_{s11}}{I_x}$$

$$A_{3,11} = \frac{cc_{st21}}{I_x}$$

$$A_{3,12} = \frac{ck_{s21}}{I_x}$$

$$A_{3,13} = \frac{-dc_{st22}}{I_x}$$

$$A_{3,14} = \frac{-dk_{s22}}{I_x}$$

$$A_{5,1} = \frac{l_f c_{st11} + l_f c_{st12} - l_r c_{st22} - l_r c_{st21}}{I_y}$$

$$A_{5,2} = \frac{l_f k_{s11} + l_f k_{s12} - l_r k_{s22} - l_r k_{s21})}{I_y}$$

$$A_{5,3} = \frac{l_f c_{st11} a - l_f b c_{st12} + l_r d c_{st22} - l_r c_{st21} c}{I_y}$$

$$A_{5,4} = \frac{(l_f a k_{s11} - b l_f k_{s12} + l_r d k_{s22} - l_r c k_{s21})}{I_y}$$

$$A_{5,5} = \frac{(-l_f^2 c_{st11} - l_f^2 c_{st12} - l_r^2 c_{st22} - l_r^2 c_{st21})}{I_y}$$

$$A_{5,6} = \frac{(-l_f^2 k_{s11} - l_f^2 k_{s12} - l_r^2 k_{s22} - l_r^2 k_{s21})}{I_y}$$

$$A_{5,7} = \frac{-l_f c_{st12}}{I_y}$$

$$A_{5,8} = \frac{-l_f k_{s12}}{I_y}$$

$$A_{5,9} = \frac{-l_f c_{st11}}{I_y}$$

$$A_{5,10} = \frac{-l_f k_{s11}}{I_y}$$

$$A_{5,11} = \frac{l_r c_{st21}}{I_y}$$

$$A_{5,12} = \frac{l_r k_{s21}}{I_y}$$

$$A_{5,13} = \frac{l_r c_{st22}}{I_y}$$

$$A_{5,14} = \frac{l_r k_{s22}}{I_y}$$

$$A_{7,1} = \frac{c_{st12}}{m_{12}}$$

$$A_{7,2} = \frac{k_{s12}}{m_{12}}$$

$$A_{7,3} = \frac{-c_{st12} b}{m_{12}}$$

$$A_{7,4} = \frac{-k_{s12} b}{m_{12}}$$

$$A_{7,5} = \frac{-c_{st12} l_f}{m_{12}}$$

$$A_{7,6} = \frac{-k_{s12} l_f}{m_{12}}$$

$$A_{7,7} = \frac{-c_{st12}}{m_{12}}$$

$$A_{7,8} = -\frac{(k_{s12} + k_{t12})}{m_{12}}$$

$$A_{9,1} = \frac{c_{st11}}{m_{11}}$$

$$A_{9,2} = \frac{k_{s11}}{m_{11}}$$

$$A_{9,3} = \frac{c_{st11} a}{m_{11}}$$

$$A_{9,4} = \frac{k_{s11} a}{m_{11}}$$

$$A_{9,5} = \frac{-c_{st11} l_f}{m_{11}}$$

$$A_{9,6} = \frac{-k_{s11} l_f}{m_{11}}$$

$$A_{9,9} = \frac{-c_{st11}}{m_{11}}$$

$$A_{9,10} = -\frac{(k_{s11} + k_{t11})}{m_{11}}$$

$$A_{11,1} = \frac{c_{st21}}{m_{21}}$$

$$A_{11,2} = \frac{k_{s21}}{m_{21}}$$

$$A_{11,3} = \frac{c_{st21} c}{m_{21}}$$

$$A_{11,4} = \frac{k_{s21} c}{m_{21}}$$

$$A_{11,5} = \frac{c_{st21} l_r}{m_{21}}$$

$$A_{11,6} = \frac{k_{s21} l_r}{m_{21}}$$

$$A_{11,11} = \frac{-c_{st21}}{m_{21}}$$

$$A_{11,12} = -\frac{(k_{s21} + k_{t21})}{m_{21}}$$

$$A_{13,1} = \frac{c_{st22}}{m_{22}}$$

$$A_{13,2} = \frac{k_{s22}}{m_{22}}$$

$$A_{13,3} = \frac{-dc_{st22}}{m_{22}}$$

$$A_{13,4} = \frac{-dk_{s22}}{m_{22}}$$

$$A_{13,5} = \frac{c_{st22}l_r}{m_{22}}$$

$$A_{13,6} = \frac{k_{s22}l_r}{m_{22}}$$

$$A_{13,13} = \frac{-c_{st22}}{m_{22}}$$

$$A_{13,14} = -\frac{(k_{s22}+k_{t22})}{m_{22}}$$

$$B_1 = \begin{bmatrix} \frac{-1}{m} & \frac{-1}{m} & \frac{-1}{m} & \frac{-1}{m} \\ 0 & 0 & 0 & 0 \\ \frac{b}{I_x} & -\frac{a}{I_x} & -\frac{c}{I_x} & \frac{d}{I_x} \\ 0 & 0 & 0 & 0 \\ \frac{l_f}{I_y} & \frac{l_f}{I_y} & -\frac{l_r}{I_y} & -\frac{l_r}{I_y} \\ 0 & 0 & 0 & 0 \\ \frac{1}{m_{12}} & 0 & 0 & 0 \\ 0 & 0 & 0 & 0 \\ 0 & \frac{1}{m_{11}} & 0 & 0 \\ 0 & 0 & 0 & 0 \\ 0 & 0 & \frac{1}{m_{21}} & 0 \\ 0 & 0 & 0 & 0 \\ 0 & 0 & 0 & \frac{1}{m_{22}} \\ 0 & 0 & 0 & 0 \end{bmatrix}$$

$$B_2 = \begin{bmatrix} 0 & 0 & 0 & 0 \\ 0 & 0 & 0 & 0 \\ 0 & 0 & 0 & 0 \\ 0 & 0 & 0 & 0 \\ 0 & 0 & 0 & 0 \\ 0 & 0 & 0 & 0 \\ \frac{k_{t12}}{m_{12}} & 0 & 0 & 0 \\ 0 & 0 & 0 & 0 \\ 0 & \frac{k_{t11}}{m_{11}} & 0 & 0 \\ 0 & 0 & 0 & 0 \\ 0 & 0 & \frac{k_{t21}}{m_{21}} & 0 \\ 0 & 0 & 0 & 0 \\ 0 & 0 & 0 & \frac{k_{t22}}{m_{22}} \\ 0 & 0 & 0 & 0 \end{bmatrix}$$

- 130 -

APPENDIX B. VEHICLE PARAMETERS

A.B.0 Quarter Car Lumped Mass Model

m_u 40kg	m_t 730kg
k_s 19.96kN/m	m_s 234kg
k_t 175.5kN/m	c_{st} 1.29kN/m

$$m_s = (m_t) \frac{l_r}{2(l_f + l_r)}$$

(A.30)

where:

m_t.the total mass of the vehicle body (excludes the mass of the unsprung mass)

A.B.1 Half Car Lumped Mass Model

m_1 40kg	m_2 35.5kg	l_f 1.011m
k_{s1} 19.96kN/m	k_{s2} 17.5kN/m	l_r 1.803m
c_{st1} 1.29kN/m	c_{st2} 1.62kN/m	I_y 1230kgm^2
k_{t1} 175.5kN/m	k_{t2} 175.5kN/m	m_s 365kg

A.B.2 Full Car Lumped Mass Model

m_{11} 40kg	m_{12} 40kg	m_{21} 35.5kg	m_{22} 35.5kg	l_f 1.011m
k_{s11} 19.96kN/m	k_{s12} 19.96kN/m	k_{s21} 17.5kN/m	k_{s22} 17.5kN/m	l_r 1.803m
c_{st11} 1.29kN/m	c_{st12} 1.29kN/m	c_{st21} 1.62kN/m	c_{st22} 1.62kN/m	I_y 1230kgm^2
k_{t11} 175.5kN/m	k_{t12} 175.5kN/m	k_{t21} 175.5kN/m	k_{t22} 175.5kN/m	I_x 1230kgm^2
a 0.761m	b 0.761m	c 0.755m	d 0.755m	m_s 730kg

A.B.3 Iltis Model

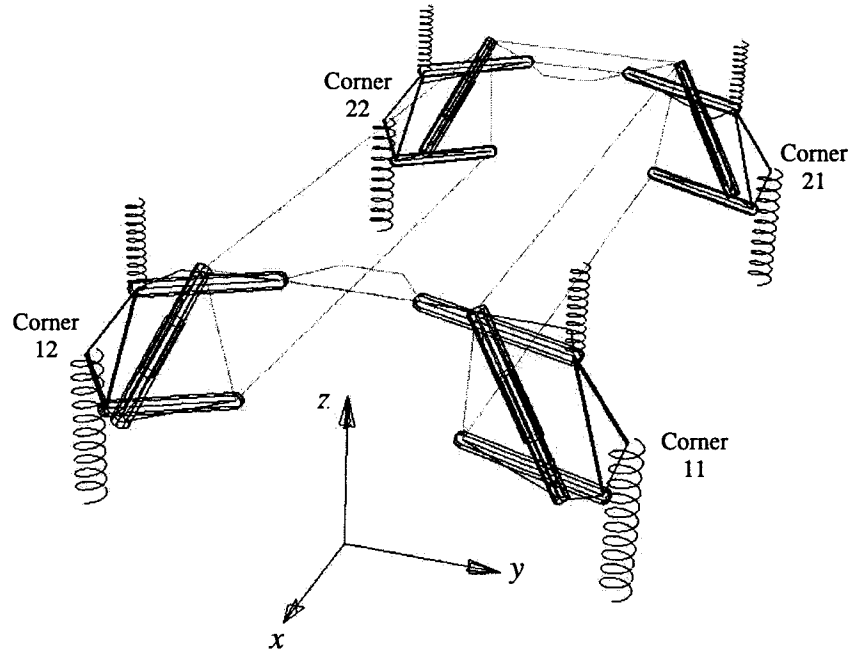*Figure A.3: Full car Iltis*

Reference origin is the center of the front and rear axles on the ground.

Legend

lca- lower control arm

uca- upper control arm

sp- spindle

cm- sprung mass

Quarter Car Model State Variables

$$x = (\dot{Z}_{cm}, Z_{cm}, \dot{\phi}_{11}, \phi_{11})^T$$

Full Vehicle Model State Variables

$$x = (\dot{\phi}_{12}, \phi_{12}, \dot{X}_{cm}, X_{cm}, \dot{\phi}_{11}, \phi_{11}, \dot{\beta}_{cm}, \beta_{cm}, \dot{\phi}_{cm}, \phi_{cm}, \dot{\phi}_{22}, \phi_{22}, \dot{\phi}_{21}, \phi_{21}, \dot{\theta}_{cm}, \theta_{cm}, \dot{Y}_{cm}, Y_{cm}, \dot{Z}_{cm}, Z_{cm})^T$$

- 132 -

Full Vehicle Model with Bushings State Variables

$\mathbf{x} = ($

$\dot{\varphi}_{LCA12}, \varphi_{LCA12}, \dot{\theta}_{LCA12}, \theta_{LCA12},$

$\dot{X}_{UCA12}, X_{UCA12}, \dot{Y}_{UCA12}, Y_{UCA12}, \dot{Z}_{UCA12}, Z_{UCA12}, \dot{\varphi}_{UCA12}, \varphi_{UCA12},$

$\dot{\beta}_{SP12}, \beta_{SP12}, \dot{\varphi}_{SP12}, \varphi_{SP12},$

$\dot{X}_{CM}, X_{CM}, \dot{Y}_{CM}, Y_{CM}, \dot{Z}_{CM}, Z_{CM}, \dot{\beta}_{CM}, \beta_{CM}, \dot{\varphi}_{CM}, \varphi_{CM}, \dot{\theta}_{CM}, \theta_{CM},$

$\dot{\beta}_{SP11}, \beta_{SP11}, \dot{\varphi}_{SP11}, \varphi_{SP11},$

$\dot{\varphi}_{UCA11}, \varphi_{UCA11}, \dot{\theta}_{UCA11}, \theta_{UCA11},$

$\dot{X}_{LCA11}, X_{LCA11}, \dot{Y}_{LCA11}, Y_{LCA11}, \dot{Z}_{LCA11}, Z_{LCA11}, \dot{\varphi}_{LCA11}, \varphi_{LCA11},$

$\dot{\beta}_{SP22}, \beta_{SP22}, \dot{\varphi}_{SP22}, \varphi_{SP22},$

$\dot{\beta}_{SP21}, \beta_{SP21}, \dot{\varphi}_{SP21}, \varphi_{SP21},$

$\dot{\varphi}_{LCA22}, \varphi_{LCA22}, \dot{\theta}_{LCA22}, \theta_{LCA22},$

$\dot{\varphi}_{LCA21}, \varphi_{LCA21}, \dot{\theta}_{LCA21}, \theta_{LCA21},$

$\dot{X}_{UCA21}, X_{UCA21}, \dot{Y}_{UCA21}, Y_{UCA21}, \dot{Z}_{UCA21}, Z_{UCA21}, \dot{\varphi}_{UCA21}, \varphi_{UCA21},$

$\dot{X}_{UCA22}, X_{UCA22}, \dot{Y}_{UCA22}, Y_{UCA22}, \dot{Z}_{UCA22}, Z_{UCA22}, \dot{\varphi}_{UCA22}, \varphi_{UCA22})^{T}$

Description	x (m)	y (m)	z (m)
wheel centre	0	-0.615	0.356
A-arm connection to spindle	0	-0.572	0.229
A-arm connection to cabin	0	-0.259	0.302
leaf spring connection to spindle	0	-0.488	0.531
leaf spring connection to cabin	0	-0.159	0.600
damper connection to A-arm	7.50e-2	-0.500	0.241
damper connection to cabin	7.50e-2	-0.297	0.632
tie rod connection to spindle	-0.140	-0.448	0.531
tie rod connection to cabin	-0.140	-0.070	0.600

Body	Center of Gravity Location (m)	Mass (kg)	I_x (kgm^2)	I_y (kgm^2)	I_z (kgm^2)
cabin	(0,0,0.570)	1260	130	1620	1670
right front wheel assembly	(0.970,-0.615,0.356)	57.35	1.2402	1.908	1.2402
left front wheel assembly	(-1.047,0.615,0.356)	57.35	1.2402	1.908	1.2402
right front A-arm	(0.97,-0.4155,0.2655)	6.00	0.052099	0.023235	0.068864
left rear A-arm	(-1.047,0.4155,0.2655)	6.00	0.052099	0.023235	0.068864

*all products of inertia are zero

Preload in the Nominal Condition

Element	Force (N)
leaf spring	2728.9
damper spring	128.0
front tire	3829.6
rear tire	3593.6

A.C.0 Lumped Mass Models

If the desired force is that which is produced by a skyhook damper then:

$$F_{desired} = c_{sky} \dot{z}_s \tag{A.31}$$

In the switching criteria, the damping coefficient may be ignored since it is a scalar and so:

$$F_D = c_{sky} \dot{z}_s \quad \text{if} \quad \dot{z}_s \dot{x}_D > 0 \tag{A.32}$$

$$F_D = 0 \quad \text{if} \quad \dot{z}_s \dot{x}_D \leq 0 \tag{A.33}$$

A.C.0.1 Quarter Car Model

With this vehicle:

$$\dot{x}_D = (\dot{z}_s - \dot{z}_u) \tag{A.34}$$

A.C.0.2 Half Car Model

With this vehicle:

$$\dot{x}_{D_{front}} = ((\dot{z}_s - l_f \dot{\theta} \cos\theta) - \dot{z}_{u1}) \tag{A.35}$$

$$\dot{x}_{D_{rear}} = ((\dot{z}_s + l_r \dot{\theta} \cos\theta) - \dot{z}_{u2}) \tag{A.36}$$

A.C.0.3 Full Car Model

With this vehicle:

Front

$$\dot{x}_{D_{11}} = ((\dot{z}_s - l_f \dot{\theta} \cos\theta + a\dot{\phi}\cos\phi) - \dot{z}_{u11}) \tag{A.37}$$

$$\dot{x}_{D_{12}} = ((\dot{z}_s - l_f \dot{\theta} \cos\theta - b\dot{\phi}\cos\phi) - \dot{z}_{u12}) \tag{A.38}$$

Rear

$$\dot{x}_{D_{21}} = ((\dot{z}_s + l_r \dot{\theta} \cos\theta + c\dot{\phi}\cos\phi) - \dot{z}_{u21}) \tag{A.39}$$

$$\dot{x}_{D_{22}} = ((\dot{z}_s + l_r \dot{\theta} \cos\theta - d\dot{\phi}\cos\phi) - \dot{z}_{u22}) \tag{A.40}$$

A.C.1 Iltis Model

Due to the complexity of the geometry, deriving an expression for $\dot{x}_D$ is not straight forward. However this algorithm can still be used by simply outputting the length of the damper element from ADAMS into Simulink. This value can then be used in the above relations to describe the switching laws.

VITA AUCTORIS

Name:	Joseph Maiorana
Place of Birth:	Scarborough, Ontario, Canada
Year of Birth:	1978
Education:	Brebeuf College, Willowdale, Ontario 1992-1997
	Queen's University, Kingston, Ontario 1997-2002, Bachelor of Science
	University of Windsor, Windsor, Ontario 2002-2004, Master of Applied Science
Contact:	maioranajoseph@yahoo.ca